REPORT DOCUMENTATION PAGE

1a. REPORT SECURITY CLASSIFICATION Unclassified	1b. RESTRICTIVE MARKINGS
2a. SECURITY CLASSIFICATION AUTHORITY	3. DISTRIBUTION / AVAILABILITY OF REPORT Approved for public release; Unlimited distribution.
2b. DECLASSIFICATION / DOWNGRADING SCHEDULE	
4. PERFORMING ORGANIZATION REPORT NUMBER(S)	5. MONITORING ORGANIZATION REPORT NUMBER(S) AFOSR-TR- 9 5 - 0 4 3 2

6a. NAME OF PERFORMING ORGANIZATION Hatfield Marine Science Center Oregon State University	6b. OFFICE SYMBOL (If applicable)	7a. NAME OF MONITORING ORGANIZATION Air Force Office of Scientific Research/NL
6c. ADDRESS (City, State, and ZIP Code) Marine Science Drive Newport, OR 97365		7b. ADDRESS (City, State, and ZIP Code) Building 410 Bolling AFB, DC 20332

8a. NAME OF FUNDING / SPONSORING ORGANIZATION AFOSR	8b. OFFICE SYMBOL (If applicable) NL	9. PROCUREMENT INSTRUMENT IDENTIFICATION NUMBER F49620-92-J-0140

8c. ADDRESS (City, State, and ZIP Code) Building 410 Bolling AFB, DC 20332-6448	10. SOURCE OF FUNDING NUMBERS			
	PROGRAM ELEMENT NO. 61102F	PROJECT NO. 2312	TASK NO. A+BS	WORK UNIT ACCESSION NO.

11. TITLE (Include Security Classification) Parallel Processing and Learning: Variability and Chaos in Self-Organization of Activity in Groups of Neurons

12. PERSONAL AUTHOR(S)
George J. Mpitsos, PI

13a. TYPE OF REPORT Final Report	13b. TIME COVERED FROM 92/1/15 TO 95/1/31	14. DATE OF REPORT (Year, Month, Day) 95/6/14	15. PAGE COUNT = 13 Plus 3 Appendices

16. SUPPLEMENTARY NOTATION

17.	COSATI CODES		18 SUBJECT TERMS (Continue on reverse if necessary and identify by block number)
FIELD	GROUP	SUB-GROUP	Parallel processing, learning, catalytic networks, attractors, gradient descent

19. ABSTRACT (Continue on reverse if necessary and identify by block number) Abstract is continued on reverse side.

GOALS: Motivated partly by our previous work, we have attempted:
(1) To determine whether there is a global mechanism that automatically adjusts the strengths of the many connections that take place between neurons.
(2) To determine the source of variations in neuronal firing observed during behaviorally meaningful neural activity, whether the variations arise from deterministic processes or nondeterministic ones, and to identify the synaptic or membrane mechanisms that may give rise to them.
Because biological systems are difficult to control, we have used computer simulations to examine these problems. The results indicate that the findings may be addressable in biological systems, particularly in cell cultures of two or three selectively connected neurons.

20. DISTRIBUTION / AVAILABILITY OF ABSTRACT ☒ UNCLASSIFIED/UNLIMITED ☒ SAME AS RPT. ☐ DTIC USERS	21. ABSTRACT SECURITY CLASSIFICATION Unclassified
22a. NAME OF RESPONSIBLE INDIVIDUAL Dr. Genevieve Haddad	22b. TELEPHONE (Include Area Code) (202) 767-5021	22c. OFFICE SYMBOL NL

DD FORM 1473, 84 MAR   83 APR edition may be used until exhausted.
 All other editions are obsolete.   SECURITY CLASSIFICATION OF THIS PAGE
 UNCLASSIFIED

1 6 JUN 1995

19. Abstract, continued.

RESULTS: Five illustrations are used in this report to discuss the major features of the results.

Figures 1 and 2 are directed to the first of the above problems. A conjecture is outlined and evaluated: If a group of neurons can sustain recurring activity whose dynamics represents an attractor, and if the synaptic strengths and thresholds are set by activity-dependent mechanisms, the dissipative properties of the attractor constrain the flow of activity among these neurons in such a way that all synapses and thresholds are optimally set with respect to one another.

Appendix-1 provides an extended discussion of this conjecture, and of other findings that emerge from it, and places it within the context of findings in the literature. Appendix-1 is presently under review in *Behavioral and Brain Sciences*.

Figures 3-5 are directed to the second of the above problems. We used the rationale that one synaptic input acts as a perturbation stimulus to another; i.e., a given synaptic input that leads to the generation of an action potential acts on membrane impedance that has been preconditioned by some preceding event. In the present series of experiments, we used a weak preconditioning delta-function current impulse as the conditioning stimulus to determine its effect on the latency of a synaptically activated action potential (spike). The findings show clearly that the membrane is highly sensitive to the temporal pattern of the input signal. The output spike train, however, has a temporal structure that is significantly altered by comparison to the input. More importantly, the information flow across the synapse is highly degenerate; i.e., that degenerate conditions may emerge naturally from a completely deterministic system. It is expected that our future work will show that variations, and other dynamical characteristics of network activity, naturally emerge from such conditions.

Appendices 2 & 3 discuss these findings in detail, and place them within the context of the literature over the past 30 years that has dealt with the possibility that neurons may be sensitive to the pattern of the input signals that they receive. Appendices 2 & 3 are near final versions of papers that will be submitted for publication in *Biological Cybernetics*.

Publication that have appeared in print over the past three years:

Andrade MA, Nuño JC, Moran F, Montero F, Mpitsos GJ (1993) Complex dynamics of a catalytic network having faulty replication into an error species. Phys D 63:21-40

Burton RM, Mpitsos GJ (1992) Event-dependent control of noise enhances learning in neural networks. Neural Networks 5:627-637

Mpitsos GJ, Burton RM (1992) Convergence and divergence in neural networks: Processing of chaos and biological analogy. Neural Networks 5:605-625

Mpitsos GJ, Soinila S (1993) In search of a unifying theory of biological organization: What does the motor system of a sea slug tell us about human motor integration? In: Newell KM, and Corcos D, (eds) Variability and Motor Control, Human Kinetics, Champaign, pp 225-290

Soinila S, Mpitsos GJ, Soinila J (1992) Enkephalin immunohistochemistry: Model studies on conjugation reaction and fixation. J Histochem Cytochem 40:231-239

Appendices:

1. Mpitsos GJ (1995) Attractor gradients: architects of developmental organization. Under review in Behavioral and Brain Sciences

2. Edstrom JL, Mpitsos GJ (1995) Predicting the influence of perturbing currents on spike latencies: Determinism and degeneracy of information in synaptic transmission. A revised version will be sent to Biological Cybernetics.

3. Edstrom JL, Mpitsos GJ (1995) Simple neuronal membrane is sensitive to the temporal structure of input signals. A revised version will be sent to Biological Cybernetics.

I. FINAL REPORT

1. Dissipative action of network firing patterns sets all synapses optimally with respect to one another

The following conjecture is examined:

(a) Assume that the network is initially randomly connected, and that the neurons are firing action potentials.

(b) Somewhere in the network, two or three neurons may have firing patterns that are sufficiently correlated with one another that their synapses undergo activity-dependent changes. If dissipative action begins to emerge, the synaptic weights in the developing network must have some interrelated range of values, else the attractor would not exist.

(c) The emerging attractor constrains the flow of activity, causing further activity-dependent changes and refinement of the attractor spatio-temporally.

(d) Neurons that converge onto the same follower neurons may compete (Merzenich, et al., 1978; Merzenich, et al., 1983a; Merzenich, et al., 1983b; Merzenich, et al., 1984; Mpitsos, et al., 1978; Recanzone and Merzenich, 1992) for occupancy of the synaptic space available on the follower neuron such that connections may be made or broken, structurally molding the neuroarchitecture

Behavior of a fixed network: To illustrate this conjecture, first consider a network that has already been set and has the strengths of all of its synapses frozen. Figure 1C shows the network. For the present discussion, we may exclude Cell4; its use is discussed in Appendix-1 where some of the details of the network are also given (detailed descriptions of the membrane and synapse characteristics are given in Appendix-2). The three cells are connected by excitatory (synapses shown by open-circle terminals) and inhibitory connections (synapses shown by filled-circles). The delay between the synapses was set at 3 msec. Simulation of electrogenic activity used the Hodgkin-Huxley model of the squid giant axon (future research will use more biologically complex neurons). The strength of the synapses is indicted by the thickness of the connection "axons" and numerically in milliSiemens. Steady depolarizing current was injected into Cell-1, causing it to fire action potentials which activated the remaining cells in the network.

Figure 1A shows a 3-cycle firing pattern in Cell2. Starting from the simulation time at 680 msec, seven intervals between the action potentials are shown, where the 3-cycle repetition sequence consists of intervals having 15.4 msec, 35.0 msec, and 46.3 msec durations. For the purposes of the illustration only two 3-cycle periods are shown, but many more 3-cycle sequences preceded them. This particular firing pattern was obtained by driving the network using steady depolarization of Cell1 and selectively adjusting the strength of the inhibitory synapse that Cell3 makes on Cell2 until the 3-cycle was obtained.

Certain other combinations of synaptic weights also give similar 3-cycle activity, just as Gardner (1990) has demonstrated that different synaptic strengths between four identified neurons in the sea slug *Aplysia* generate similar network function. The dashed line below the action potential trace shows the time during which the network was perturbed by injecting Cell2 with a 125 msec electrical current pulse that pushed the membrane potential below the threshold level for the genesis of action potentials, except for one action potential (labeled by a "1") arising from strong activity in one of the other cells in the network. After the cessation of the applied current, the cell rebounded with a rapid burst of three action potentials (labeled "2", "3", "4"), and then recovered to its original firing pattern.

The pattern of intervals shown in Fig. 1A may be plotted in a return map in which one interval in the sequence is plotted on the horizontal axis and the succeeding interval is plotted on the vertical axis. One hundred intervals were used to construct the 3-cycle of the unperturbed activity; all fell sequentially on the three filled circles in Fig. 1B. The return-map positions of the intervals during and after the application of the 125 msec perturbation pulse are shown by the numbered and open triangles. The identifying numbers in the return map are the

same as those in the trace shown in Fig. 1A, where the number over a given action potential indicates the interval between that action potential and the preceding one.

Behavior of a changeable network: The schematic in Fig. 2 shows how the network examined previously may be altered following a perturbation stimulus. The original network is shown in Fig. 2A. It is the same as the one shown in Fig. 1, as are the activation conditions, but the strengths of the synapses are now made available for activity-dependent changes. If Cell2 is depolarized for an arbitrary length of time, it begins to generate action potentials initially at a higher frequency than before, but soon the balance of excitatory and inhibitory feedback readjusts its rate of firing. The activity-dependent changes in a synapse depend on the temporal correlations of activity in the presynaptic and postsynaptic cells which will vary over time. The dynamics giving rise to these correlations is extremely complicated and time dependent, but Fig. 2B has caught the changed synapses at a stage (shown by the numbers next to the axons) that cause Cell2 to generate a 6-cycle firing pattern. The open triangles in the return map of Fig. 2B show the values of the six intervals between the action potentials. The filled circles show the original 3-cycle.

When Cell2 is released from the depolarizing current (Cell1 is under continuous depolarization to keep the network active), its firing pattern may remain in the 6-cycle state, but if the attractor is not sufficiently well formed, genesis of action potentials in the three neurons may drift to some other set of patterns, or it may eventually settle back to the original 3-cycle state (and perhaps with a different set of synaptic strengths between the neurons).

The aim here is not to say that the 6-cycle *per se* is formed, nor that the original 3-cycle is regenerated in the recovery, but that some attractor is generated, and that its gradients are what adjusts or globally "directs" the local activity-dependent synaptic changes. This is different than would be imagined were we to view networks as switchboards or reflexes by which change is based only on local activity-dependent effects. From such effects it might be postulated, for example, that associative learning in whole animals is based on changes in individual synapses; reviewed in. By the conjectured gradient method, however, it is obvious that changing one synapse causes changes in all of them. Local rules are a work, but they are guided by a more global principle.

Appendix-1 places this in the context of findings in artificial neural networks, and discusses how dissipative mechanisms may lead to a number of effects, such as the limitations of the functional size of the network and the types of information that may be stored among the connections in the network.

2. Sensitivity of a neuron to the pattern of input stimuli, & the emergence of degeneracy in the information flow across a simple synapse

How much of the input stimulus pattern does the output firing pattern of a neuron represent? How does the membrane transform the input signal? What are the filter properties of neuron membrane? Does the membrane of postsynaptic neurons act as a filter that is sensitive to the pattern of the input data stream arriving from presynaptic neurons? Being able to describe the membrane as a linear filter in order to understand the answers to such questions has been a subject of interest for many decades, as discussed in Appendix-2. Moreover, the possibility that neurons may be sensitive to the temporal patterns of input signals has important implications in our understanding of neurointegrative mechanisms (Softky, 1995).

We have devised experiments that address such questions in computer simulations. The work described in Appendices 2 & 3 uses simple synapses and neuron membrane, as may be found in the giant synapse and axon of the squid. Subsequent studies will extend the work to more complex neurons and synapses. The results give some insight into the above questions, and also provide a basis for understanding how at least one source of nondeterministic variation in the firing patterns of neurons may emerge naturally from a deterministic process. The rationale for starting with studies that examine the membrane within its linear response range is also discussed in the Introduction and Discussion of Appendix-2.

The results in Fig. 3 provide the foundation for the work covered in Appendices 2 & 3, and for much of our work that we shall be doing over the next several years. The design of the experiments used to obtain the results is a simple perturbation method. The family of curves shown in Fig. 3 C &D are the composite of many 40 msec simulation sweeps. In each sweep, a

single excitatory postsynaptic current (EPSC) was activated at 25 msec into the sweep. This produced a constant-latency action potential (Fig. 3B) when the postsynaptic neuron was not presented the conditioning, perturbation stimuli. The effects of perturbations are shown in Fig. 3 C & D , and are compared against this standard response as a changes in the spike latency. A single excitatory (solid-line traces) or inhibitory (dotted-line traces) current impulse, lasting one integration step, was presented during the first 30 msec of each simulation sweep. In Fig. 3 C & D, the position of the impulse was moved progressively from left to right in the simulation sweep. Each curve was generated using one impulse amplitude. Progressing outwardly from the zero-latency change, the amplitudes in multiples of 10^{-10} Amp were ($\pm$) 2, 4, 6, 8, 10.

The most important finding in Fig. 3 is that a given latency can be produced by many different temporal positions of the impulses. A horizontal line drawn in Fig. 3 to represent a given latency intersects not only one curve in two places, but many other curves as well: i.e., the input/output function of synapses under perturbation produce a many-to-one mapping. An observer of the output-spike latencies is ignorant of the temporal positions of the stimuli that produced the latency changes because a given latency can not be used to uniquely identify the timing of the perturbation impulse that generated it.

This raises many important research questions relating to strategies that biological systems may have taken to accommodate to such degeneracies. One possibility is that the degeneracy may be useful in generating response variations that may be useful in controlling how networks settle into or exit response patterns. The relationship of these input/output functions to studies in biological systems of the impulse response function (IRF), the average current trajectory (ACT), and membrane impedance is discussed in Appendix-2.

3. Sensitivity of simple neuron membrane to the pattern of input signals

(a) Random stimulation over the temporal range of input/output functions shows that the membrane acts as a nonrandom filter. The experiments shown in Fig. 4 are the same as those in Fig. 3 except that the timing of the perturbing impulses was randomly controlled. 100,000 simulation sweeps were run. The histogram in Fig. 4B shows that the timing of the impulses covered the 7-30 msec interval of the simulations evenly. The input/output function in Fig. 2 is rotated vertically by comparison to the curves in Fig. 3 so that the time-axis extends upward and the latency-axis extends horizontally from left to right. Only one input/output curve is shown because all of the impulses had the same 4×10^{-10} Amp amplitude. Figure 4C shows that the histogram of the output latencies is significantly distorted by comparison to the distribution of the impulses that produced the latency changes, showing that membrane of the postsynaptic cell imposes structure on the signals that it receives. How this occurs is shown more explicitly below.

(b) Stimulation of different temporal regions within the range of the input/output functions shows that the membrane filter imposes structure on its input signals and that the output is more complex than the input stimulus pattern. These experiments are the same as those shown in Fig. 4 except that the temporal position of the perturbing impulses was controlled by the recursive chaotic logistic, $f(x) = 3.7(1-x)x$, where x is in the unit interval; the output of this function was scaled so that it covered different regions of the simulation sweep. Return-map plots of this quadratic function, in which one value $f(x)$ is plotted against the preceding one, produce a typical inverted-U map a quadratic function that can be compared to the return maps of the spike latencies.

The effect of changing the position and range of the impulses is shown in Fig. 5. The presentation times of seven different sets of input stimulus trains are shown by the filled circles; they are shifted vertically with respect to one another in order to illustrate their positions. Figure 5B shows the return maps of the spike latencies; each map is identified numerically by the temporal range of the input stimulus times that generated it. The return maps of the latencies are significantly distorted by and non-quadratic; i.e., whereas the input of the quadratic logistic is a simple second-order polynomial, the multi-looped maps of the latency return maps require fourth or higher-order polynomials to define them.

Additionally, the ends of the spike-latency return-maps may cross. This occurs whenever the stimulus pattern sufficiently spans a humped (vertically convex or concave) region of the i/o functions. An example is shown in Fig. 5B by the map labeled "14-19." These crossed-loop maps are degeneracies that cannot exist in an deterministic system since the flow

of events at the crossing point is not uniquely determined. However, this can be resolved by plotting the return maps in three dimensions (not shown) where one latency (X) is mapped on the x-axis, the next interval (X_{n+1}) is on the y-axis, and the third interval (X_{n+2}) in succession if mapped on the z-axis. Rotating this 3-dimensional image shows that the maps do not actually cross, but that they only appeared to do so because the 2-dimensional return map is a projection of the 3-dimensional one. Dynamically, the input data stream is a 1-dimensional process, whose dynamics can be characterized in two-dimensional return-map embedding. The output data stream is also a 1-dimensional process, but it requires at least three-dimensional embedding to resolve. Thus, the filter properties of the postsynaptic neuron produces an output firing pattern whose temporal characteristic are not only a distortion of the dynamics in the input signal, they also produce an output whose dynamics live an embedding space having a higher dimension than the dynamics of the input data stream.

SIGNIFICANCE:

These findings raise a number of serious questions about how information is transferred across synapses, and how neurons or circuits of neurons may have accommodated to the complexities produced by the input/output functions. It is conceivable that the variations may play a beneficial role in neurointegrative processes. It is particularly interesting that a completely deterministic process may generate non-deterministic responses. Unlike chaos, in which the variations themselves are deterministic, the degeneracies indicated by the findings in Fig. 4 & 5 may lead to nondeterministic variations. The findings shown in Figs. 1 & 2 provide a rationale with which to conceive of how complex neuropil may be formed, and attractors provide a functional way to understand how information distributed widely in a network. We believe that many integrative functions, that may not be follow easily from traditional biological studies, naturally emerge from the findings outlined above. Future work will inquire into these possibilities.

LITERATURE CITED

Gardner D (1990) Paired individual and mean postsynaptic currents recorded in 4-cell networks of *Aplysia*. J Neurophysiol 63:1226-1240

Merzenich MM, Kaas JH, Sur M, Lin CS (1978) Double representation of the body surface within cytoarchitectonic Areas 3b and 1 in "S-I" in the owl monkey *Aotus trivirgatus*. J Comp Neurol 181:41-74

Merzenich MM, Kaas JH, Wall JT, Nelson RJ, Sur M, Felleman DJ (1983a) Progression of change following median nerve section in the cortical representation of the hand in areas 3b and 1 in adult owl and squirrel monkeys. Neurosci 10:639-665

Merzenich MM, Kaas JH, Wall JT, Nelson RJ, Sur M, Felleman DJ (1983b) Topographic reorganization of somatosensory cortical areas 3b and 1 in adult monkeys following restricted deafferentation. Neurosci 8:33-55

Merzenich MM, Nelson RJ, Stryker MP, Cynader MS, Schoppmann JM, Zook JM (1984) Somatosensory cortical map changes following digit amputation in adult monkeys. J Comp Neurol 224:591-605

Mpitsos GJ, Collins SD, McClellan AD (1978) Learning: A model system for physiological studies. Science 199:497-506

Recanzone GH, Merzenizh MM (1992) Alterations in the functional organizaiton of primary somatosensory cortex following intracortical microstimulation or behavioral training. In: Squire LM, Weinberger NM, Lynch G, and McGaugh JL, (ed) Memory: Organization and Locus of Change, Oxford University Press, New York, pp 217-238

Softky WR (1995) Simple codes versus efficient codes. Curr Opin Neurobiol 5:239-247

FIGURE LEGENDS

FIGURE 1. Dissipative action in the simulation of small biologically realistic networks. The network (C) was activated by steady, low-level depolarizing current applied to Cell1. A: Time series of action potentials obtained from Cell2. The activity consists of a 3-cycle in which three intervals between action potentials repeatedly appear, as shown by the first seven action potentials. A 125 msec hyperpolarizing perturbation pulse was presented to Cell2 (marked by the dashed line). One action potential escaped during the hyperpolarization. After the release of the hyperpolarizing pulse, Cell2 rebounded, generating three action potentials in rapid succession, and then relaxed toward the original 3-cycle intervals. B: Shows the return map of the original 3-cycle (filled circles) and the post-perturbation recovery (open triangles). The numbers in (B) are the same as in A, and represent the interval between the numbered action potential and the action potential preceding it. C: Structure of the network: the thickness of the connections are proportional to the maximal synaptic strengths; the numbers show the strengths in milliSiemens. Excitatory synapses (open circles) have a reversal potential of 45 mV. Inhibitory synapses (filled circles) have a reversal potential of -82 mV. Open and close time constants for both types of synapses are 3 and 20 msec, respectively. Transmission delays were 3 msec. The simulations were run GENESIS obtained from the California Institute of Technology, Pasadena, and used squid axon membrane (Hodgkin & Huxley, 1952).

FIGURE 2. Attractors may adjust synaptic strengths globally. A: The same network that produced the 3-cycle activity shown in Fig. 1 is used here. B: Activity-dependent emergence of new connection strengths: The network was activated using Cell1 to produce the 3-cycle. After start-up transients were dissipated, Cell2 was depolarized tonically while maintaining the depolarization applied to Cell1. All synapses in the network were allowed to change using a variant of Hebb's rule. The new synaptic strengths are indicated by the thickness of the connection lines between the neurons and by the numerical values placed next to the lines (compare A and B). C: A return map showing that the new connection strengths generate a 6-cycle pattern (open circles) in the firing of Cell2; the original 3-cycle is shown by the filled symbols. When shorter or weaker stimuli are presented to Cell2, the synaptic strengths do not settle sufficiently into the values required to generate the 6-cycle. The synaptic strengths may fluctuate as the interrelated firing patterns of the cells in the network seek one gradient or another. The temporal structure of these patterns may drift until a strong enough gradient emerges which then forces the interrelated strengths of the synapse into some more stable set. The activity dependent changes in the synaptic strengths, discussed a little later, used Mike Vanier's implementation of Hebbian synapses in GENESIS.

FIGURE 3: The timing of single preconditioning current impulses produces complex changes in action potential latencies. A single current impulse was given in each 40 msec simulation sweep; the timing was allowed to overlap the EPSC. The design of the experiment was aimed at understanding how the temporal position of the impulse affected the latency of the spike produced by the EPSC. A series of such experiments defined input/output functions that relate impulse timing to spike latency. A: Onset (25 msec) and time course of the EPSC. B: Action potential produced by the EPSC in the absence of a preconditioning current pulse. C & D: latencies of action potentials produced in hyperpolarized (-9.5 x 10^{-11} Amp) and normal membrane in response to depolarizing (solid curves) and hyperpolarizing (dotted) current pulses. Each curve was obtained using a different amplitude of the current pulse. The incomplete lines in some of the negative current isopleths indicate suppression of the EPSC-evoked action potential at those current/time combinations. The interval between the points on the curves is 250 msec. The amplitude for the five 0.010 ms depolarizing and hyperpolarizing current pulses was, in multiples of 10^{-10} Amp: ($\pm$) 2, 4, 6, 8, 10. G_{syn} = 3 x 10^{-8} Siemens at the normal resting potential and 4.0536 x 10^{-8} Siemens at the hyperpolarized potential, a value chosen by trial and error to give the same unperturbed action potential latency as the normal control EPSC. Integration time step = 0.010 ms.

FIGURE 4: Recent history of impedance changes that occur under random perturbation generates nonrandom firing of EPSC-evoked action potentials. A: Relation of impulse

presentation time (vertical axis) to action potential latency (horizontal axis). B: Density of randomly generated impulse presentation times; vertical axis is the same as in (A). A single randomly timed current impulse (4×10^{-10} Amps, lasting one .010 ms integration step) was presented in the 7-30 ms interval of each 35 ms simulation sweep. A suprathreshold EPSC was initiated 25 ms into the simulation. C: Histogram of the EPSC-evoked action potentials the resulted from 100,000 simulation sweeps.

FIGURE 5: The temporal position along the latency input/output functions represent different distortions of the structure of the input function generating the perturbation pulses. A: The thin line shows the action potential latencies arising from a composite of logistic-activated sequence of current pulses having constant amplitude (9×10^{-10} Amp; .010 ms). Seven of these sequences are shown by the dotted curves which have been shifted vertically to identify them. The irregular spacing between the dots in each line arises from the logistic scaling function T described in the text. B: Return maps of the intervals in six of the sequences in (A). The numbers identify the approximate range of times spanned by each sequence along the input/output function.
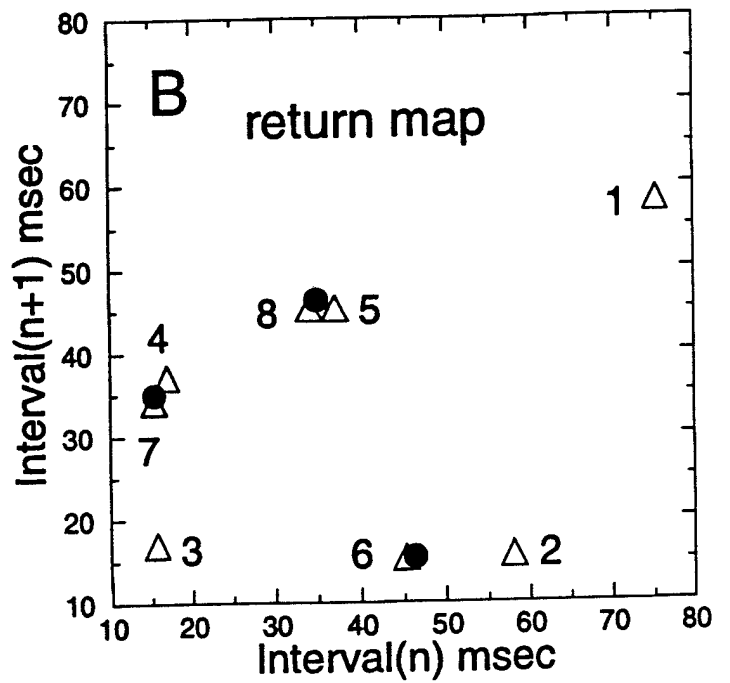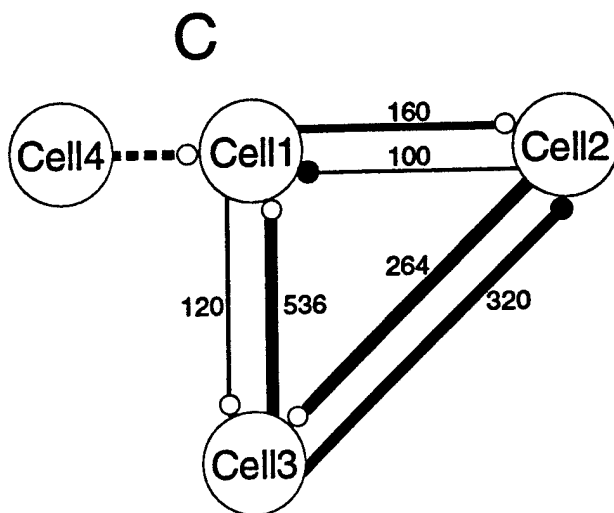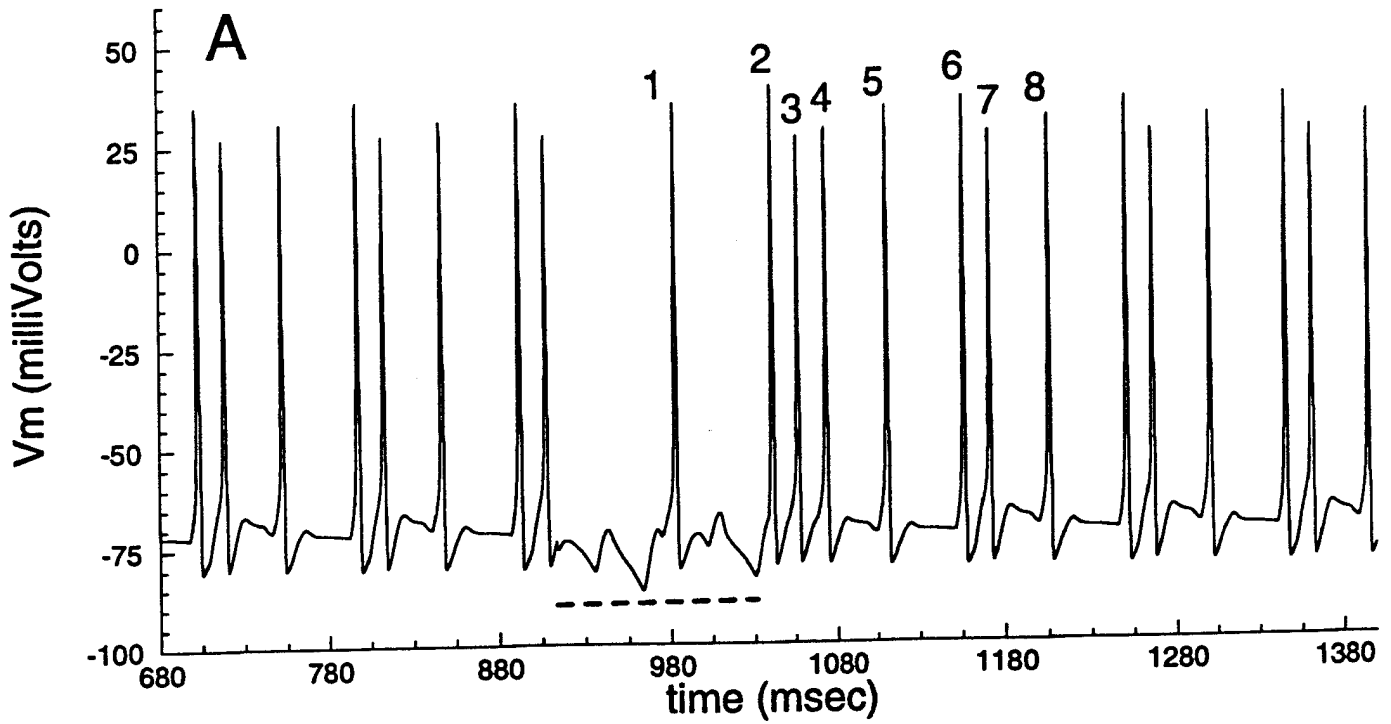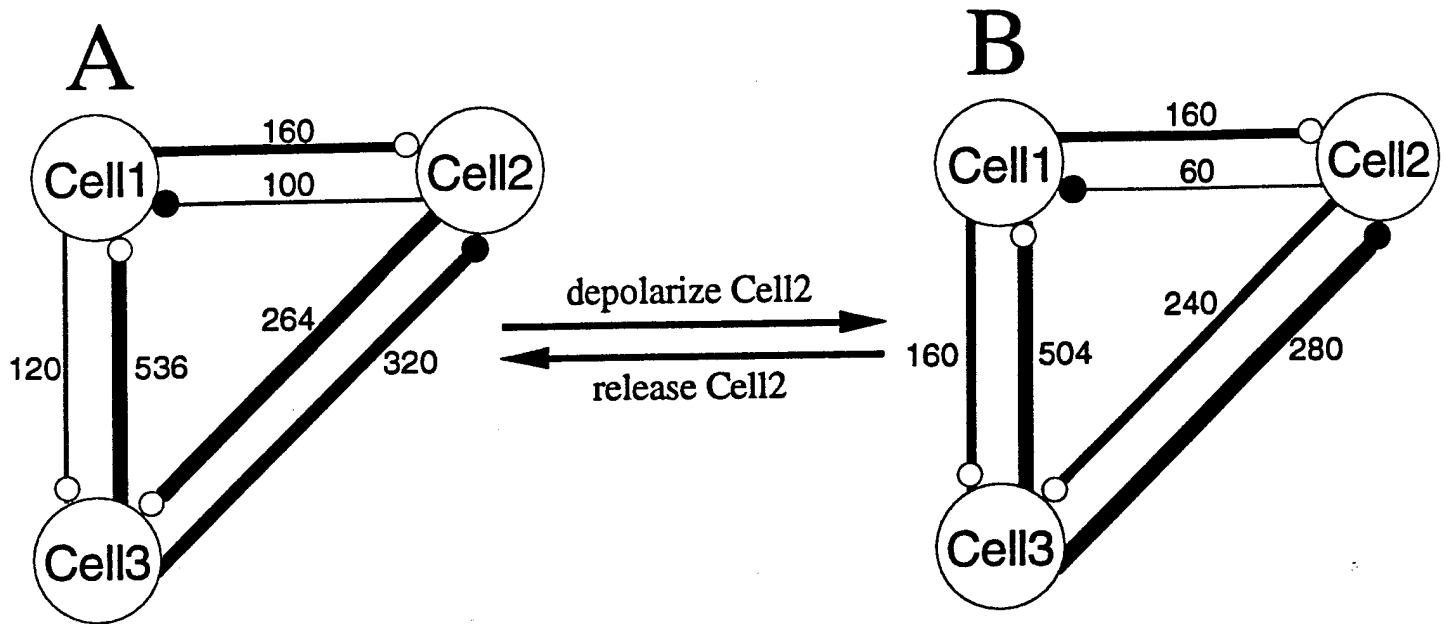
Fig 1

Fig 2
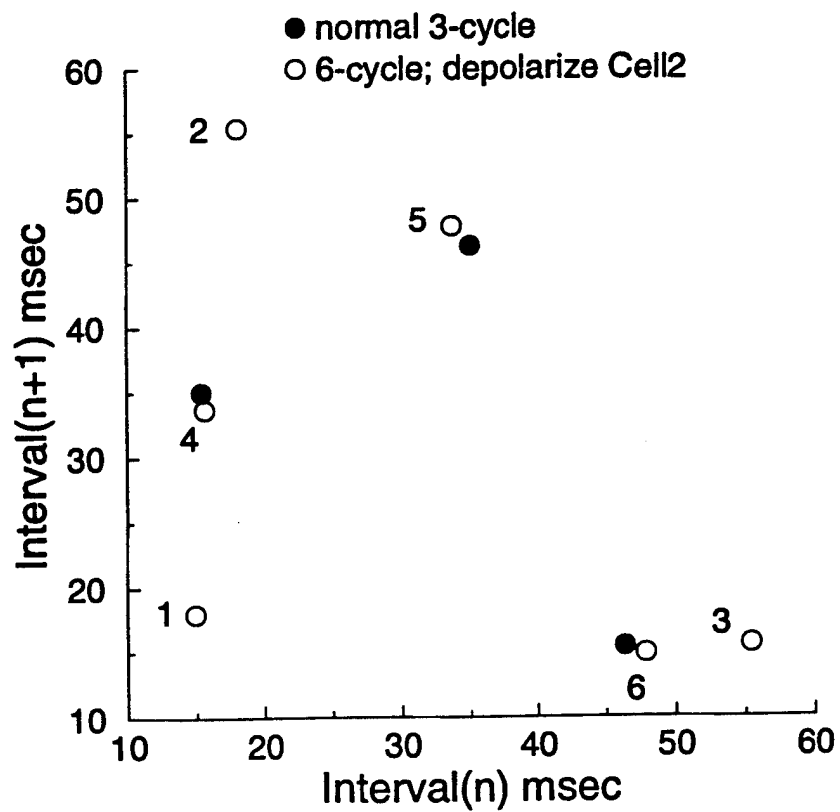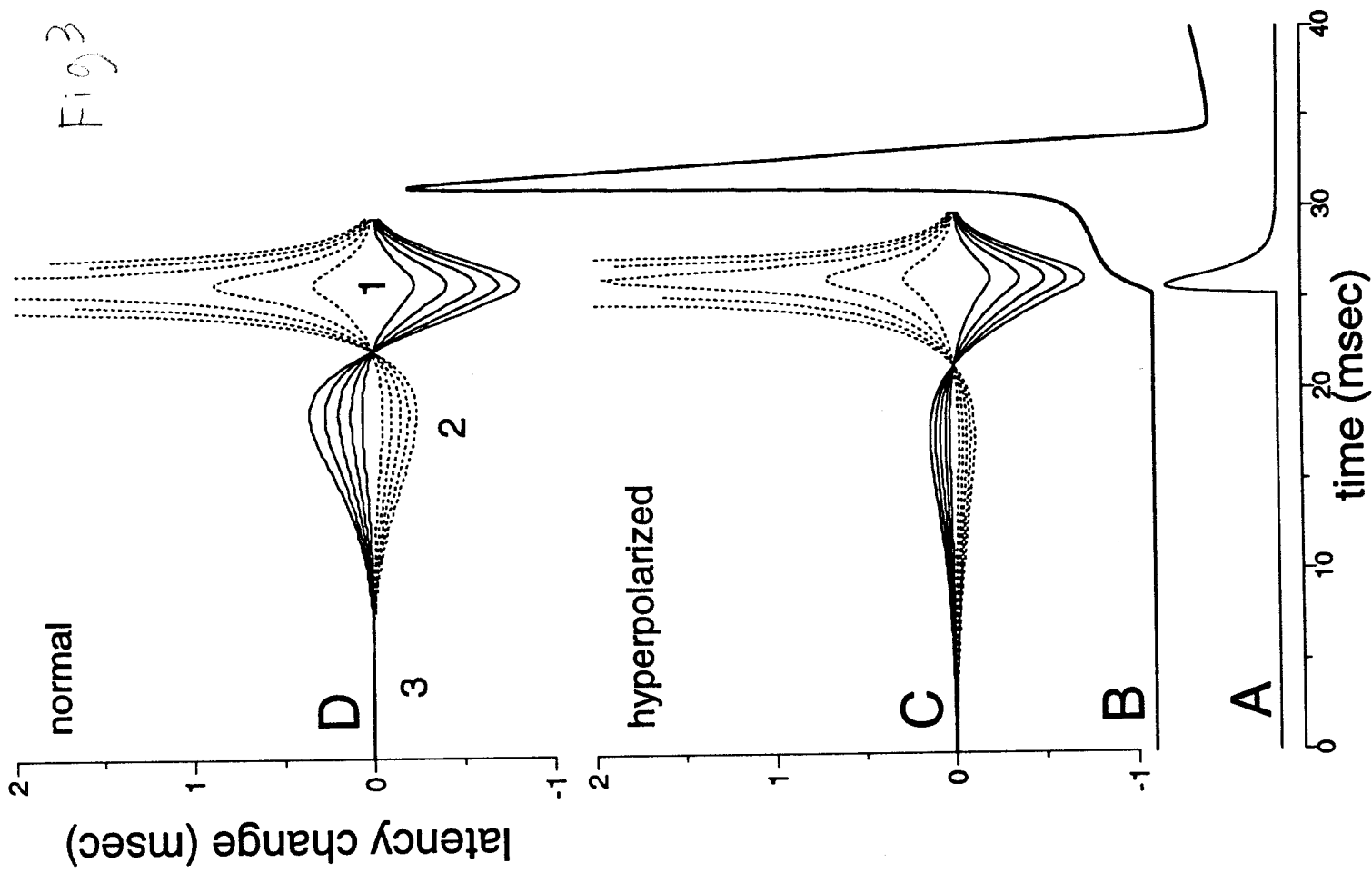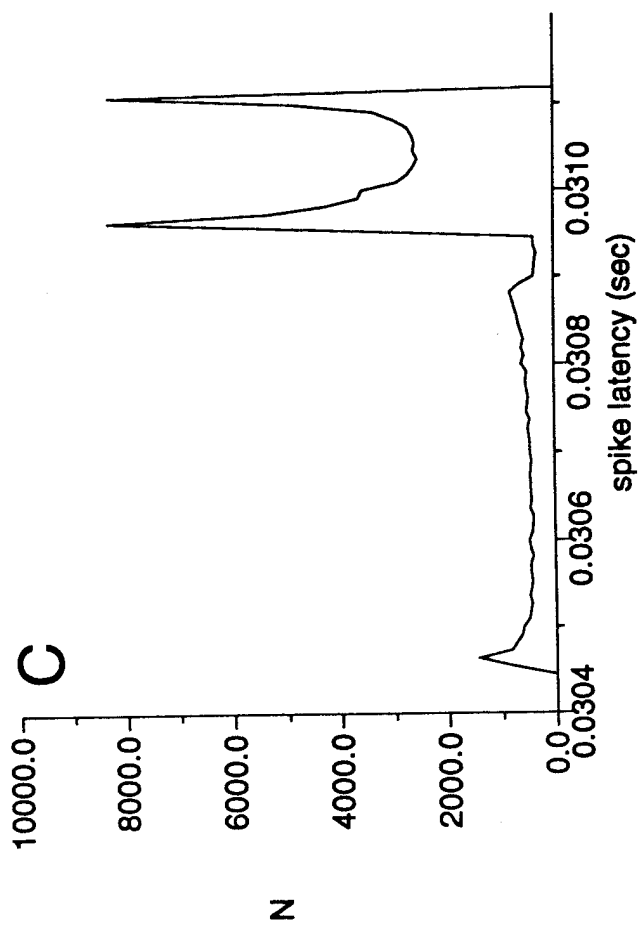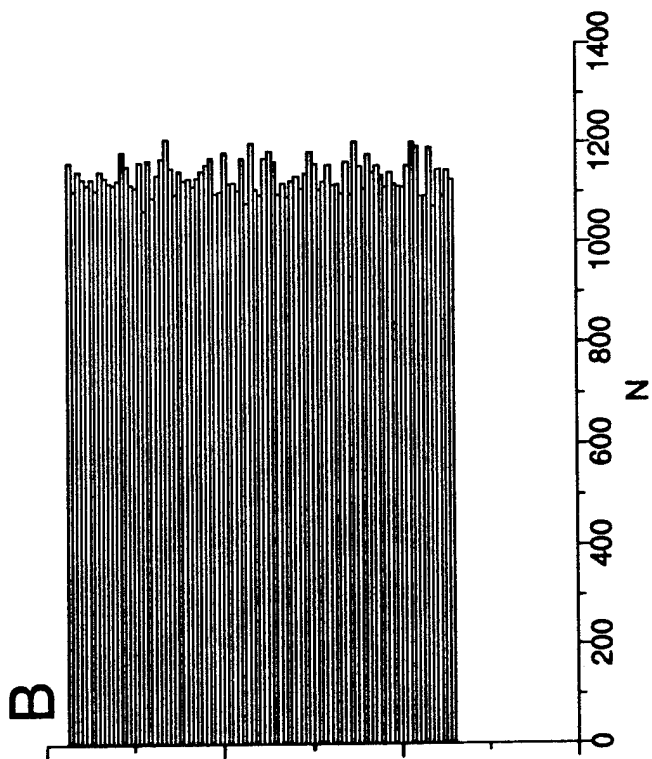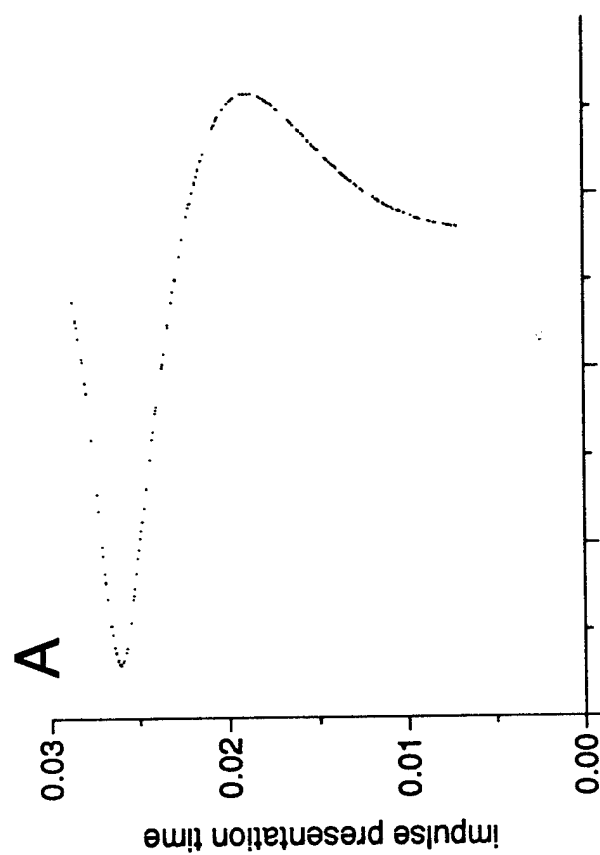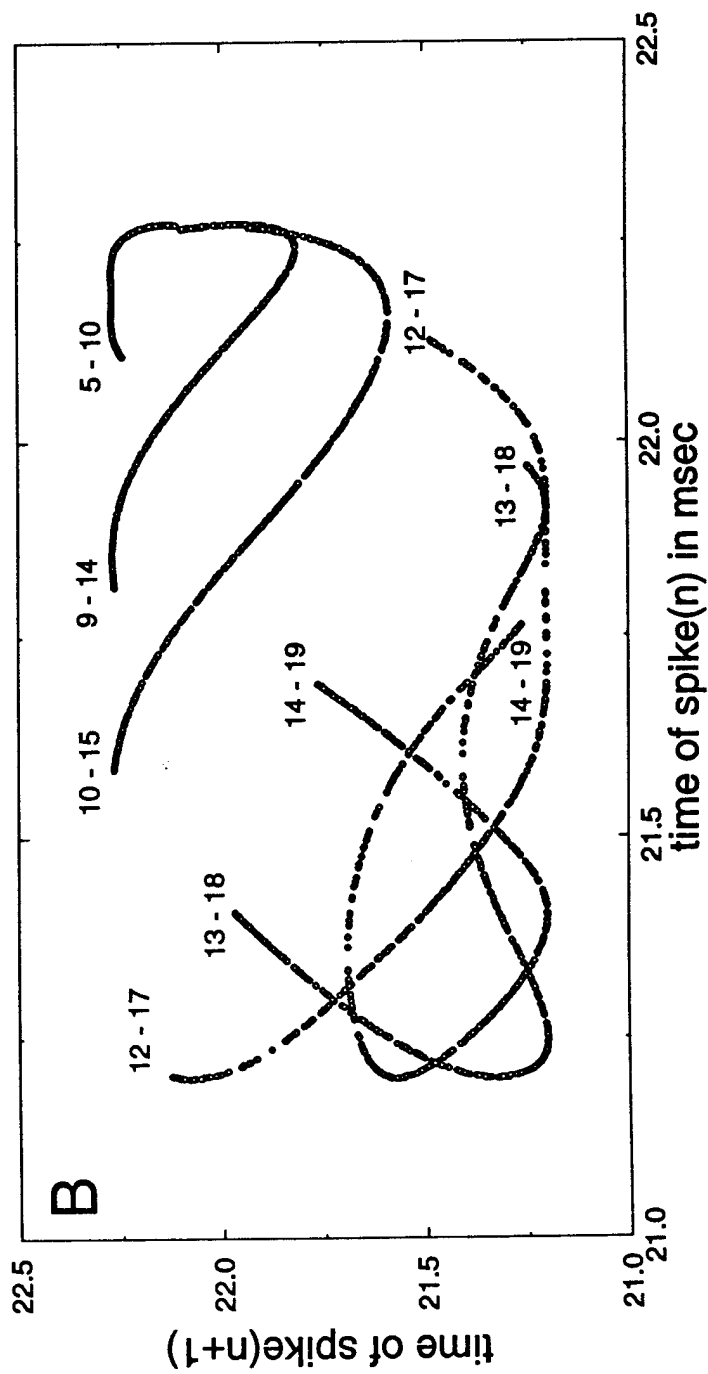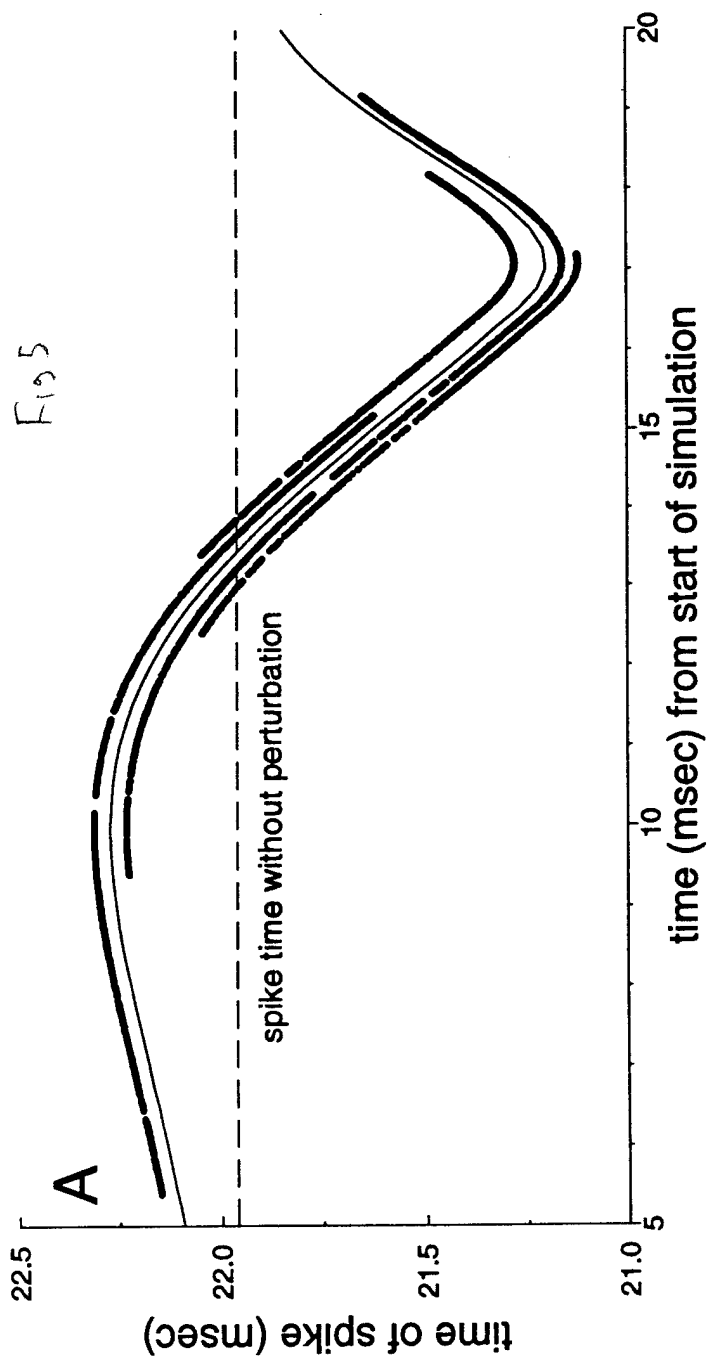
A

B

depolarize Cell2 →
← release Cell2

C

- normal 3-cycle
○ 6-cycle; depolarize Cell2

Fig 3

Fig 4

A

B

C

impulse presentation time

spike latency (sec)

N

N

Fig 5

A

spike time without perturbation

time (msec) from start of simulation

time of spike (msec)

B

5 - 10

9 - 14

10 - 15

12 - 17

13 - 18

14 - 19

14 - 19

12 - 17

13 - 18

time of spike(n) in msec

time of spike(n+1)

-13-

APPENDIX-1

Attractor Gradients: Architects of Developmental Organization

George J. Mpitsos
Mark O. Hatfield Marine Science Center
Oregon State University
Newport, OR 97365
gmpitsos@slugo.hmsc.orst.edu

SHORT ABSTRACT

Biological systems have many interacting components that together produce coherent actions under conditions in which each component has relatively limited information. How coherence emerges in such complex systems is presently unclear. Using findings from biological, computational neural network, and dynamical system studies, I discuss how system-wide attractor gradients may provide a global organizing principle that: adjusts the local interactions optimally with respect to one another; limits network size; sculpts the neuroarchitecture, further redefining the gradients themselves; and imposes new types of stored information. Problems encountered in defining the existence of attractors are discussed.

ABSTRACT

All biological systems are composed of many parts that must work together to produce coherent adaptive responses. The many nonlinear interconnections between neurons in an assembly or between individuals in any population pose analogous questions to analytical studies, e.g: How does one handle the many degrees of freedom to know how the system as a whole functions? How does global function emerge from the action of individuals whose decisions are based on local information? Many simplifications may occur if the system is dissipative; i.e., if it has an attractor such that it tends to return to a characteristic state in response to external perturbation. I discuss possibilities emerging from studies in neural networks and dynamical systems to examine how: (a) Spatio-temporal attractor basins act as a global force on populations of neurons, restricting the correlations between their activities. (b) If the strengths of the connections are activity-dependent, gradients set the connection strengths between all neurons, and the response thresholds of individual neurons, optimally with one another, (c) limit network size, and (d) control the types of information that a system stores. The findings may provide insight into mechanisms that might not have been considered from classical approaches that view brain function as arising from simple reflexes and "switchboard" circuitry. Similar effects may occur in many different systems, from cellular to societal ones, that generate attractors and in which the response thresholds and strengths of interactions between the component parts are adjusted by activity-dependent mechanisms.

Key words: Self-organization, neural networks, multifunctional systems, activity-dependent changes, gradient systems, thresholds, central pattern generators, neural development, learning, population dynamics.

INTRODUCTION

Common conceptual and experimental problems. All biological systems, whether cellular ones, organismal ones, or ones involving populations of organisms, have the common feature of being composed of many parts that must work together to produce coherent responses or behaviors. Because of these attributes, similar conceptual and experimental problems arise in widely disparate systems such that studies in the social sciences are faced with many of the same difficulties as those in the neurosciences. For example, individual persons or neurons communicate with many others within the potentially coactive populations, yet must generate responses based largely on local rules because no single individual has information about the population as a whole or about the context within which the population must act. The present paper deals with the organization of neural tissues, but the findings that are discussed may also extend heuristically to other systems. The problem will be examined of how a globally acting principle may emerge from local interactions in the system and, if the connections are changeable, how it affects the connections themselves.

I shall discuss that attractors may provide one such principle. Attractors are an old idea (Abraham & Shaw, 1983), and have long been thought to be useful in developing a biological and computational theory relating to disparate systems, from chemical ones, to cellular ones, to ones composed of populations of animals and possibly even to evolution (Waddington, 1968-1972). There are many sources dealing with the use of attractors and the qualitative shift in dynamics or bifurcations in forced and unforced systems, e.g., (Andrade, et al., 1993; Chay & Rinzel, 1985; Cohen & Grossberg, 1983; Eigen & Schuster, 1979; Farmer, et al., 1987; Farmer, et al., 1986; Guckenheimer & Holmes, 1983; Haken, 1983; Hirsch & Smale, 1974; Hofbauer & Sigmund, 1988; Holden, 1985; Hopfield, 1982; Küppers, 1983; Le Cun, et al., 1991; Schnabl, et al., 1991; Skarda & Freeman, 1987; Ueda, 1992; Widrow & Stearns, 1985). Additionally, a large literature has emerged, based on the seminal work of (Grassberger & Procaccia, 1983; Packard, et al., 1980; Takens, 1981) aimed at computing attractor dimensions and the minimal number of degrees of freedom or dimensions required to define attractors from experimental observations. A recent review by Abarbanel et al. (1993) is a useful account of some of the methods and directions for future work. A critical account of a number of these methods, methods for controlling the dynamics of a system, methods for determining whether the responses of an experimental system are deterministic, and software for making such assessments, have recently been published in an issue of the journal *Integrative Physiological and Behavioral Science (Vol 29, No. 3, 1994)*.

A defining feature of attractors is dissipation; i.e., that they relax to some characteristic state following perturbation. There are formal connections between the dissipative and attractor generating qualities of a system (Hale & Koçak, 1991, p. 394), but, as discussed a little later, the formalism may not be

applicable to many biological systems. Given these constraints, the aim will be to follow the notion that attractors exist based on the observation of relaxation dynamics, and to see what might be a consequence of this dynamics, rather than, for example, attempting to compute its "fractal" dimension. A number of studies provide examples of such an approach, e.g., (Garfinkel, 1983; Garfinkel, et al., 1992; Schiff, 1994; Skarda & Freeman, 1987; Weiss, et al., 1994).

Pathways for communication. Complex systems must have some method for distributing information among their components. In neural systems, single neurons make synaptic connections with many others; anatomically, this is referred to as divergence. Conversely, many neurons make synaptic connections onto common target neurons; this is referred to as convergence. In the visual cortex of mammals, the number of diverging connections that a single neuron makes is in the order of 5,000 to 10,000, and each neuron receives roughly the same number of converging inputs. The situation one encounters in studies even of "simple" invertebrate animals, such as sea slugs, is illustrated in Fig. 1 which shows that a few cell bodies (shown by the bright circular objects having a greenish color) send tangles of profusely diverging axons and neurites (bright green strands) throughout a region of the ganglion known as the neuropil where most of the synapses between neurons take place. Some of the neuron cell bodies appear greener than others because they contain a four-peptide neurotransmitter FMRF-amide. The axons and neurites divide into thinner and thinner branches as they form, what seems to the human eye, a entangled web in the neuropil. Other neurons send similarly profuse projections to converge in the same areas. How such extensive connections become established and whether there is any interrelationship among the strengths of the connections are questions that remain unanswered.

FIGURE 1 HERE

Dynamic readjustment of network function. An additional difficulty is that the responses of biological systems are often short-lived, variable, possibly nonstationary, and are continuously subjected to many different types of "external" stimuli that perturb them. As a result, the functional role of a neuron in an assembly may be vary from one time to another, and may best be described by the context of the actions expressed by other individuals with which it becomes active (for discussions and a review of some of the literature on the subject, see Mpitsos & Soinila, 1993).

Figure 2 provides an interesting example of a network dynamically adjusting to a perturbation. The illustration shows the time evolution of electrical potentials obtained from neurons; the overall pattern relates to feeding behavior. The trace labeled BCN is from a neuron that takes part (with about 20 other BCNs) in generating the pattern of activity for opening and closing of the jaws.[1] The term "pattern" refers to the sequences of action potentials, sharp voltage spikes recorded from single neurons and from nerve

roots. This cyclical activity is generated within the central nervous system; i.e., it is a central pattern generator (CPG) because the fundamental oscillations do not depend on sensory feedback. When the BCN is forced to stop firing action potentials, by selectively applying hyperpolarizing electrical current to it (arrows in Fig. 2), the pattern in the rest of the traces initially stops and then restarts while the BCN is still suppressed. Although the CPG and related activity initially depended on the actions of the BCN, they soon recover from the loss. How such reconfigurations happen is a an important and interesting problem facing studies of the complex brains in mammals (Lindsey, et al., 1992), as well as of "simple" nervous system in the sea slug.

FIGURE 2 HERE

The themes introduced in Figs. 1 and 2 are observed in all animals. Given the large number of possible pathways that activity can follow from one neuron to another, the activity observed at different times may be variable or unstable (Adey, 1972; Braitenberg, 1989; Freeman, 1994; John, 1972; Lindsey et al., 1992; Mpitsos, 1989; Mpitsos & Cohan, 1986a; Mpitsos & Cohan, 1986b; Mpitsos, et al., 1988b; Wu, et al., 1989). This makes it quite difficult to correlate the activity of a neuron or a circuit of neurons with a particular function or behavior, suggesting that a new way of viewing function, some new language or set of concepts, is needed other than what is provided by the idea of simple reflexes. In mammalian studies, Adey (1972), John (1972), and Freeman (see (Skarda & Freeman, 1987) for a review) were perhaps the first to stress the notion of functional variability in neural tissues. Adey, asks whether the brain is adaptively a "noisy processor." John contrasts the notion of a circuit or "switchboard", akin to the circuits in a computer board, against statistical properties. Freeman (1994) views chaotic variations and instabilities as a search mechanism by which neural tissues find meaningful firing patterns in changing ensembles of neurons. From an anatomical perspective, Braitenberg (1989) speaks of the neuron-to-neuron firing pathways through visual cortex as taking a random walk. Such findings indicate that we must re-examine the notion and the applicability of the reflex, defined nearly 100 years ago (Sherrington, 1906).

Activity-dependent changes in connection strengths. The proposition, discussed later, is that attractors emerging from a population of neurons globally cause the connections within this population to change in such a way that the dynamics is strengthened. To implement this mechanism, the connections between neurons must be able to change based on some locally acting rule governed by the firing patterns of the neurons. It has been shown in biological systems that at least some synapses are established by *activity-dependent* mechanisms, e.g., (Kater & Mills, 1990; Lipton & Kater, 1989; Mattson & Kater, 1989). All such mechanisms bear some similarity to a rule stated by Hebb (1949) which has found considerable utility in biological and artificial neural network studies. It states that if there is appropriate timing in the activity between two connected neurons, the synapses undergo metabolic or structural changes that affect its function.

GRADIENTS AND FACTORS THAT CONTROL THEM

Phase space visualization of attractors. Considering systems that are definable by differential equations, there are three types of attractors: point attractors, limit cycles (or, more generally, periodic and quasiperiodic cycles), and chaotic attractors. A rapid way to examine all of them is to construct *phase portraits*. For example, to examine the dynamics of the movement of a simple, friction-damped pendulum after it has been set into motion, a phase portrait can be constructed by plotting the position of the swing of the pendulum against its velocity. The succession of the position-velocity states from moment to moment constitutes a *trajectory* showing how the system evolves over time, though time is an implicit variable in such plots. The characteristic state of such a pendulum is the resting point at the bottom of its swing. We may think of the momentary stimulus that set the pendulum into motion as a perturbation pulse. The element that dissipates this pulse is friction. Operationally, the dissipative or relaxation process appears as an asymptotic spiral or gradient leading toward the resting point in the phase plot. Phase portraits of limit-cycle attractors contain trajectories that form a single closed loop; other periodic attractors have closed trajectories with two or more loops. Phase plots of chaotic attractors exhibit infinitely many loops of the trajectory, but with the proviso, as required by the Jordan curve theorem and the Poincaré-Bendixson theorem (Hirsch & Smale, 1974; Hofbauer & Sigmund, 1988), that the trajectory never closes and that the interrelated positions of the loops mix in a certain way, e.g., (Andrade et al., 1993; Thompson & Stewart, 1986, p. 165).

In the smooth dynamics of systems defined by differential equation, one speaks of flows in state space. Use of an artificial network model will serve as a example to illustrate phase space and fixed points. The exact specifics of this system have been described in detail elsewhere (Andrade et al., 1993). Briefly, it is composed of a set of four coupled differential equations that describe molecular catalytic action, where each variable represents the concentration of one of the catalytic species; a single species may catalyze the replication of more molecules of its own species, or of other species. The mathematical formulation resembles equations describing the dynamics of disparate systems, from population dynamics to neural network function (Cohen & Grossberg, 1983). By changing the parametric setting of one of its catalytic constants (equivalent to changing the strength of a neuronal synapse, as will be done later here), the system generates many different patterns of activity representing all three types of attractors mentioned above. Such constants are called bifurcation parameters. Changes in these parameters usually produces little change in system dynamics, but at certain critical points small parameter changes cause the system to respond qualitatively differently.

The operations used to determine the presence of attractors graphically are illustrated in Fig. 3 for the catalytic network in periodic and chaotic

regimes (only species X1 and X2 are shown). The time-evolution of the concentrations in both regimes are shown before and after a brief perturbation was applied by increasing the concentration of molecular species X1 for a single integration step. Since X1 is coupled to the other catalytic species, the pulse of externally applied extra copies of X1 affects the concentrations of all species. Following the perturbation pulse, the periodic oscillations (but not the phase) in the concentration original pattern. The method has been widely used in studies from CPGs in neural systems to circadian rhythms in humans. A similar relaxation process occurs in the chaotic regime, but owing to the variations that occur naturally in chaos, the recovery is difficult too assess using time-series data.

FIGURE 3 HERE

A view of the pre- and post-perturbation conditions is more clearly shown graphically by the phase portraits at the bottom of Fig. 3 than by the time-series data alone. The unperturbed state of the periodic activity, a limit cycle, is shown by the thick trajectory. The thin-line trajectories show the recovery that occurs after the perturbation stimulus is applied. These trajectories eventually lead back to the original limit cycle. In the chaotic regime, the relaxation process also occurs, but, since chaotic processes are sensitive to initial conditions, the trajectory never returns exactly to the original thick line; i.e., the attractor is represented by the overall structure of the phase portrait rather than a particular set of trajectories. To obtain a view of the gradient fields or *basins of attraction*, it is necessary to repeat the same experiment many times using different concentrations in the perturbation pulse; and pulses may be applied to all of the molecular species, as well.

In the pendulum with friction, dissipation occurs through heat loss. In the catalytic network, dissipation occurs through two interrelated components. In one, the replication process is error-prone, and error copies of all of the different molecular species are ejected from the network into an error-species. The second component arises from competition between the various molecular species for a substrate substance from which they make copies of themselves. However, the total number of molecules of all species in the mixture that can be produced by replication from substrate material is capped at some upper limit. The pulse of externally applied molecules of X1 causes a new set of conditions for competition for substrate, but as long as the excess copies are present, the total number of molecules exceeds the capped limit. The relative proportions of the various species readjusts nonlinearly since the extra copies of X1 cause the synthesis of other species, so adding X1 causes a redistribution in the population of all species. At the same time, error copies are ejected from the mixture, slowly redistributing the relative concentrations progressively back to the distributions relating to each dynamical regimes.

Fixed points control system responses and define gradient space. Fixed points represent conditions when the state of a system does not changing over time (Andrade et al., 1993; Seydel, 1988); synonyms are steady

states, equilibria, stationary points. The quality of the fixed points determines whether they attract or repel trajectories in state space. Figure 4 illustrates the relationship between the trajectory and fixed points in unperturbed and perturbed conditions of a periodic regime. The circles show four of the points, all saddles. Point-1 is the only fixed point at which all four species {X1,X2,X3,X4} coexist. For some parameter settings, the point is stable, attracting flows to it in all directions and creating conditions in which the concentrations of all species remain constant. For other settings, the flows are stable toward the point in two directions and unstable in the other two. Points 2 and 3 show the unstable saddles for species-states {X1,X2,X4} and {X1,X2}, respectively. Point-4 is an unstable spiral saddle for the steady state {X1,X2,X3}, and as in points 2 and 3, there is one unstable direction of flow. Stability or instability along each axis is determined by the eigenvalues that characterize the quality of the fixed points. Negative eigenvalues indicate stable directions of flow; positive ones indicate unstable ones.

FIGURE 4 HERE

The quality of all of the fixed points together defines the characteristic features of the potential surface of attainable concentrations. This surface consists of a set of local maxima and minima, hills, valleys, saddles, etc., comprising a landscape whose local features must be navigated by the dynamics of the four coupled molecular species. The effects of the fixed points extend as gradients, so the course of nearby trajectories is determined by the "push" and "pull" of all the fixed points that exist in a given dynamical regime. Consequently, in order to know how a network will respond under the variable conditions that an animal may experience in the natural environment, it is necessary to understand what the gradient fields are and how perturbations move the trajectory around them.

Attractors have zero volume. The attracting limit set has vanishingly small volume. This is indicated by the spectrum of Lyapunov exponents. These provide a measure of the rate at which nearby trajectories converge or diverge with respect to one another. There is an exponent for each dimension of the system. For the system to remain bounded, the sum of all of the Lyapunov exponents must be negative, though in chaos at least one exponent must be positive to produce stretching along a given dimension, e.g., see (Seydel, 1988; Wolf, et al., 1985). The post-transient behavior of the attractor is to approach zero-phase space volume. The rate of contraction in bits per second is given by $2^{(\lambda_1 + \lambda_2 + \lambda_3 + \lambda_4)t}$. If all exponents were negative (loss of information in each direction of flow), the activity would collapse into a single point in all directions. In the example shown in Fig. 4C, the exponents are {+2.94, 0, -49.06,-239.59} (Andrade et al., 1993). The positive value of the principal exponent indicates that there is stretching or gain of information in that direction of phase space. The next exponent is vanishingly small, leading neither to expansion or contraction. The third exponent is strongly negative and is required to constrain the activity in phase space. The fourth exponent is

even more negative than the third such that information in this dimension is lost extremely rapidly. The exponents of periodic activity are all negative, except for the first which is zero. So, for all three types of attractors, there is overall contraction in phase space.

The spectrum of Lyapunov exponents describes the local flows in the system and is an invariant measure of the attractor, regardless of the wild swings that may occur in the overall structure of the unperturbed attractor in phase space. As such, they provide an instantaneous indicator of an attractor, and they can an be used to estimate other invariants, such as the attractor dimension (Kaplan & Yorke, 1979; and see examples in Andrade et al., 1993; Wolf et al., 1985). Being local-flow measures that apply to the attractor as a whole, it is a rather interesting speculation that they may provide an immediate way for a network to detect the pattern of activity it receives as opposed to detecting it based on the large-scale aspects of its evolution which would require much longer sampling time.

ATTRACTORS IN BIOLOGICAL SYSTEMS: SOME CAVEATS

Before going on to a discussion of how attractors might affect networks, it is necessary first to point out problems or constraints that must be consider when positing the existence of attractors in biological adaptation.

Effects produced by action-potential activated synapses. Much of what is known formally of dynamical systems, and partly described above, has come from studies of differential and difference equations, or of systems that can be put in these forms. In neural systems, the Hodgkin-Huxley (1952) model of the squid axon has had its success, and fostered much research on the dynamics of nerve membrane, e.g., (Canavier, et al., 1990; Chay & Rinzel, 1985; Evans, et al., 1982; Fitzhugh, 1961; Fitzhugh, 1969; Jalife, 1990; Rinzel & Keller, 1973; Rinzel & Miller, 1980) partly because it can be modeled as a system of differential equations. The same is true in neural network studies when the communication between neurons is controlled by smoothly graded synaptic potentials (Wang & Rinzel, 1992; Rowat & Selverston, 1993), and in many studies dealing with psychophysical problems (Cohen & Grossberg, 1983; Grossberg, 1980; Grossberg, 1988; Zanone & Kelso, 1992).

The situation becomes much more complex when neurons communicate with one another using the pulses of action-potential activated synapses. A major reason for the increase in complexity is that the differently timed and differently shaped synaptic inputs act as perturbation pulses to subsequent synaptic inputs. Even for a simple model, such as the catalytic network discussed above, it would be impossible to determine how the system would behave in response to a series of differently shaped perturbation pulses that arrive at irregular times.

Instability and ergodicity. The goal-directed, self-organizing behavior of biological systems can be unstable (Freeman, 1994). Examples of spontaneous shifts of motor patterns in our experimental system are given in Figs. 18 and 19 in (Mpitsos et al., 1988b). Extended discussions of the problems

may be found in (Mpitsos, 1989; Mpitsos & Soinila, 1993). Perhaps the most difficult problem to address is the finding that behaviors and motor patterns may blend into one another (Mpitsos & Cohan, 1986a; Mpitsos & Cohan, 1986b); i.e., if attractors underlie behaviors, does blending imply that attractors blend into one another to create intermediates? Even if the number of systems that exhibit such variabilities is small, Freeman's comments are a fair warning that we must consider instabilities in order to gain a fuller (alternative?) understanding of self-organizing behavior, and, especially, how classical dynamical constructs such as attractors take part in the process, or whether they apply.

Ideal multi-component systems in which transients and other instabilities have died out, and in which all available states are equally probable, may be thought of as being in statistical or thermodynamic equilibrium. This condition, which stems from ergodic theory (Eckmann & Ruelle, 1985; Friedman, 1970; Smale, 1980), may provide a principle that can be used to understand how complex biological systems organize globally. It is necessary to consider ergodicity because the aim here will be to say that the emergence of the "cooperative" assembly of neurons is a post-perturbation residue that emerges from a larger population through a common driving force. This force is the gradient action of the attractor.

Ergodic conditions are difficult to prove in model systems, let alone in biological ones. A simple model system can be run long enough that it closely approximates statistical equilibrium, but biological systems, almost by definition, are far from equilibrium. During embryonic development, and learning, and in the normal moment to moment states that do not involve development or learning, biological systems are continuously bombarded by many extraneous stimuli; biological systems are always changing and are subjected to many perturbations such that asymptotically stable conditions seldom arise. It is necessary, therefore, to soften the statement of ergodicity to say that gradient-seeking activity in biological systems *tends* toward ergodic conditions, though it may be far off. Similarly, it is necessary to speak not of an attractor, which is an ideal equilibrium condition reached asymptotically, but rather of gradient behavior as the state of a system tends or is drawn toward the attractor.

Does simple function emerge from complex structure? Although there are only about 20 BCNs on each side of the bilaterally symmetric nervous system of *Pleurobranchaea*, they are embedded in larger networks. In the motor ganglion in which the BCNs are located, there are roughly 400 neurons, some of which are shown in Fig. 1. The BCNs connect to other neurons in this ganglion and in other ganglia, and receive feedback from them directly or indirectly through other neurons. Overall, several thousand neurons, located in different parts of the nervous system, may take part in generating the pattern of neural activity underlying a bout of feeding behavior. However, many oscillatory patterns (though not all) that are generated by such networks recover rapidly from perturbations. Although phase information may be lost,

biological systems are observed to be homeostatic, and even if many different states are possible, small perturbations of a given state usually leads to its recovery. Because of such a relaxation process there is a tendency for the activity representing the attractor to contract spatially. This suggests, as in the case of the BCNs in Fig. 2, that fewer than the several thousand neurons that are active during the feeding motor pattern may be required to generate the dynamics underling the behavior. This relates to the above idea that the sum of the Lyapunov exponents must be negative for the system to remain bounded; overall, there must be contraction in phase space in the responses of individual neurons, and in the interrelated firing between neurons. The notion of spatial contraction is used in the sense of exclusion from the final cooperative ensemble. It does not imply that the final generative set necessarily consists of adjacently located cell bodies. The excluded neurons may become quiescent or they may continue to fire independently of the attractor, or they may be driven by the attractor yet may not be part of the neural machinery that generates the attractor.

Having said all that, it is necessary to point out that fundamental attractor features, such as fixed points, are not definable in most biological networks that rely on action potentials for communication between neurons, even in simple model networks such as the ones discussed below. Neither do we understand the specifics of how different spatio-temporal regimes emerge or how to define them from the perspective of how individual neurons take part in the process, though considerable work has been done along that line, e.g. (Freeman, 1994; Skarda & Freeman, 1987). Neither is it fully understood as to how to assess the state of a system or attractor quantitatively. The publication by Grassberger and Procaccia (1983) of a method for estimating attractor and embedding dimensions provided one easily applicable avenue for making assessments at least for the number of variables or dimensions that may sustain an attractor. Over the years, a number of important refinements have been proposed to improve the methods for determining attractor dimensions, whether chaos is present, or whether there are nonlinearities in the data, e.g., (Grassberger, 1990; Judd, 1992; Kaplan, 1993; Kaplan & Glass, 1992; Mayer-Kress, 1986; Schiff, et al., 1994; Skinner, et al., 1994; Theiler, 1986; Theiler, 1987; Theiler, 1993; Theiler, et al., 1992), but as Theiler (1994) has pointed out, much "black art" is involved. Moreover, as Theiler and Rapp (1995), Mayer-Kress, Barczys and Freeman (1991), Glass and Kaplan (1993) point out, evidence for low dimensionality and chaos in measurements of biological activity is inconclusive. Although electrical stimulation methods, potentially applicable to the control of epileptic foci, have been developed that use the characteristics of unstable fixed points to obtain evidence both of periodic activity and chaos in hippocampal slices (Schiff, 1994), the majority of the quantitative assessments of activity in the same tissue point to stochastic processes rather than to low-dimensional chaos (Schiff et al., 1994). In our own studies, the evidence for chaos was state explicitly as being only circumstantial (Mpitsos, et al., 1988a; Mpitsos et al., 1988b). Although we have

not yet exhausted the available methods on estimates of low embedding space, e.g., such as the neural network methods described in (Abarbanel et al., 1993), use of surrogates (Theiler, 1994) indicates that though there is structure in the firing patterns of individual BCNs and motor neurons that they drive, the evidence for low-dimensional embedding space is also wanting. This is remarkable because the neurons we have examined and the neural firing patterns that they generate are related to identifiable behaviors, whereas the firing, for example, of compound action potentials in hippocampal slices (Schiff et al., 1994) need not and probably do not represent any particular behavior. Moreover, in our experience, motor patterns appear less variable when obtained from isolated nervous systems than in whole animals, indicating that the numerical evidence for low dimensional (periodic or chaotic) attractors in whole animals should be even less conclusive.

The problem in our own studies, and in other studies mentioned above, may be only one of quantitative verification, for which the appropriate methods have not been developed yet, or that we may not have conducted experiments that yielded the appropriate data. Alternatively, perhaps the search for crisply definable determinism may be equivalent to the search to identify a network anatomically as the neural correlate of behavior (Mpitsos & Soinila, 1993). But, following Adey (1972) and John (1972), it may be worthwhile to consider further the utility of stochastic processes. One of the reasons may be that while synaptic transmission involving action-potential evoked synapses, as opposed to smooth graded transmission, may be deterministic, it also appears that degeneracy of information flow across the synapse may also occur (Edstrom & Mpitsos, 1995b).

The dynamics of spatio-temporal recovery may also not be simple. We can not just say that the recovery process reestablishes the set of neurons generating the attractor before the system was perturbed and leave it at that. The reason for this is that the generation of an attractor may not require the activity in any particular neuron. Even fewer than the 20 BCNs may be necessary for generating the CPG or the behaviors that the CPG drives. The effect shown in Fig. 2 is an extreme example of this. Other examples, not presented here, show that the interrelated firing of neurons in a cooperative set may vary over time, and the removal of some BCNs may have essentially no effect on the oscillatory patterns (Mpitsos & Cohan, 1986b). In a sense, there is a kind of redundancy in a population of neurons that generate attractors. Up to a point one can remove neurons, and the system can rearrange itself to give the same attractor as before, though eventually a minimal population may be reached from which we can not remove neurons and retain the attractor (Selverston, 1980; Selverston, 1993; Rowat & Selverston, 1993). Under the most general conditions, the terminal group may be different, depending on which neurons were removed at the beginning. Therefore, in the recovery of attractor systems, the crucial element is not necessarily what neurons remain, but whether certain gradient can be sustained.

ATTRACTORS IN SIMULATION OF BIOLOGICAL NETWORKS

The network shown in Fig. 5C will be examined here and used subsequently to examine how activity affects network structure. This particular architecture was chosen as part of a larger experiment aimed at studying both periodic and complex firing patterns, though only simple patterns will be examined here. The network consists of three cells; Cell4 is external to the network because it receives no feedback from the other cells. A number of network constants that may be used as control parameters with which to produce "bifurcations", qualitative changes in the interrelated patterns of action potentials produced by the three cells: (a) Changing the firing level of Cell4 by injecting it with different sustained levels of depolarizing electrical current. (b) Keeping Cell4 quiescent, but injecting depolarizing current into one of the other cells in the network to adjust its firing level. (c) Or by selectively changing the synaptic strength of one of the synapses.

FIGURE 5 HERE

Figure 5A shows a 3-cycle firing pattern in Cell2. Starting from the simulation time at 680 msec, seven intervals between the action potentials are shown, where the 3-cycle repetition sequence consists of intervals having 15.4 msec, 35.0 msec, and 46.3 msec durations. For the purposes of the illustration only two 3-cycle periods are shown, but many more 3-cycle sequences preceded them. This particular firing pattern was obtained by driving the network using steady depolarization of Cell1 and selectively adjusting the strength of the inhibitory synapse that Cell3 makes on Cell2.

The values for the synaptic strengths giving this 3-cycle are illustrated in Fig. 5C, but certain other combinations of synaptic weights give similar 3-cycle activity, just as Gardner (1990) has demonstrated that different synaptic strengths between four identified neurons in the sea slug *Aplysia* generate similar network function. The dashed line below the action potential trace shows the time during which the network was perturbed by injecting Cell2 with a 125 msec electrical current pulse that pushed the membrane potential below the threshold level for the genesis of action potentials, except for one action potential (labeled by a "1") arising from strong activity in one of the other cells in the network. After the cessation of the applied current, the cell rebounded with a rapid burst of three action potentials (labeled "2", "3", "4"), and then recovered to its original firing pattern.

The pattern of intervals shown in Fig. 5A may be replotted in a return map in which one interval in the sequence is plotted on the horizontal axis and the succeeding interval is plotted on the vertical axis. One hundred intervals were used to construct the 3-cycle of the unperturbed activity; all fell sequentially on the three filled circles in Fig. 5B. The return-map positions of the intervals during and after the application of the 125 msec perturbation pulse are shown by the numbered and open triangles. The identifying numbers in the return map are the same as those in the trace shown in Fig. 5A,

where the number over a given action potential indicates the interval between that action potential and the preceding one.

What causes dissipation in biological networks? The friction-damped pendulum and the catalytic network described above have known dissipative mechanisms with which to conceptualize the recovery process, but there is no obvious anchor in networks such as the one shown in Fig. 5C. It is not simply that there are inhibitory synapses in the network. Although, the excitatory and inhibitory synapses were chosen to produce expansion and contraction qualities in the firing patterns among the three neurons, modeled after Rössler (1976), dissipative firing can be obtained by using, for example, only excitatory synaptic connections. An understanding of the cellular processes underlying dissipative action in biological systems may shed light in how individual neurons take part in group action (Edstrom & Mpitsos, 1995a), but the subject has been largely bypassed in neurobiological applications of dynamical theory.

Effect of gradient-seeking activity on biological networks. Gradient-seeking behavior in neural networks has been a subject of interest for a long time, and a large literature has emerged, e.g., (Cohen & Grossberg, 1983; Hopfield, 1982; Le Cun et al., 1991; Perlmutter, 1992; Plaut, et al., 1986; Rumelhart, et al., 1986; Werbos, 1974; Widrow & Stearns, 1985). The possibilities that gradients may change biological networks is considered in the following scenario:

(1) Assume that the network is initially randomly connected, and that the neurons are firing action potentials.

(2) Somewhere in the network, two or three neurons may have firing patterns that are sufficiently correlated with one another that their synapses undergo activity-dependent changes. If dissipative action begins to emerge, the synaptic weights in the developing network must have some interrelated range of values, else the attractor would not exist.

(3) The emerging attractor constrains the flow of activity, causing further activity-dependent changes and refinement of the attractor spatiotemporally.

(4) Neurons that converge onto the same follower neurons may compete (Merzenich, et al., 1983a; Merzenich, et al., 1983b; Merzenich, et al., 1984; Mpitsos et al., 1978) for occupancy of the synaptic space available on the follower neuron such that connections may be made or broken, structurally molding the neuroarchitecture; i.e., attractors are the ultimate architects of neural tissues (or of any biological system governed by gradient-seeking behavior).

A concrete example of this would be useful to visualize the process. Our work on this is very preliminary, but it is worth discussing to illustrate the above conjecture. The schematic in Fig. 6 shows how the network examined previously may be altered following a perturbation stimulus. The original network is shown in Fig. 6A. It is the same as the one shown in Fig. 5, as are the activation conditions, but the strengths of the synapses are now

made available for activity-dependent changes. If Cell2 is depolarized for an arbitrary length of time, it begins to generate action potentials initially at a higher frequency than before, but soon the balance of excitatory and inhibitory feedback readjusts its rate of firing. The activity-dependent changes in a synapse depend on the temporal correlations of activity in the presynaptic and postsynaptic cells which will vary over time. The dynamics giving rise to these correlations is extremely complicated and time dependent, but Fig. 6B has caught the changed synapses at a stage (shown by the numbers next to the axons) that cause Cell2 to generate a 6-cycle firing pattern. The open circles in the return map of Fig. 6C show the values of the six intervals between the action potentials. The filled circles show the original 3-cycle.

FIGURE 6 HERE

When Cell2 is released from the depolarizing current (Cell1 is under continuous depolarization to keep the network active), its firing pattern may remain in the 6-cycle state, but if the attractor is not sufficiently well formed, genesis of action potentials in the three neurons may drift to some other set of patterns, or it may eventually settle back to the original 3-cycle state (and perhaps with a different set of synaptic strengths between the neurons).

The aim here is not to say that the 6-cycle *per se* is formed, nor that the original 3-cycle is regenerated in the recovery, but that some attractor is generated, and that its gradients are what adjusts or globally "directs" the local activity-dependent synaptic changes. This is different than would be imagined were we to view networks as switchboards or reflexes by which change is based only on local activity-dependent effects. From such effects it might be postulated, for example, that associative learning in whole animals is based on changes in individual synapses; reviewed in (Mpitsos & Lukowiak, 1985). By the conjectured gradient method, however, it is obvious that changing one synapse causes changes in all of them. Local rules are a work, but they are guided by a more global principle.

GRADIENTS OF LEARNING IN ARTIFICIAL NEURAL NETWORKS

The above ideas are derived from the extensive studies on artificial networks, though their effect is only beginning to become apparent in biological studies. I shall discuss the results of simple artificial neural network studies (Burton & Mpitsos, 1992; Mpitsos & Burton, 1992), based on the backpropagation algorithm (Rumelhart et al., 1986), to examine possibilities that might not have been conceived from studies on biological networks. The backpropagation algorithm relies on a negative-gradient mechanism to minimize error as synapses and thresholds are changed during training. Gradner (1993) has suggested cellular mechanisms by which backpropagation might take place in biological systems, and backpropagation methods have been used to address specific cases in biology, such as the mechanism of local bending in the leech (Lockery & Sejnowski, 1992). However, rather than addressing a particular application or biological system, I shall examine some

of the more rudimentary effects that might arise generally in networks from gradient-seeking mechanisms.

The network examined here is shown in Fig. 7(Top). The input consists of a single neuron whose synapses are distributed to a set of "interneurons", or hidden neurons, labeled h. The number of hidden units varies, depending on the experiments. The hidden units converge onto a single output neuron. The input signal consisted of a sequence of discrete values generated by the chaotic logistic function $f(x) = 3.95(1-x)x$, where x is in the unit interval. One of the aims of the original studies was to determine whether a single-input network with no bypass connections could predict a chaotic signal, but in order to keep the illustrations as simple as possible, the discussion here is of training using the identify function as the teacher whereby the output is required only to reproduce the input. Despite its simplicity, the identity function provides insight into the effects of gradients and permits the use of simple graphics to demonstrate effects. An on-line training method was used in which synapses, and threshold levels, are adjusted after each training trial. In this way the network is given information only of a single error-point relating to the gradient fields of the teacher function. Batch training updates the synapses after a number of trials, providing more information about the teacher function than on-line training.

FIGURE 7 HERE

Gradient descent during learning adjusts synaptic strengths optimally with respect to one another. The network was trained until the difference between its output and the teacher requirement converged to some minimum error. The synapses and thresholds were frozen at the trained values, and training effects were excluded during subsequent manipulations of the network. One synapse at a time was then set at a series of arbitrarily selected values while holding all other synapse at their trained value. For each value, the network was presented a number of input values of the logistic to obtain the average error as a function of the changes in each synapse (Fig. 7 Bottom). As should be expected of backpropagation training, the error-gradients generated during training set the synapses optimally with respect to one another, as was proposed for biological simulations in Fig. 6.

Two-dimensional error gradients or surfaces may be constructed using by measuring the error as a function of changes in two synaptic weights. The asterisk in Fig. 8 shows the location of the two weights that gave the minimum error. By adding a third synapse, the gradients become more complex, as shown in Fig. 9, where color represents error. Minimum error is somewhere inside the box of Fig. 9A. A series of slices through the box (Fig. 9B) reveals the location of the minimum error which is indicated by deep blue in the top horizontal slice. This slice is identical to the surface shown in Fig. 8; the dark blue spot in the middle corresponds to the asterisk in Fig. 8. Different initialization parameters yield a different set of final optimal weights, as occurred in the simulations in Figs. 5 and 6, and as reported in comparisons of

the connections between a set of four identifiable neurons in different specimens of the sea slug *Aplysia* (Gardner, 1990).

FIGURES 7, 8 & 9 HERE

Gradients limit the number of neurons in a cooperative assembly. The common intuitive impression of the effect of the size of the network is "the bigger, the better." This proved to be true to some extent (Mpitsos & Burton, 1992), but after some optimal small number of hidden units was reached, increasing the number further rapidly led to learning failure. The more complicated the learning task, the sooner the detrimental effects occur, even for learning the identity function.

There are at least three interrelated factors underlying size limitation, all related to gradients. The top horizontal slice in Fig. 9B contains obvious gradients leading to an optimal solution of for weights {W1,W2,W3}; other slices contain large areas of flat gradients. Comparing Figs. 7-9 shows that changing from 1 to 3 degrees of freedom increases the possibility of encountering large flat gradient fields. As the number of trainable synapses or units increases, the surrounding high-error region grows exponentially by comparison to the central low error (Fig. 10). This makes the distances that the network must traverse through weight-error space from high too low error during training extremely long and the gradients flat in all directions.

FIGURE 10 HERE

Contributing to size limitation is the on-line training method since in each training trial the network is exposed to a single error-point rather than to the structure of the entire error surface. The error fields in Fig. 7-9 were constructed artificially after the network was trained, but the training method contained no information about the structure of the error fields, making learning difficult.

The third factor limiting network size is introduced by a type of "stiffness" in gradient decent. This arises from cross correlations in the input matrix to neurons that receive multiple synapses (for a detailed discussion see Le Cun et al., 1991). If no cross correlations exist, the rate of gradient decent is the same in all directions, generating symmetric error fields in all directions. Ideally, minimum error can be reached in a single time step. If correlations exist, the rate of descent is not symmetric causing distortion and stretching of error fields. Analogous stiffness occurs in numerical integration of differential equations having disparate time scales. High-dimensionality and complex teachers (gradients) exacerbate this problem, slowing or preventing learning.

Biological systems are inherently high-dimensional, far from ideal, and probably possess conditions for analogs of stiffness to exist. The neural network findings suggest that the rate at which coherent activity emerges in large biological networks will be slower than in smaller networks. In embryonic development, for example, certain rules (perhaps genetic ones) may limit the number of neurons in a cooperative assembly, but these rules may be assisted by the limitations imposed by gradient descent into attractors. Smaller populations of neurons may reach "consensus" to generate an attractor

faster than much larger ones, and may generate stronger attractors since smaller networks may have less chance of falling into non-optimal connection configurations that generate weak attractors. It is perhaps not just a humorous exaggeration to extend the notion of stiffness to consensus-building or lack thereof in university faculty meetings and in the United States Congress.

Adjustable thresholds are essential for learning to occur. The presence of adjustable response thresholds in neurons, in addition to the presence of adjustable synaptic strengths between neurons, is necessary for learning to occur properly (Mpitsos & Burton, 1992). The above mentioned deficits relating to stiffness can be largely overcome for simple learning tasks in our network by slowing the rate of learning in the output unit, but even this does not make up for the reported deficits that emerge when networks do not contain trainable thresholds. Recent studies (Leshno, et al., 1993) provide a general proof for the necessity of thresholds in certain artificial networks, and findings in networks of biological neurons in culture (Turrigiano, et al., 1994) indicate that adjustments in firing thresholds may stabilize firing patterns.

The facilitating effect of thresholds arises from that fact that they act as a bias (Rumelhart et al., 1986). This bias shifts the mid-region of the sigmoidal output functions selectively to different regions on the activation axis (Fig. 11; thin-line curves), allowing the network to reach activation states that would only be asymptotically reachable in the absence of thresholds (Fig. 11; thick-line curve). The activation of an output unit may be thought of as a polynomial function of the inputs from the hidden units. Selective control of all thresholds allows fine adjustments to the polynomial, allowing network function to conform to the error-field requirements of the learning task. Given that attractors in biological systems may have considerably more complicated gradients than the identity function shown here, it is expected that adjustable thresholds may be important when learning involves attractors. However, compared to the extensiveness of studies on synaptic changes during learning in biological systems, little attention has been paid to threshold changes and how such changes affect the computational ability of networks.

FIGURE 11 HERE

Networks encode multiple forms of information. The term *encoded information* typically refers to processes that are evoked among neurons in a network to produce an output. The output of the network can be sent to other networks for further computation or for producing behavior. A given network may contain the information for generating one or more processes (Mpitsos & Cohan, 1986a; Mpitsos & Cohan, 1986b; Sejnowski & Rosenberg, 1987; Skarda & Freeman, 1987). Ultimately, this information is "laid down in structure" (Lorenz, 1974), such as in the strength of synapses, in the structure of the neurocircuit itself, and even in changes relating to gene expression.

Networks may contain a second form of encoded information that does not become obvious until networks are required to learn something new (Burton & Mpitsos, 1992). In these experiments, noise was injected into the adjustments that were applied to the synapses and thresholds in order to

improve the rate of learning. Interestingly, it also optimized the rate of learning of a subsequent task when noise was not given. Networks that were not given noise during the first training session eventually learned the first task equally as well as ones that received noise (i.e. all networks reached the same level of performance), but they learned the second task more slowly.

To account for this, consider the error surfaces in Figs. 8 and 9. Without noise, the trajectory through weight-error space flows relatively smoothly, covering only a small region the potential errors. With noise-adjusted synapses, the network is forced to produce large error shifts during which the trajectory covers a relatively large portion of the potential error space. The two networks reach the same minimum error, but sample the error-space differently. This suggests that the second form of information contained in a set of connections may relate to not so much to the actual final task but to the error gradients that must be navigated during learning.

If new tasks or teacher functions involve error gradients having any structural similarity to the gradients relating to previously learned functions, the networks that had been trained with noise should learn them faster because they already contain more information about these gradient fields than do networks whose adjustments had been made without noise. Conversely, if the old and new tasks involved quite different gradients, the ability of the two types of networks to learn the new task should be reversed. This occurs because the errors that are generated during learning of the second task result from the relative change between the gradient fields of the old and new tasks.

The potential to store such different types of information may provide a form of generalization in biological systems. The first form of encoded information results from learning-related adaptation to one or more conditions. Given sufficient similarity between the new challenge and previous ones, biological systems may gain considerable adaptive advantage by having the additional information about the attractor gradients.

CONCLUSION

The aim here has been to use attractors to make sense of the functional structure in large neural assemblies. To do this I have discussed attractors as existing wholly within the nervous system. Learned perceptions in animals and humans (Freeman & Skarda, 1990; Grossberg, 1988) and CPGs and are examples of such internal representations. These examples are equivalent because they require sensory cueing only for triggering or sustaining them, although they may incorporate sensory or external elements as part of the pattern generating process or modification of it (Kater & Rowell, 1973; Mellon, 1969). What this says is that if the aggregate activity of neurons in a network can not be altered so as to generate a particular basin of attraction, the network will not be able to adjust its connections to encode the information pertaining to that perception or motor pattern. Similarly, a network whose connections between the neurons have already been set will not produce a

particular pattern of activity when driven by some external signal if the fixed points represented by the connection strengths do not provide the gradients that will express such patterns. In either of these cases, the network exhibits "no workable solution" in its ability to learn or to respond to the driving force of an external stimulus once the synapses have been set. Ultimately, in adaptive behavior, the time varying neural output underlying a behavior emerges from a tension or dialectic between the goal-directed needs of the animal and a shifting and unknowable environment (Mpitsos & Cohan, 1986a). The final "attractor" is not fixed hard; it is variable and moldable.

The conjecture discussed here does not unravel the specific connections that we observe in complex biological systems as those shown in Fig. 1. It save to say that they will never be known in detail. We may gain some assurance in the validity of the conjecture by examining increasingly more complex networks in simulation or testing the conjecture in biological networks in cell culture, and showing that the settings of the connections follow a pattern that is established by the dissipative dynamics of the system. But as in Weinberg's (1992) use of reductionism, the conjecture provides the principle, not the details, though the effects of this principle should be testable.

FOOTNOTE

[1]The BCNs are involved in many different jaw-mouth behaviors; i.e., they are multifunctional. The animal exhibits several stages of feeding. Like all good carnivores, it actively exhibits regurgitation of noxious substances that have been ingested. It "rejects" ingested substances, by a process that resembles "reverse play-back" of bite-swallow behavior. It exhibits defensive biting behavior toward noxious attacks. And, interestingly, it not only cleans its gill, it also cleans the gill of other *Pleurobranchaea*, despite the fact that the animals are cannibalistic. *Pleurobranchaea* also exhibits rapid associative learning of several forms using mouth/head responses, eg., (Mpitsos & Cohan, 1986c; Mpitsos & Collins, 1975; Mpitsos, et al., 1978; Mpitsos, et al., 1988c).

REFERENCES

Abarbanel, H. D. I., Brown, R., Sidorowich, J. J., & Tsimring, L. S. (1993) The analysis of observed chaotic data in physical systems. *Reviews of Modern Physics* 65: 1331-1392.

Abraham, R. H., & Shaw, C. D. (1983) *Dynamics--The Geometry of Behavior, Parts 1-4*. Santa Cruz: Aerial Press.

Adey, R. W. (1972) Organization of brain tissue; Is the brain a noisy processor? *Int. J. Neurosci.* 3: 271-284.

Aihara, K., & Matsumoto, G. (1986) Chaotic oscillations and bifurcation's in squid giant axons. In: *Chaos*, A. V. Holden, ed. Princeton: Princeton Univ. Press. 257-269

Andrade, M. A., Nuño, J. C., Moran, F., Montero, F., & Mpitsos, G. J. (1993) Complex dynamics of a catalytic network having faulty replication into an error species. *Phys. D.* 63: 21-40.

Braitenberg, V. (1989) Some arguments for a theory of cell assemblies in the cerebral cortex. In: *Neural Connections, Mental Computations*, L. Nadel, L. A. Cooper, P. Culicover & R. M. Harnish, eds. Cambridge, MA: MIT Press. 137-145

Burton, R. M., & Mpitsos, G. J. (1992) Event-dependent control of noise enhances learning in neural networks. *Neural Networks* 5: 627-637.

Canavier, C., Clark, J. W., & Byrne, J. H. (1990) Routes to chaos in a model of a bursting neuron. *Biophys J* 57: 1245-1251.

Chay, T. R., & Rinzel, J. (1985) Bursting, beating, and chaos in an excitable membrane model. *Biophys. J.* 47: 357-366.

Cohan, C. S. (1980) *Centralized control of distributed motor networks in Pleurobranchaea californica*. Ph. D., Case Western Reserve University,

Cohen, M. A., & Grossberg, S. (1983) Absolute stability of global pattern formation and parallel memory storage by competitive neural networks. *IEEE Trans.Syst., Man, and Cybern.* 13: 815-826.

Eckmann, J.-P., & Ruelle, D. (1985) Ergodic theory of chaos and strange attractors. *Rev. Mod. Phys.* 57: 617-656.

Edstrom, J., & Mpitsos, G. (1995a) Membrane mechanism for dissipation of perturbations in network function. *In Preparation* :

Edstrom, J. L., & Mpitsos, G. J. (1995b) Predicting the influence of perturbing currents on spike latencies: Determinism and degeneracy of information transfer across simple synapses. *In Preparation* :

Eigen, M., & Schuster, P. (1979) *The Hypercycle. A Principle of Natural Self-Organization*. New York: Springer-Verlag.

Evans, J. W., Fenichel, N., & Feroe, J. A. (1982) Double impulse solutions in nerve axon equations. *SIAM J. Appl. Math.* 42: 219-234.

Farmer, D. J., Kauffman, S. A., Packard, N. H., & Perelson, A. S. (1987) Adaptive dynamic networks as models for the immune system and autocatalytic sets. *Ann Rev New York Acad Sci* 504: 118-131.

Farmer, J. D., Kauffman, S. A., & Packard, N. H. (1986) Autocatalytic replication of polymers. *Physica* 22D: 50-67.

Feroe, J. A. (1982) Existence and stability of multiple impulse solutions of a nerve equation. *SIAM J. Appl. Math* 42: 235-246.

Fitzhugh, R. (1961) Impulses and physiological states in theoretical models of nerve membrane. *Biophysic. J.* 1: 445-466.

Fitzhugh, R. (1969) Mathematical models of excitation and propagation in nerve. In: *Biological Engineering*, H. P. Schwan, ed. New York: McGraw-HIll. 1-85

Freeman, W. J. (1994) Role of chaotic dynamics in neural plasticity. *Prog. Brain Res.* 102: 319-333.

Freeman, W. J., & Skarda, C. A. (1990) John Searle and His Critics. In: *Chapter 7, Mind/BrainScience: Neuroscience on Philosophy of Mind*, E. Lepore & R. van Gulick, eds. Oxford: Blackwell. 115-127

Friedman, N. (1970) *Introduction to Ergodic Theory*. Princeton: Van Nostrand.

Gardner, D. (1990) Paired individual and mean postsynaptic currents recorded in 4-cell networks of *Aplysia. J. Neurophysiol.* 63: 1226-1240.

Gardner, D. (1993) Statistical determinants of synaptic strength. In: *The Neurobiology of Neural Networks*, D. Gardner, ed. Cambridge, MA: MIT Press. 21-70

Garfinkel, A. (1983) A mathematics for physiology. *Amer. J. Physiol.* 245: R445-R466.

Garfinkel, A., Spano, M. L., Ditto, W. L., & Weiss, J. N. (1992) Controlling cardiac chaos. *Science* 1230-1235:

Glass, L., & Kaplan, D. (1993) Time series analysis of complex dynamics in physiology and medicine. *Med. Prog. Technol.* 19: 115-128.

Grassberger, P. (1990) An optimized box-assisted algorithm for fractal dimensions. *Phys. Rev. Lett* 45: 346-349.

Grassberger, P., & Procaccia, I. (1983) Characterization of strange attractors. *Phys. Rev. Lett.* 50: 346-349.

Grossberg, S. (1980) *Studies of Mind and Brain*. Boston: Reidel Publishing Co.

Grossberg, S., ed. Neural Networks and Natural Intelligence. Cambridge, MA: MIT Press.

Guckenheimer, J., & Holmes, P. (1983) *Nonlinear Oscillations, Dynamical Systems, and Bifurcations of Vector Fields*. New York: Springer-Verlag.

Haken, H. (1983) *Synergetics: An Introduction. Nonequilibrium Phase Transitions and Self-Organization in Physics, Chemistry, and Biology*. New York: Springer-Verlag.

Hale, J., & Koçak, H. (1991) *Dynamics and Bifurcations*. New York: Springer-Verlag.

Hastings, S. (1982) Single and multiple pulse waves for the Fitzhugh-Nagumo equations. *SIAM J. Appl. Math.* 27: 247-260.

Hebb, D. (1949) *Organization of Behavior-A Neuropsychological Theory*. New York: Wiley.

Hirsch, M. W., & Smale, S. (1974) *Differential Equations, Dynamical Systems, and Linear Algebra*. New York: Academic Press.

Hodgkin, A., & Huxley, A. F. (1952) A quantitative description of membrane current and its application to conduction and excitation in nerve. *J. Physiol.* 117: 500-544.

Hofbauer, J., & Sigmund, K. (1988) *The Theory of Evolution and Dynamical Systems.* Cambridge, MA: Cambridge University Press.

Holden, A. V., ed. Chaos. Princeton: Princeton University Press.

Hopfield, J. J. (1982) Neural networks and physical systems with emergent computational abilities. *Proc. Natl. Acad. Sci. USA* 79: 2554-2558.

Jalife, J., ed. Mathematical Approaches to Cardiac Arrhythmias.

John, E. R. (1972) Switchboard versus statistical theories of learning and memory. *Science* 177: 850-864.

Judd, K. (1992) An improved estimator of dimension and some comments on providing confidence intervals. *Physica D* 56: 216-288.

Kaplan, D. T. (1993) Evaluating deterministic structure in maps deduced from descrete-time measurements. *Int. J. Bifurcation and Chaos* :

Kaplan, D. T., & Glass, L. (1992) Direct test for determinism in a time series. *Phys. Rev. Lett.* 68: 427-430.

Kaplan, J., & Yorke, J. (1979) Chaotic behavior of multidimensional difference equations. In: *Lecture Notes in Mathematics: Functional Difference Equations and Approximation of Fixed Points*, H.-Å. Peitgen & H.-O. Walther, eds. New York: Springer. 204-227

Kater, S. B., & Mills, L. R. (1990) Neurotransmitter activation of second messenger pathways for the control of growth cone behaviors. In: *Molecular Aspects of Development and Aging of the Nervous System*, J. M. Lauder, ed. New York: Plenum Press. 217-225

Kater, S. B., & Rowell, C. H. F. (1973) Integration of sensory and centrally programmed components in generation of cyclical feeding activity of *Helisoma trivolvis. J. Neurophysiol.* 36: 142-155.

Küppers, B. O. (1983) *Molecular Theory of Evolution.* Berlin: Springer-Verlag.

Le Cun, Y., Kanter, I., & Solla, S. A. (1991) *Second order properties of error surfaces: Learning time and generalization.* Morgan Kaufmann Publishers, Inc., 918-924.

Leshno, M., Lin, V. Y., Pinkus, A., & Schocken, S. (1993) Multilayer feedforward networks with a nonpolynomial activation function can approximate any function. *Neural Networks* 6: 861-867.

Lindsey, G. B., Hernandez, Y. M., Morris, K. F., Shannon, R., & Gerstein, G. (1992) Dynamic reconfiguration of brain stem neural assemblies: Respiratory phase-dependent synchrony versus modulation of firing rates. *J. Neurophysiol.* 67: 923-930.

Lipton, S. A., & Kater, S. B. (1989) Neurotransmitter regulation of neuronal outgrowth, plasticity, and survival. *TINS* 12: 265-270.

Lockery, S. R., & Sejnowski, T. J. (1992) Distributed processing of sensory information in the leech. III. A dynamical neural network model of the local bending reflex. *J. Neurosci.* 12: 3877-3895.

Lorenz, K. Z. (1974) Analogy as a source of knowledge. *Science* 185: 229-234.

Matsumoto, G., Kim, K., Uehara, T., & Shimada, J. (1980) Electrical and computer simulations upon the nervous activities of squid giant axons at and around the state of spontaneous repetitive firing of action potentials. *J. Phys. Soc. Jap.* 49: 906-914.

Mattson, M. P., & Kater, S. B. (1989) Excitatory and inhibitory neurotransmitters in the generation and degeneration of hippocampal neuroarchitecture. *Brain Res* 478: 337-348.

Mayer-Kress, G., ed. Dimensions and Entropies in Chaotic Systems. New York: Springer-Verlag.

Mayer-Kress, G., Barczys, C., & Freeman, W. J. (1991) Attractor reconstruction from event-related multi-electrode EEG-data. In: *Proceedings of the International Symposium: Mathematical Approaches to Brain Function Diognostics of the International Brain Research Organization*, A. V. Holden, ed. New Jersey: World Scientific. 1-31 (available as a Tech Report-91-01-007 from the Santa Fe Institute)

Mellon, D., Jr. (1969) The reflex control of rhythmic motor output during swimming in scallop. *Z. für vergl. Physiol.* 62: 318-336.

Merzenich, M. M., Kaas, J. H., Wall, J. T., Nelson, R. J., Sur, M., & Felleman, D. J. (1983a) Progression of change following median nerve section in the cortical representation of the hand in areas 3b and 1 in adult owl and squirrel monkeys. *Neurosci.* 10: 639-665.

Merzenich, M. M., Kaas, J. H., Wall, J. T., Nelson, R. J., Sur, M., & Felleman, D. J. (1983b) Topographic reorganization of somatosensory cortical areas 3b and 1 in adult monkeys following restricted deafferentation. *Neurosci.* 8: 33-55.

Merzenich, M. M., Nelson, R. J., Stryker, M. P., Cynader, M. S., Schoppmann, J. M., & Zook, J. M. (1984) Somatosensory cortical map changes following digit amputation in adult monkeys. *J. Comp. Neurol.* 224: 591-605.

Mpitsos, G. J. (1989) Chaos in brain function and the problem of nonstationarity: A commentary. In: *Dynamics of Sensory and Cognitive Processing by the Brain*, E. Basar & T. H. Bullock, eds. New York: Springer-Verlag. 521-535

Mpitsos, G. J., & Burton, R. M. (1992) Convergence and divergence in neural networks: Processing of chaos and biological analogy. *Neural Networks* 5: 605-625.

Mpitsos, G. J., Burton, R. M., Creech, H. C., & Soinila, S. O. (1988a) Evidence for chaos in spike trains of neurons that generate rhythmic motor patterns. *Brain Res. Bull.* 21: 529-538.

Mpitsos, G. J., & Cohan, C. S. (1986a) Comparison of differential Pavlovian conditioning in whole animals and physiological preparations of *Pleurobranchaea:* Implications of motor pattern variability. *J. Neurobiol.* 17: 498-516.

Mpitsos, G. J., & Cohan, C. S. (1986b) Convergence in a distributed motor system: Parallel processing and self-organization. *J. Neurobiol.* 17: 517-545.

Mpitsos, G. J., & Cohan, C. S. (1986c) Differential Pavlovian Conditioning in the Mollusk *Pleurobranchaea. J. Neurobiol.* 17: 487-497.

Mpitsos, G. J., & Collins, S. D. (1975) Learning: Rapid aversive conditioning in the gastropod mollusc *Pleurobranchaea. Science* 188: 954-957.

Mpitsos, G. J., Collins, S. D., & McClellan, A. D. (1978) Learning: A model system for physiological studies. *Science* 199: 497-506.

Mpitsos, G. J., Creech, H. C., Cohan, C. S., & Mendelson, M. (1988b) Variability and chaos: Neurointegrative principles in self-organization of motor patterns. In: *Dynamic patterns in complex systems*, J. A. S. Kelso, A. J. Mandell & M. F. Shlesinger, eds. Singapore: World Scientific. 162-190

Mpitsos, G. J., & Lukowiak, K. (1985) Learning in gastropod molluscs. In: *The Mollusca*, A. O. D. Willows, ed. New York: Academic Press. 95-267

Mpitsos, G. J., Murray, T. F., Creech, H. C., & Barker, D. L. (1988c) Muscarinic antagonist enhances One-trial food-aversion learning in Pleurobranchaea. *Brain Res Bull* 21: 169-179.

Mpitsos, G. J., & Soinila, S. (1993) In search of a unifying theory of biological organization: What does the motor system of a sea slug tell us about human motor integration? In: *Variability and Motor Control*, K. M. Newell & D. Corcos, eds. Champaign: Human Kinetics. 225-290

Packard, N. H., Crutchfield, J. P., Farmer, J. D., & Shaw, R. S. (1980) Geometry from a time series. *Phys. Rev. Lett.* 45: 712-716.

Perlmutter, B. (1992) *Gradient descent: Second-order momentum and saturating error*. Morgan Kaufmann Publishers, Inc., 887-894.

Plaut, D. C., Nowlan, S. J., & Hinton, G. E. (1986) Experiments in learning by back propagation. *Carnegie-Mellon University Technical Report* CMU-CS-86-126:

Rinzel, J., & Keller, J. B. (1973) Traveling wave solutions of a nerve conduction equation. *Biophys J.* 13: 1313-1337.

Rinzel, J., & Miller, R. N. (1980) Numerical calculations of stable and unstable periodic solutions to the Hodgkin-Huxley equations. *Mathematical Bioscience* 49: 27-59.

Rössler, O. E. (1976) An equation for continuous chaos. *Phys. Lett.* 57A: 397-398.

Rowat, P., & Selverston, A. (1993) Phase-setting in a model of the gastric mill CPG in the lobster. *Society for Neuroscience Abstr.* 19: 406.7.

Rumelhart, D. E., McClelland, J. L., & PDP Group, eds. Parallel distributed processing: Explorations in the microstructure of cognition. Cambridge: MIT Press.

Schiff, S. J. (1994) Controlling chaos in the brain. *Nature* 370: 615-620.

Schiff, S. J., Jerger, K., Chang, T., Sauer, T., & Aitken, P. G. (1994) Stochastic versus deterministic variability in simple neuronal circuits: II. Hippocampal slice. *Biophys. J.* 67: 684-691.

Schnabl, W., Stadler, P. F., Frost, C., & Schuster, P. (1991) Full characterization of a strange attractor: Chaotic dynamics in low-dimensional replicator systems. *Physica D* 48: 65-90.

Sejnowski, T. P., & Rosenberg, C. R. (1987) Parallel networks that learn to pronounce English text. *Complex Syst.* 1: 145-168.

Selverston, A. I. (1980) Are central pattern generators understandable? *Behav. Brain Sci.* 3: 335-371.

Selverston, A. I. (1993) Modeling of neural circuits: What we have learned. *Ann. Rev. Neurosci.* 16:: 531-546.

Seydel, R. (1988) *From Equilibrium to Chaos. Practical Bifurcation and Stability Analysis.* New York: Elvesier.

Sherrington, C. S. (1906) *The Integrative Activity of the Nervous System.* New Haven: Yale University Press.

Sil'nikov, P. (1967) The existence of a denumberable set of periodic motions in four-dimensional space in an extended neighborhood of a saddle-focus. *Math. Dokl.* 8: 54-106.

Sil'nikov, P. (1970) A contribution to the problem of the structure of an extended neighborhood of a rough equilibrium state of saddle-focus type. *Math. USSR Sbornik* 10: 91-102.

Skarda, C. A., & Freeman, W. J. (1987) How brains make chaos in order to make sense of the world. *Behav. Brain Sci.* 10: 161-195.

Skinner, J. E., Molnar, M., & Tomberg, C. (1994) The point correlation dimension: Performance with nonstationary surrogate data and noise. *Integrative Physiological and Behavioral Science* 29: 217-234.

Smale, S. (1980) On the problem of reviving the ergodic hypothesis of Boltzman and Birkhoff. *Ann. N. Y. Acad. Sci.* 357: 260-266.

Soinila, S., & Mpitsos, G. J. (1991) Immunohistochemistry of diverging and converging neurotransmitter systems in molluscs. *Biol. Bull.* 181: 484-499.

Takens, F. (1981) Detecting strange attractors in turbulence. In: *Dynamical Systems and Turbulence,* D. A. Rand & L. S. Young, eds. Berlin: Springer-Verlag. 366-381

Theiler, J. (1986) Spurious dimension from correlation algorithms applied to limited time-series data. *Physical Rev A* 34: 2427-2432.

Theiler, J. (1987) Efficient algorithm for estimating the correlation dimension from a set of descrete points. *Physical Rev A* 36: 4456-4462.

Theiler, J. (1993) Don't bleach chaotic data. *Chaos* 4: 1-12.

Theiler, J. (1994) Two tools to test time series data for evidence of chaos and/or nonlinearity. *Integrative Physiological and Behavioral Science* 29: 211-216.

Theiler, J., Eubank, G., Longtin, A., Galdrikian, D., & Farmer, J. D. (1992) Testing for nonlinearity in time series: The method of surrogate data. *Physica D* 58: 77-94.

Theiler, J., & Rapp, P. E. (1995) Re-examination of the evidence for low-dimensional, nonlinear structure in the human electroencephalogram. *In Preparation* :

Thompson, J. M. T., & Stewart, H. B. (1986) *Nonlinear Dynamics and Chaos.* New York: John Wiley and Sons.

Tufillaro, N., Abbott, T., & Reilly, J. (1992) *An Experimental Appoach to Nonlinear Dynamics and Chaos*. Redwood City, CA: Addison-Wesley.

Turrigiano, G., Abbott, L. F., & Marder, E. (1994) Activity-dependent changes in the intrinsic properties of cultured neurons. *Science* 264: 974-977.

Ueda, Y. (1992) *The Road to Chaos*. Aerial Press.

Waddington, C. H., ed. Towards a Theoretical Biology. An IUBS Symposium. Chicago: Aldine Publishing Co.

Wang, X.-J., & Rinzel, J. (1992) Alternating and synchronous rhythms in reciprocally inhibitory model neurons. *Neural Commputation* 4: 84-97.

Weinberg, S. (1992) *Dreams of a Final Theory*. New York: Pantheon Book.

Weiss, J. N., Garfinkel, A., Spano, M. L., & Ditto, W. L. (1994) Chaos and chaos control in biology. *J. Clin. Invest.* 93: 1355-1360.

Werbos, P. J. (1974) *Beyond regression. New tools for prediction and analysis in the behavioral Sciences*. PhD, Harvard,

Widrow, B., & Stearns, S. D. (1985) *Adaptive Signal Processing*. Englewood Cliffs, NJ: Printice-Hall, Inc.

Wolf, A., Swift, J. B., Swinney, H. L., & Vastano, J. A. (1985) Determining Lyapunov exponents from a time series. *Physica* 16D: 285-317.

Wu, J.-Y., Falk, C. X., Höpp, H.-P., & Cohen, L. B. (1989) Trial-to-trial variability in the neuronal response to siphon touch in the *Aplysia* abdominal ganglion. *Soc Neurosci Abstr* 15: 1264.

Zanone, P. G., & Kelso, J. A. (1992) Evolution of behavioral attractors with learning: Nonequilibrium phase transitions. *J. Exp. Psychol. Hum. Percept. Perform.* 18: 403-421.

Zecevic, D., Wu, J.-Y., Cohen, L. B., London, J. A., Höpp, H.-P., & Falk, C. X. (1989) Hundreds of neurons in the *Aplysia* abdominal ganglion are active during the gill-withdrawal reflex. *J Neurosci* 9: 3681-3689.

FIGURE LEGENDS

Figure 1. "Massively" parallel network connections. Photomicrograph of immunofluorescence for the neurotransmitter FMRF-amide in the right half of a 400-neuron ganglion responsible for generating rhythmic feeding movements in the sea slug, *Pleurobranchaea californica*. Circular objects are neuron cell bodies, several of which exhibit the green fluorescence indicative of FMRF-amide. The tangle of neurites in the large area next to the cell bodies is the neuropil where most of the synapses between neurons take place. Exhaustive anatomical examination of the ganglion by slicing it layer by layer and reconstructing the results shows that the massive tangle of connections in the neuropil comes from only a few of the neurons in the buccal ganglion (and other ganglia); i.e., that there is extensive divergence in the connections between neurons. A survey of over a dozen neurotransmitters in complete serial sections of all ganglia in *Pleurobranchaea* and another sea slug, *Aplysia*, has shown similar profusely diverging projections of a few neurons containing a particular neurotransmitter into vast areas of the neuropil. Neurons containing other transmitters send converging projections into the same areas. Physiological work confirms the high degree of connectivity in *Pleurobranchaea* (Mpitsos & Cohan, 1986b) and *Aplysia* (Zecevic, et al., 1989). Modified from (Soinila & Mpitsos, 1991).

Figure 2. Biological networks compensate for the loss of a neuron. Traces show the action potentials in single neurons (BCN and M) and in nerves containing the axons of many neurons (top four traces). The sequential bursts of action potentials relate to feeding behavior, where bursts in R1 drive muscles that open the jaws and bursts in R3 drive muscles that close the jaws. Cessation of firing in the BCN, caused by applying electrical current to the BCN (between the arrows), stops the oscillatory activity, but that the oscillations recover despite the fact that the BCN remains quiescent. The BCN is one of about 20 neurons that comprise the oscillator (CPG) for opening and closing the jaws. M is one of the motor neurons in the mouth nerve MN. The SOVN carries axons of nerves that control muscles in the lips and mouth. Modified from (Mpitsos & Cohan, 1986b).

Figure 3. Dissipative processes in a computer simulation of periodic and chaotic changes in the concentration of two of the molecular species in a four-species catalytic network. Top four traces: time series of the concentrations of molecular species X1 and X2 before and after a perturbation pulse was applied (asterisk). The perturbation was applied by increasing the concentration of X1 for one integration step and then allowing the network to recover. Bottom two illustrations: phase portraits of preperturbed (thick lines) and perturbed post-transient responses (thin lines starting at asterisk) in the two regimes.

Figure 4. Four-dimensional phase portrait showing relationship between four of the fixed points in periodic (A and B) and chaotic (C) regimes and the system trajectories. The concentration of molecular species X1, X2, X4 are plotted on the three axes, and X3 is shown by thickness of trajectory. Circles (spheres) show the

location of the fixed points. A: Unperturbed system. B. Perturbation induced by injecting extra copies of X1 for one integration step. C: Fixed points are not shown because they would be obscured by the trajectories. (A and B) are modified from (Andrade et al., 1993).

Figure 5. Dissipative action in the simulation of small biologically realistic networks. The network (C) was activated by steady, low-level depolarizing current applied to Cell1. A: Time series of action potentials obtained from Cell2. The activity consists of a 3-cycle in which three intervals between action potentials repeatedly appear, as shown by the first seven action potentials. A 125 msec hyperpolarizing perturbation pulse was presented to Cell2 (marked by the dashed line). One action potential escaped during the hyperpolarization. After the release of the hyperpolarizing pulse, Cell2 rebounded, generating three action potentials in rapid succession, and then relaxed toward the original 3-cycle intervals. B: Shows the return map of the original 3-cycle (filled circles) and the post-perturbation recovery (open triangles). The numbers in (B) are the same as in A, and represent the interval between the numbered action potential and the action potential preceding it. C: Structure of the network: the thickness of the connections are proportional to the maximal synaptic strengths; the numbers show the strengths in milliSiemens. Excitatory synapses (open circles) have a reversal potential of 45 mV. Inhibitory synapses (filled circles) have a reversal potential of -82 mV. Open and close time constants for both types of synapses are 3 and 20 msec, respectively. Transmission delays were 3 msec. The simulations were run GENESIS obtained from the California Institute of Technology, Pasadena, and used squid axon membrane (Hodgkin & Huxley, 1952).

Figure 6. Attractors may adjust synaptic strengths globally. A: The same network that produced the 3-cycle activity shown in Fig. 5. B: Activity-dependent emergence of new connection strengths: The network was activated using Cell1 to produce the 3-cycle. After start-up transients were dissipated, Cell2 was stimulated tonically in addition to Cell1, and all synapses in the network were allowed to change using a variant of Hebb's rule. The new synaptic strengths are indicated by the thickness of the connection lines between the neurons and by the numerical values placed next to the lines (compare A and B). C: A return map showing that the new connection strengths generate a 6-cycle pattern (open circles) in the firing of Cell2; the original 3-cycle is shown by the filled symbols. When shorter or weaker stimuli are presented to Cell2, the synaptic strengths do not settle sufficiently into the values required to generate the 6-cycle. The synaptic strengths may fluctuate as the interrelated firing patterns of the cells in the network seek one gradient or another. The temporal structure of these patterns may drift until a strong enough gradient emerges which then forces the interrelated strengths of the synapse into some more stable set. The activity dependent changes in the synaptic strengths, discussed a little later, used Mike Vanier's implementation of Hebbian synapses in GENESIS.
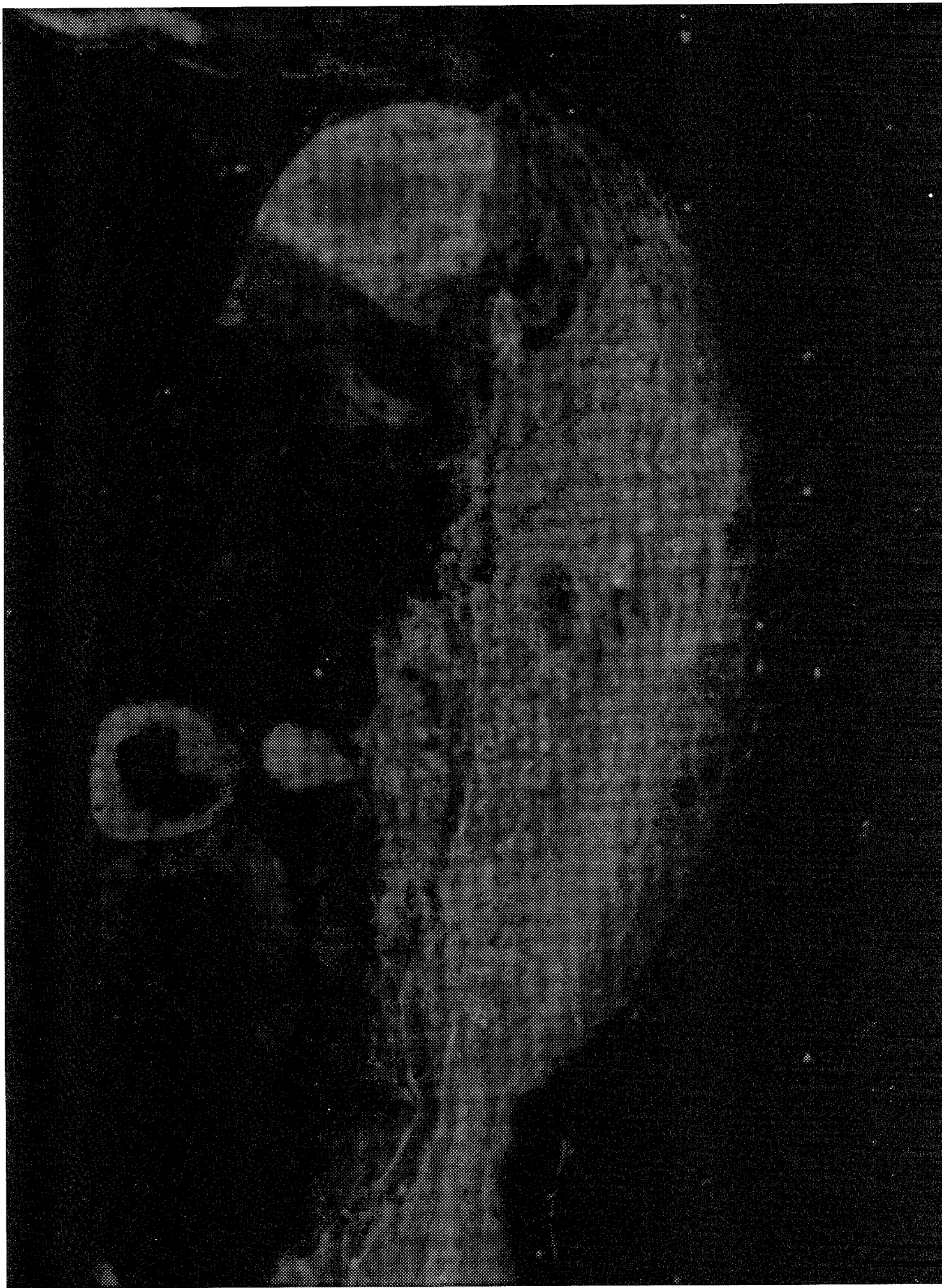
Figure 7. Backpropagation training of an artificial neural network sets synaptic strengths optimally with respect to one another. Top: Schematic showing a network having 1 input neuron, 1 output neuron and n-number hidden neurons (h). wh_i, and wo_i: synapses on hidden and output units. th_i and th_o, thresholds of hidden and output units; here, $i = 1,..,4$. Bottom: Training sets all synapses optimally with respect to one another. Dashed vertical line: synaptic strength set during training. Curves: Error as a function of changes in a single synapse while holding others at their trained values. Network as in Fig. 7. Modified from (Mpitsos & Burton, 1992).

Figure 8. Two-dimensional error surfaces. Same procedure as in Fig. 7 except that two synapses at a time were arbitrarily adjusted. The optimum combination of synaptic strengths (shown by the asterisk) in the selected synapses (using all other synapses at their trained value) is identical to the values obtained during training. Note high-error hill, nearly flat plateaus, and the steeply sloping gradients of the valley leading to the lowest error point.

Figure 9. Error gradients in 3-dimensions. Red represents high error, and the color change from red to blue shows decreasing error. Same procedure as in Figs. 7-8, except that now the strength of three synapses were adjusted. A: Low error resides somewhere within the block. B: Slices uncover minimum error. The top horizontal slice is identical to the error surface shown in Fig. 8, except that the image here is rotated -90 degrees. Non-optimal slices show flat gradients.
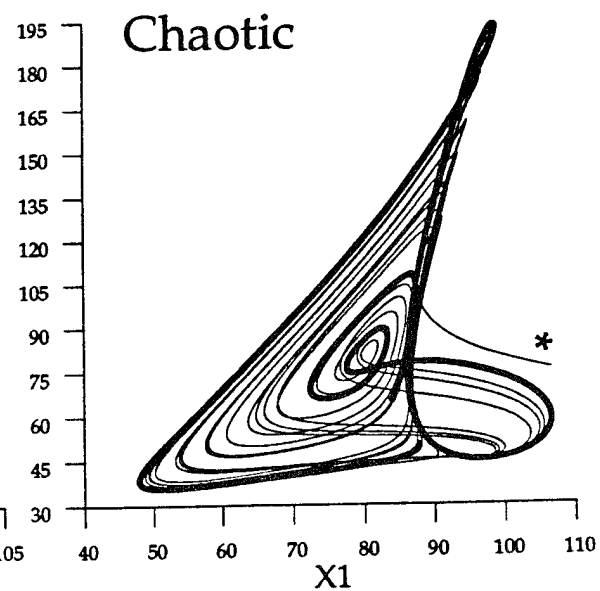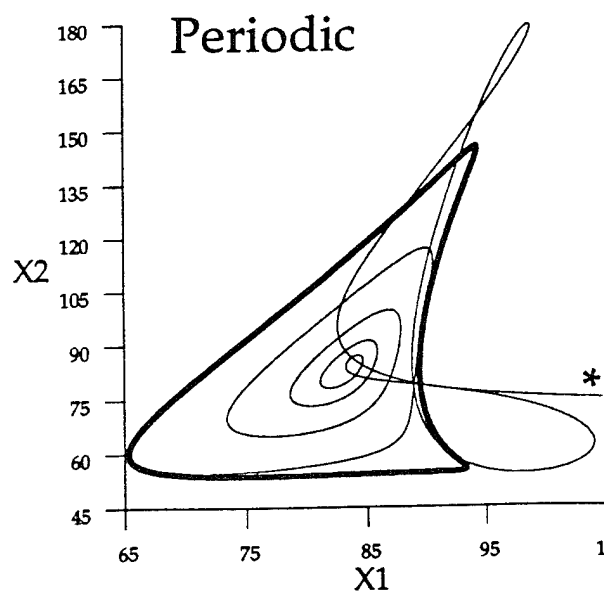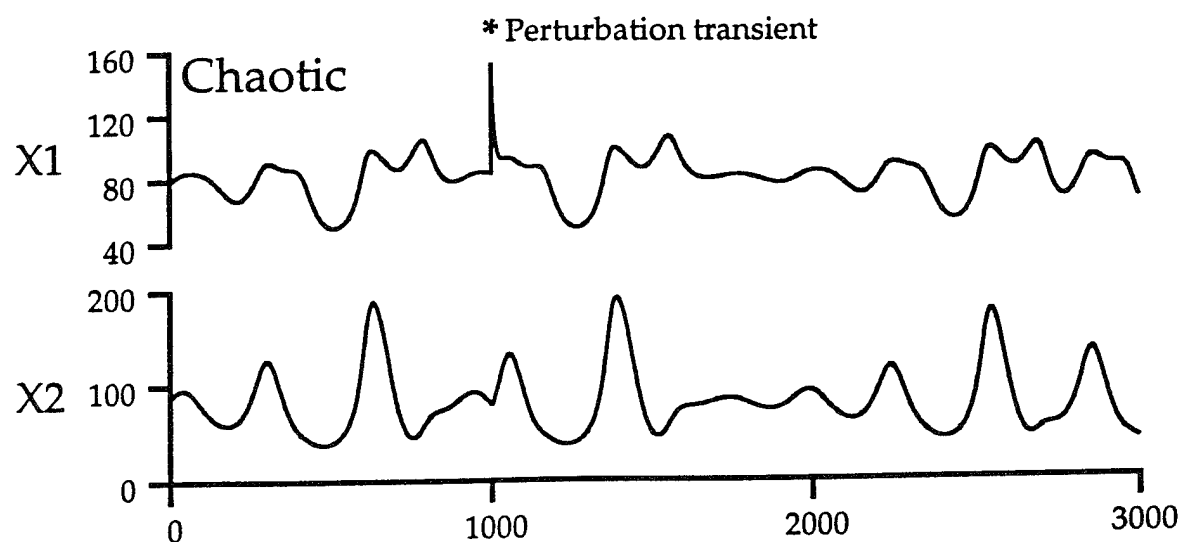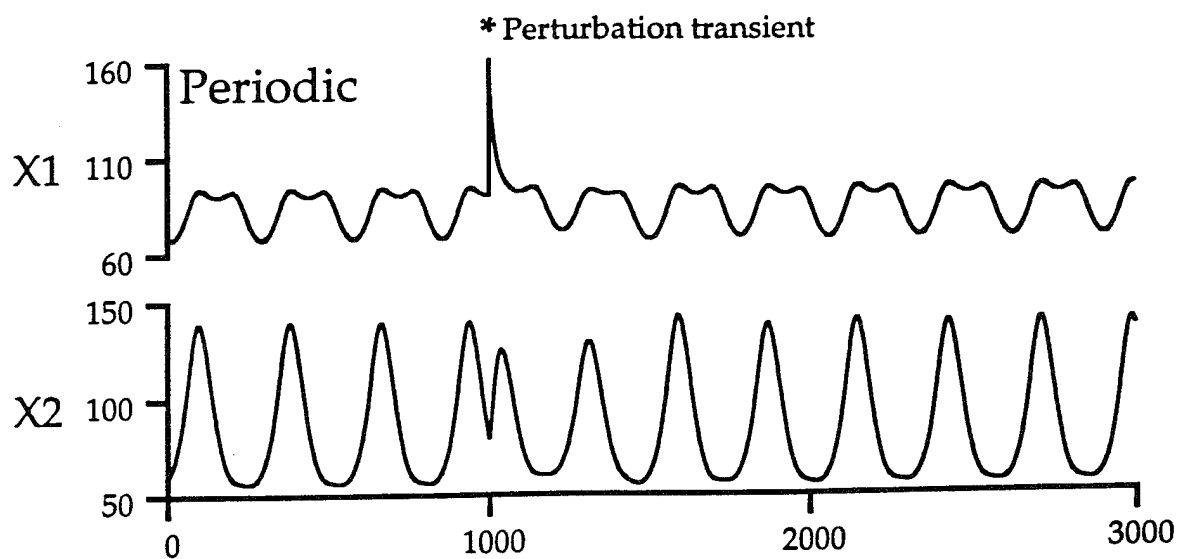
Figure 10. High-error space grows exponentially larger than low-error space as the number of trainable neurons increases. A: Schematic of the error-surface shown in the top horizontal slice of Fig. 9. Central low-error region has been made 5 times larger by comparison to the high-error region in the surround. B: Increasing to 120 trainable synapses reverses the relative sizes such that the volume of the surround-space is about 100,000 larger than the center one; the difference is a power function given by $(R_a)^d - (R_b)^d$, where d is the number of trainable synapses.

Figure 11. Thresholds (θ_i) act as a bias that shifts the sigmoidal output functions (Output$_i$) of hidden units selectively to different positions on the activation axis (a_i) which would only be reached by asymptotic regions of output functions when there are no thresholds (thick curve labeled No θ's). a_i is the product of the synaptic strength and the value of the input signal, less the threshold value.
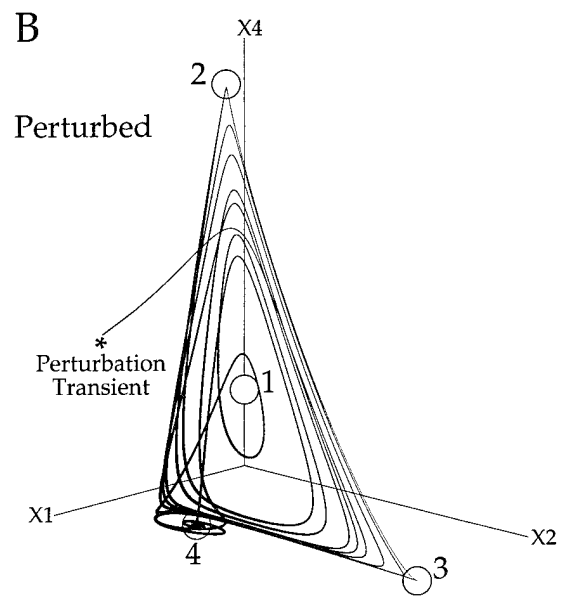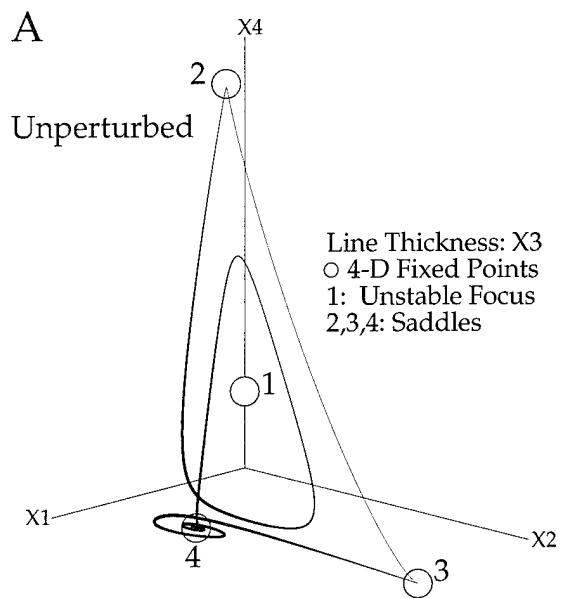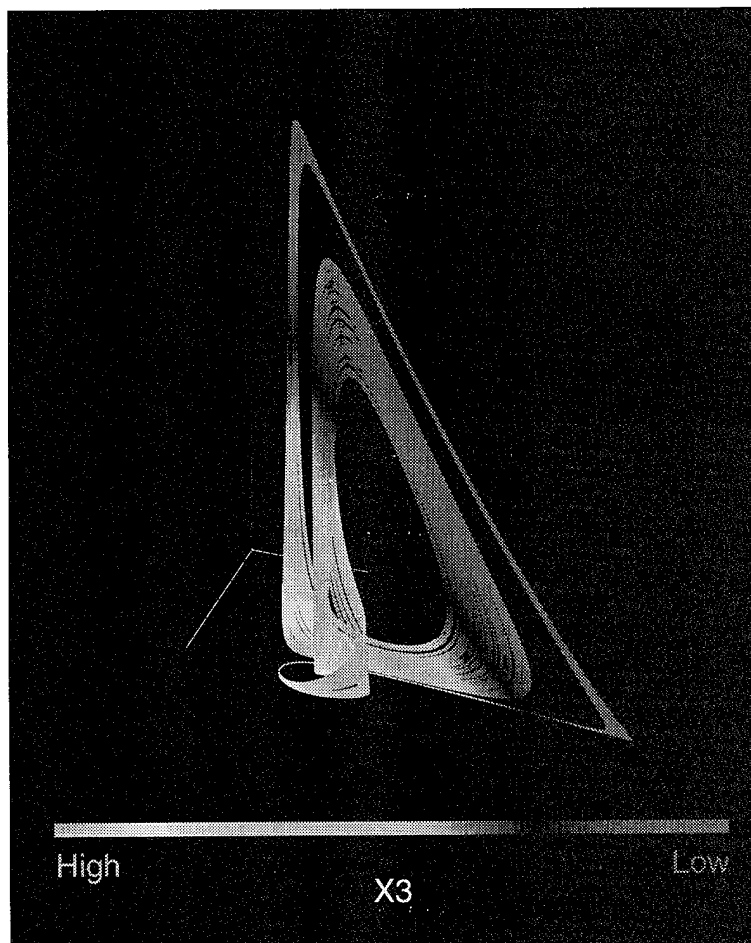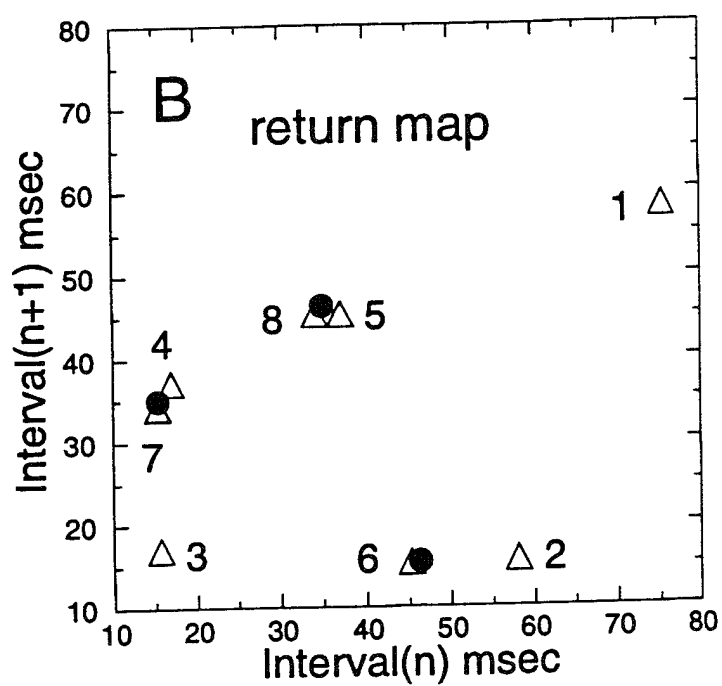
-Fig.2-

* Perturbation transient

Periodic

X1

X2

* Perturbation transient

Chaotic

X1

X2

Periodic

X2

X1

Chaotic

X1

-Fig.3-

A

Unperturbed

Line Thickness: X3
○ 4-D Fixed Points
1: Unstable Focus
2,3,4: Saddles

X4

2

1

X1

4

X2

3

B

Perturbed

X4

2

*
Perturbation
Transient

1

X1

4

X2

3

C

High   X3   Low

A

Cell1 — 160 — Cell2
Cell1 — 100 — Cell2
120   536   264   320
Cell3

depolarize Cell2 →
← release Cell2

B

Cell1 — 160 — Cell2
Cell1 — 60 — Cell2
160   504   240   280
Cell3

C

● normal 3-cycle
○ 6-cycle; depolarize Cell2

Interval(n+1) msec vs Interval(n) msec

-6-

-Fig. 7-

-Fig. 8-

A

W2

-35

35

35

W1

-35

-35 W3 35

B

W2

-35

35

35

W1

-35

-35 W3 35

-8.2 Ln(Error)^2 -0.5

—9—

A — w_2 (strength of synapse 2) vs w_1 (strength of synapse 1); $R_b = 1.0$, $R_a = 1.1$

B — surround - center vs d (number of synapses)

-Fig. 10-

-Fig. 11-

APPENDIX-2
(A revised version will be sent to *Biological Cybernetics*)

Predicting the Influence of Perturbing Currents on Spike Latencies: Determinism and Degeneracy in Synaptic Transmission

By

John Edstrom

and

George J. Mpitsos
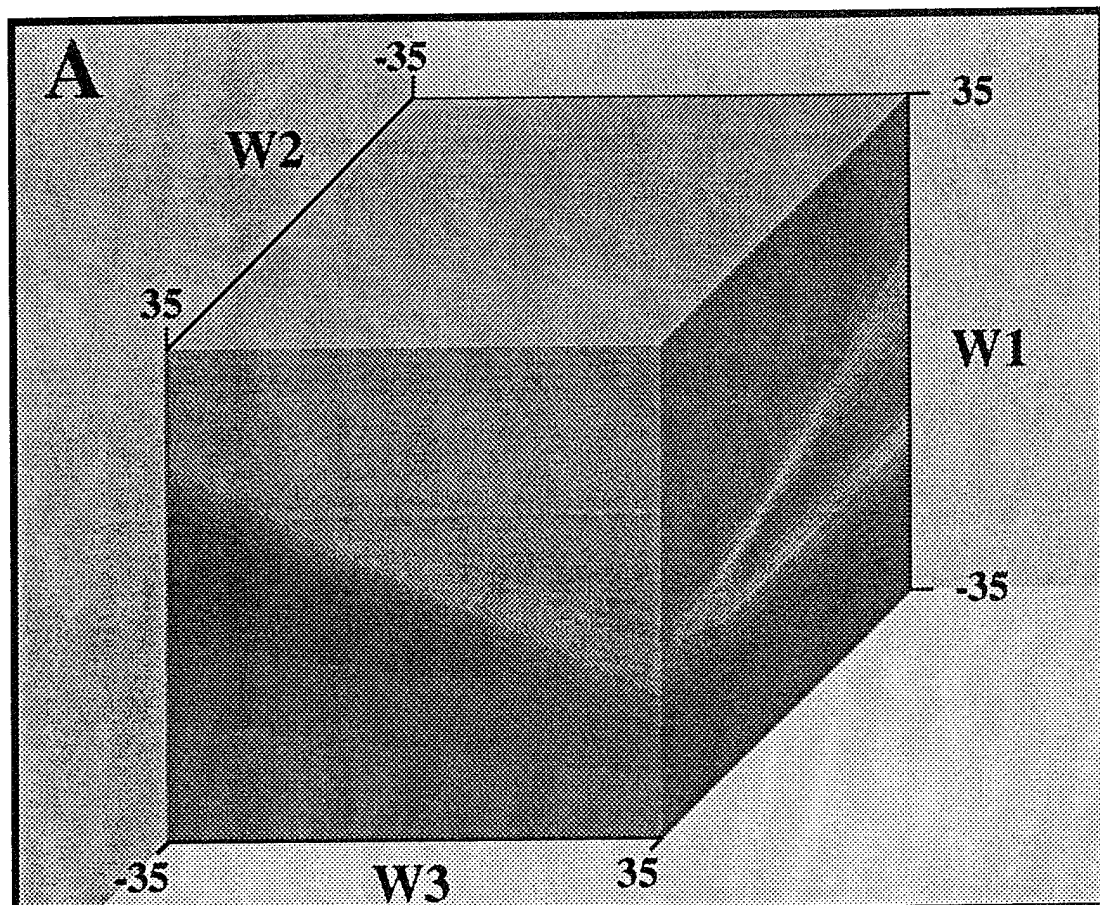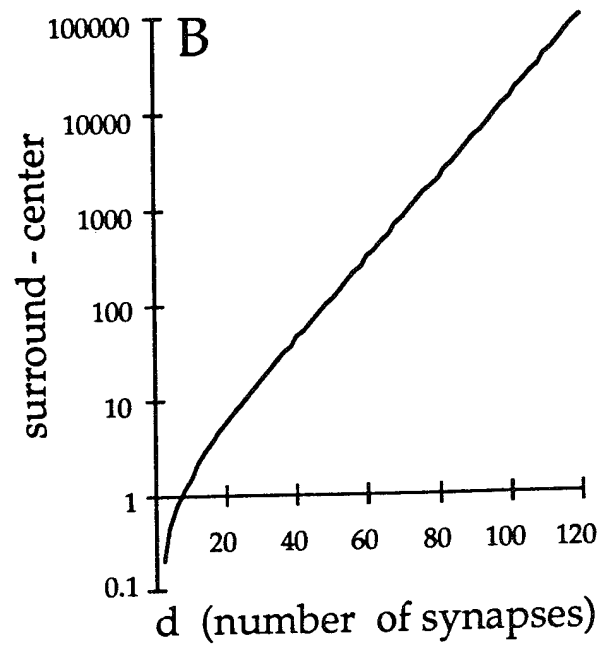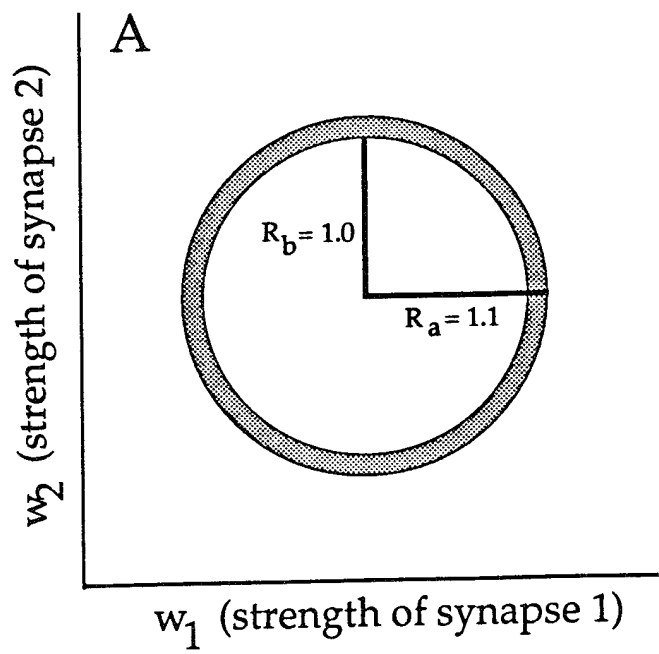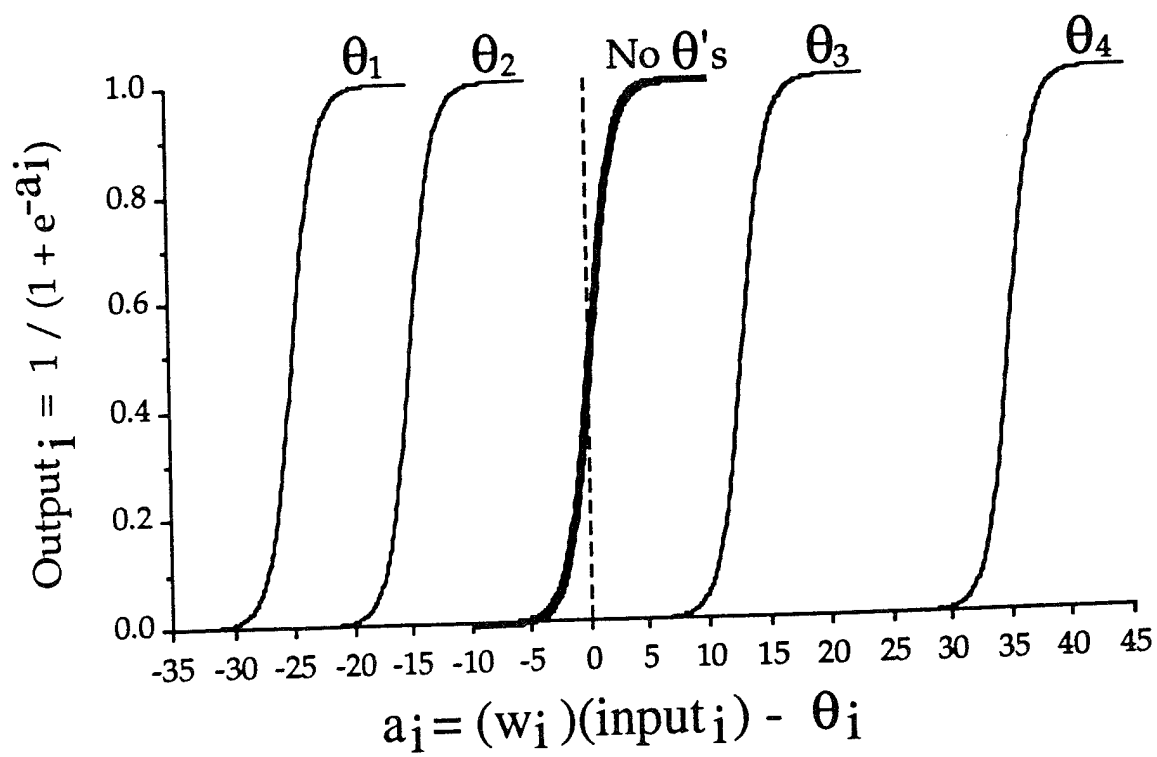
Oregon State University
The Mark. O. Hatfield Marine Science Center
Newport, OR 97365
USA
gmpitsos@slugo.hmsc.orst.edu

Abstract. The general principles by which a neuron transforms the structure of afferent synaptic currents to an output firing pattern are essentially unknown. To address this problem we explored the interaction between injected current and the intrinsic membrane conductances during the generation of firing patterns. This was done by performing perturbation studies in simulations of a simple model neuron comprising a single compartment possessing the electrical properties of the well-studied squid giant axon as originally described by Hodgkin and Huxley [Hodgkin, 1952 #750]. The injected current consisted of delta-function current impulses, sustained white noise, synaptic current or some combination of these. Three sets of experiments were performed: (1) Subthreshold white noise was used to characterize the impulse-impedance function (IRF) of the model neuron. (2) Suprathreshold white noise was used to obtain the average current trajectory (ACT), which is an approximation of the first-order Wiener kernel for action potential (spike) genesis. (3) A suprathreshold excitatory postsynaptic current (EPSC) was given as a time-dependent source of unimodal. The EPSC provided a test condition for determining how the latency of spikes it evoked was influenced by the timing of single current impulses. The stimulus/response (i/o) functions obtained from all three methods have complex multiphased shapes, indicating that over short periods of time linear, subthreshold and suprathreshold responses are governed by the same impedance process. These shapes also indicate that there may be considerable degeneracy in the transfer of information across synapses. Unlike neurons that are coupled by smoothly graded synaptic potentials, the dynamics of those relying on action-potential evoked synapses may may not be definable using systems of ordinary differential equations, though the numerical integrations generating the dynamics are deterministic.

1 *Introduction*

Our knowledge about neurons falls roughly into two main categories. There is a private or local world of ionic conductances, and a public or non-local world of action potentials and firing patterns, or, in the case of nonspiking neurons, of interneuronal communication that occurs via graded potentials. The fact that communication exists between neurons implies that some form of information is processed locally and transmitted to other neurons globally. For the moment, we use the term "information" broadly to mean simply some definable characteristic (or lack thereof) in the afferent signal that a neuron receives and in the output that the local processes generate. This characteristic may be as simple as the mean firing frequency of an otherwise stochastic process, or it may contain complex temporal structure.

The local and public worlds must be related since the local conductance mechanisms transduce extrinsic influences and support the public events evoked by them. The general consensus is that the interactions among the local events process afferent information within a neuron and export relevant information about the afferent stream in a efferent firing pattern to other neurons or to effector organs. Equivalently, neurons that do not generate action potentials, use graded potentials to broadcast the processed information to other neurons. In the present paper we begin the reports of our studies using findings obtained from model neurons that generate action potentials.

The electrophysiology of the single neuron stands at the confluence of these private and public domains. The character of this frontier, the laws and principles governing communication of information between domains, is mostly obscure to our understanding despite work and knowledge from both fields individually. Our understanding of the basic mechanisms of electrophysiology come from Hodgkin and Huxley [, 1952 #750] who were the first to present a theory of excitable membrane potential based on variable specific ionic conductances. These conductances were hypothesized to result from the presence, in a virtually impermeable membrane, of numerous independent molecules capable of controlling the permeability of specific ions through channels in the membrane.

These postulated channels possessed complicated time- and voltage- sensitive characteristics which offered a good quantitative explanation of the action potential and subthreshold phenomena. Subsequent work has essentially confirmed the original theory. Recordings from single channels has established the relation between the microscopic conductances of single channels, on the one hand, and the macroscopic conductances and their control parameters, on the other hand, that Hodgkin and Huxley described [Patlak, 1991 #881]. The theory of specific ionic conductances has

been successfully applied to a wide range of bioelectric phenomena such as synaptic transmission, sensory generator potentials and hormonal influences on neural activity.

The study of the public domain, of neuronal firing patterns, goes back to the 1920s when Adrian [, 1928 #921] showed that changes in the records from vertebrate peripheral sensory nerves during stimulation were due to changes in the firing rate of single units rather than to changes in their shape. Since then it has become clear that firing rate alone is not the only relevant parameter in neuronal firing patterns. It has been known for a long time that the firing patterns of neurons are often not random and show significant structure [Gerstein, 1964 #916]. Studies in visual systems suggest that various types of information about the visual field can be carried simultaneously in the firing patterns of single axons in optic nerve [Chung, 1970 #871] and monkey visual cortex [McClurkin, 1991 #872]. There are numerous studies showing that the times of occurrence of action potentials in many neurons are not independent of one another [Nakahama, 1977 #873], and that the degree of dependence varies with physiologically relevant variables [Grüneis, 1989 #875; Yamamoto, 1983 #876].

It is also known that single neurons can distinguish patterns in the sequences of synaptic activity and are potentially able to exploit this structure as a source of information. Random or constant-interval stimulation completely changes the firing pattern of pacemaker neurons [Perkel, 1964 #878] and computer model neurons [Segundo, 1968 #879]. Stimulating nerves with different interstimulus intervals at a constant mean rate yields different firing patterns in identified *Aplysia* neurons [Segundo, 1963 #880]. Single sustaining fibers in crayfish visual system are capable of carrying information relating to three different types of stimuli, average illumination, spatial frequency, and the e-vector of polarized light [Glantz, 1976 #908; Glantz, 1984 #910; Glantz, 1988 #909]. Subtle changes in subcellular biochemical processes are also sensitive to the structure of activity in the afferents to the neuron. For example, in vitro and in vivo studies in rat, long-term potentiation (LTP) of rat hippocampal neurons exhibits stimulus-pattern dependencies that may have mechanisms in common with the LTP induced by the standard procedure of equally-spaced high- frequency stimulation [Diamond, 1988 #839; Rose, 1986 #838; Tsukada, 1994 #917]. Moreover, simulation studies have shown that dendritic arrays are capable of responding differentially to different patterns of synaptic input volleys [Rall, 1977 #911].

Such studies indicate that neurons are able both to recognize and to create temporal structure in spike trains. These structures appear to have precise relationship to the structure of the input signal. For example, information about the movement of the visual field of the blowfly is recoverable from the structure of the firing pattern of visual units [Bialek, 1991 #870]. The amount of information that is extractable from the firing patterns using linear filter models can resolve movements smaller than the sensory field of single visual units, and approaches the noise level of the optic detectors. Recent work

on another arthropod, the crayfish, lends further support to the notion that the firing patterns for motion detection may be describable as linear filters [Glantz, 1994 #919]. It would seem, therefore, that linear filter models of the neuron might provide a bridge in our understanding of the relationship between the local computational properties of the neuron and firing patterns that they generate.

The filtering properties of neural membranes have been known since the late 1930's, and linear models of dynamic membrane conductances [Cole, 1968 #920; Koch, 1984 #922; Mauro, 1970 #882; Sabah, 1969 #924; Stein, 1972 #925] have established the relationship between the conventional Hodgkin-Huxley theory of specific ionic conductances and complex impedances of neurons and other excitable cells. However, the systems of conductances supporting bioelectric phenomena in neurons are unambiguously nonlinear. Linear models are only applicable over narrow ranges of membrane potentials, usually well below threshold (e.g., see [Koch, 1984 #922]), whereas much larger ranges of voltage excursions appear to be important or necessary for information processing in spiking neurons. For this reason, linear filter models are not often considered generally useful for describing spike generation or single neuron computation. Nonlinear models have been developed to account more accurately for the structure in spike trains of biological systems, e.g., [French, 1989 #888].

Nevertheless, the empirical success of linear filter models to account for the input/output relations in many neurons [Bryant, 1976 #815; Enroth-Cugell, 1983 #972; Frishman, 1987 #973; Krause, 1980 #971; Sakuranaga, 1985 #844; Sakuranaga, 1985 #843; Sakuranaga, 1983 #845], and the linear-filter decoding of the spike trains of motion detectors in the blow fly visual system [Bialek, 1991 #870], suggest that linear filter models may be more generally applicable than is usually believed. The presence of high-precision information in the temporal structure of firing patterns in the blowfly motion detectors suggests the presence of robust membrane mechanisms that preserve and respond to small changes in structure of input signals [Bialek, 1991 #870; Bialek, 1993 #915]. Although questions of the effects of nonlinearities must be addressed, the work of Guttman, Feldman and Lecar [, 1974 #914] on squid axon membrane suggests that violations of linearity produce only weak in the filter properties. The linear approximations to nonlinear activity in cockroach tactile sensory hairs [French, 1989 #888] suggest the same conclusion. Linear analytical methods often provide excellent characterizations of invariant measures of the nonlinear dynamics generated by systems of coupled differential equations, e.g., [Andrade, 1993 #635; Canavier, 1990 #517; Wolf, 1985 #55]. Taken together such studies suggest that it is reasonable to revisit the subject of how linear filter models of membrane mechanisms may be involved in the computational functions of neurons.

In the series of studies reported here we inquire into plausible explanations of how subthreshold linear filter interactions in neuron membrane can govern the

structure of nonlinear processes comprising spike trains. We show how a minimally complex membrane model can both preserve and transform temporal information. We suggest that these preserving and transforming effects may be largely explained by a linear filter model operating near a threshold nonlinearity. We then introduce some basic consequences of the insights concerning single neuron computation which will be considered more fully in later publications.

2. Methods

2.1 The simulation neuron

All of the computer simulations in this study used SWIM, version 1.5, a simulator for real neural networks (Ekeberg, et al., 1990), obtained from the Department of Numerical Analysis and Computing Science, Royal Institute of Technology, Stockholm, Sweden. The integrations employed the Crank-Nicholson method. The size of the integration steps ranged between 1 and 100 μsec, depending on the purpose of the experiment. The SWIM source was compiled with GNU gcc version 2.4.8 (Free Software Foundation Inc.) using IEEE standard compliant double precision floating point arithmetic libraries.

The SWIM source was modified to accept novel current sources that were not part of the original program. The modifications dealt strictly with adding novel current sources; none of the integration or other code was altered. These modification include the ability to read arbitrary current waveforms from script files, a white noise current source, transient current pulses lasting single time steps, synaptic conductances with bi-exponential time courses and ionic conductances using the Hodgkin and Huxley [Hodgkin, 1952 #750] specifications for squid giant axon. It was also modified to perform event triggered signal averaging used in the ACT experiment. A shifting buffer containing the recent history of injected current was maintained. When an action potential occurred the contents of the buffer were used to update a buffer of sums and sum of squares of the recent current history.

In all cases we modeled a simple spherical neuron comprising a single compartment with no axons, dendrites or other added complexities. We used three simulation models which differ only in the types of current used to drive the modeled neuron. In one, white current noise was used. In the second, a generic simulated presynaptic neuron was used to generate an EPSC in conjunction with a single current pulse, lasting one integration step, located at various times in the simulation epoch. In the third case the neuron was driven by current waveforms obtained from edited portions of the ACT, obtained from a previous white noise simulation, that were read as a current command script.

The neuronal membrane parameters, described below, are taken verbatim from the description of the squid giant axon at 6.3 C° by Hodgkin and Huxley [Hodgkin, 1952 #750]. The parameters listed below were normalized to take into account the size of the neuron.

Model Neuron Parameters:

a) Constant Parameters

Radius of Neuron: 44×10^{-6} m; Area = 6.082×10^{-9} m^2

Membrane capacitance: $C_m = 0.01$ Farads/m^2

Maximum conductances: $\bar{g}_{Na} = 1200$ S/m^2 ; $\bar{g}_K = 360$ S/m^2; $\bar{g}_{Leak} = 3$ S/m^2

Reversal potentials: $E_{Na} = 0.055$ V; $E_K = -0.072$ V; $E_{Leak} = -0.0604$V

b) Voltage-Dependent Characteristics of the Squid Giant Axon

$$\frac{dV}{dt} = \frac{I_{Na} + I_K + I_L + I_i + I_{syn}}{C_m} \tag{1}$$

$$\frac{dV}{dt} = \frac{1}{C_m}\left[g_{Na}(V - E_{Na}) + g_K(V - E_K) + g_L(V - E_L) + I_i + I_{syn}\right] \tag{2}$$

$$\frac{dV}{dt} = \frac{1}{C_m}\left[m^3 h \bar{g}_{Na}(V - E_{Na}) + n^4 \bar{g}_K(V - E_K) + \bar{g}_L(V - E_L) + I_i + I_{syn}\right] \tag{3}$$

$$\frac{dm}{dt} = \alpha_m(1 - m) - \beta_m m \tag{4}$$

$$\frac{dh}{dt} = \alpha_h(1 - h) - \beta_h h \tag{5}$$

$$\frac{dn}{dt} = \alpha_n(1 - n) - \beta_n n \tag{6}$$

c) Steady State Resting Parameter Values

$$m = 0.0355402$$
$$n = 0.260777$$
$$h = 0.705487$$
$$E_m = -0.0631 \text{ V}.$$

The functions and parameters used to obtain the rate constants (α_m, β_m, α_h, β_h, α_n, β_n) for opening and closing of the ion gates (m, h, n) were identical to those described by Hodgkin and Huxley [Hodgkin, 1952 #750].

2.2 Synaptic conductances

The time course for the EPSC was modeled to roughly resemble the squid giant synapse, as described by Llinas, Steinberg, and Walton [Llinas, 1980 #831]. With the parameters given below, the model synaptic conductance reaches a peak of approximately 25% of its maximum value (g_{syn}) after about 0.5 msec. The maximum synaptic conductance was chosen by trial-and-error to be just superthreshold at the normal resting potential.

EPSC Parameters:

Reversal potential (E_{syn}):	0 volts.
Maximum conductance ($\bar{g}_{syn}$):	3.8×10^{-8} Siemens.
Delay after presynaptic action potential:	variable.
EPSC activation time constant (τ_1):	0.00035 sec.
EPSC inactivation time constant (τ_2):	0.0007 sec.

The time course of the synaptic current is by the following equations, where V is the time-dependent membrane voltage:

$$I_{syn} = g_{syn} (V - E_{syn}) \tag{7}$$

$$g_{syn} = \bar{g}_{syn} \left[(1 - e^{-t/\tau_1}) - (1 - e^{-t/\tau_2}) \right] \tag{8}$$

2.3 Average current trajectory (ACT)

Use of the ACT asks the questions, given the occurrence of a sequence of action potentials, what can we predict of the history of the applied current that lead to these action potentials? One could ask the opposite question, given the history of the applied current, what can we predict of firing of a neuron? For the present paper, we restrict the

presentation to the first question. The term "trajectory" refers to the time course of the shape of the average membrane current that precedes the generation of action potentials. The methods used here closely follow those of Bryant and Segundo [Bryant, 1976 #815] who examined the ACT in identified neurons of *Aplysia*.

To obtain the ACT, low-level Gaussian white-noise current $X(t)$ was injected into a neuron at each integration step, and only one neuron was used; i.e., it was not synaptically activated. The response $Y(t)$ of the membrane to the applied current was a function only of the injected current $X(t)$. $Y(t)$ was converted to a delta function representing the sequence of action potentials that were generated over time, by the following algorithm:

$$Y(t) = \sum_{i=1}^{N} \delta(t - t_i) \tag{9}$$

$$\delta(t - t_i) = \begin{cases} 1, & \text{if } t = t_i \\ 0, & \text{otherwise,} \end{cases} \tag{10}$$

where t_i represents the time of occurrence of action potentials which were detected using a threshold of -30 mV in the membrane potential.

The ACT was calculated using an averaging function $S(\tau)$ that correlates the occurrence of action potentials with the membrane current that precedes them:

$$S(\tau) = \frac{1}{N} \sum_{i=1}^{N} \sum_{j=1}^{M} X(t_i - \tau_j). \tag{11}$$

N represents the total number of action potentials in the recorded spike train, t_i represents the time at which each action potential occurs, and τ_i is the time preceding the action potentials. Here $\tau_j = \Delta t$, for $j = 1,...,M$, where Δt is the integration step size. The total observation time T before the action potentials is defined by $T = M\Delta t$.

To compute the ACT, $S(\tau)$ is evaluated for all N action potentials by summing all of the currents injected at each τ_j Therefore, the ACT shows the average current injected at a series of M points before the appearance of an action potential. Thus, the ACT is both a normalizing and an averaging process. It scans all records for the occurrence of action potentials, sets that as time "zero" and then examines the average current across the membrane for a series of times preceding the action potential.

Depending on the length of time one uses to obtain the ACT and the firing frequency, one action potential can interfere with another. To avoid such artifacts, we selected the noise variance of the injected current such that the interval between action potentials was usually greater than 50 msec, the interval used to calculate the ACT.

Action potentials were excluded from the analysis that were preceded by another action potential by less than 70 msec.

2.4 Complex impedance (Z) and the impulse response function (IRF)

The complex impedance Z is the frequency domain image of the ratio of the complex frequency domain image of voltages with respect to the complex frequency domain image of the applied current: $Z = \frac{FFT(V(t))}{FFT(I(t))}$. FFT is the fast Fourier transform. $V(t)$ is the membrane potential time series calculated by SWIM in response to the applied white-noise current $I(t)$, which is described below, both of which are in the time domain. Signal processing routines were taken from Stearns and David [Stearns, 1993 #864]. Our methods follow closely after Puil, Gimbarzevsky, and Miura [Gimbarzevskey, 1986 #865]. The reported impedances are averages of ten 60 msec "sweeps", each sweep consisting of a different simulation run. A different set of random signals was used in each simulation sweep.

The IRF is obtained from Z by simply calculating the inverse Fourier transform to transpose the complex impedance vector to the time domain. These white-noise injection methods were the same as those used to obtain the data used for the ACT, except that the mean noise level was kept low enough to prevent the generation of action potentials. A second difference is that while the data for the ACT was obtained using continuous simulations to obtain tens of thousands of action potentials, the method for obtaining the data for the IRF used short 60 msec sweeps.

2.4 Random current

The white noise was generated using the ran0 and gasdev functions from [Press, 1988 #836], pp. 207-208, which uses the algorithm of Bays and Durham described in [Knuth, 1981 #835]. The random number generator was seeded with the current clock time when the program was run to avoid repeatedly using the same random series. This algorithm produces a normally distributed deviate with zero mean and unit variance. SWIM was modified so that at each integration step of the simulation, a new current intensity was selected from a Gaussian distribution with an appropriately specified variance. Different variances were used under different circumstances to control the range of the current signal. A variance of 2×10^{-12} amps was used for estimating the membrane impedance and 0.9×10^{-9} amps was used in the ACT experiment. The former produced strictly subthreshold noise and the latter produced occasional action potentials.

The membrane of the simulated neuron acts as a low pass filter and its transfer function falls rapidly between 10 and 100 Hz. The components of the stimuli with frequencies above 100 Hz have negligible effect on the membrane potential but are susceptible to phase distortions. To reduce this source of noise and restrict the signal power to a relevant range of frequencies in the experiments estimating the membrane impedance, we used a three-stage Butterworth low-pass filter [Stearns, 1993 #864] with a cutoff frequency of 400 Hz. The white-noise current used to obtain the ACT were filtered using a seven-point centered weighted running average to reduce large transients which made averaging difficult. Since the ACT was obtained using integration steps of 0.050 msec or less, whatever correlations the filtering produced were maintained within short time spans of only about 0.350 msec. In both cases blocks of random numbers were calculated and filtered in chunks to provide consistent and smooth filtering properties over the course of each simulation run.

3. Results

We are interested in understanding how current signals affect the activity of neurons. In a general sense, the effects produced by a perturbing current signal depend on two independent factors. The structure of the current (the current amplitude over time) and the electrical characteristics of the membrane.

The structure of the current is largely determined non-locally by the network in which the neuron is embedded or by the nature of the pulses that are applied experimentally. However, the local membrane characteristics, which are themselves complexly varying dynamic products of history, determine how the structure of the current is processed by a neuron at any given time. It is therefore necessary to consider the two factors together as a single functional unit.

We choose to restrict our attention here to stable cells at rest with no sustained activity resulting from intrinsic pacemaker conductances, conspicuous bursting tendencies or constant superthreshold depolarizing current. Neither do we concern ourselves here with overwhelmingly large synaptic currents. Instead, we look at the interactions of combinations of simple, transient currents with small to intermediate magnitudes in otherwise quiescent neurons where the sole source of afferent information is contained in the structure of the current signal.

It is first necessary to appreciate the degree to which different components of a current signal can be treated unequally. Synaptic interactions are often informally referred to as "spatial and temporal summation." However, the membrane is a variable and complex electronic filter and the relation between current and voltage is substantially more complex than this suggests and involves frequency-dependent

distortions of signal amplitude and phase. This relation is described by the membrane impedance.

3.1 *Membrane Impedance*

Impedance relates voltage to applied current in the same way that resistance relates voltage to current in Ohm's law except that while Ohm's law applies only to circuits comprising constant, frequency-insensitive components (resistance), impedance also describes the voltage distribution across and current flow among frequency-sensitive components (capacitance and inductance). The effects of applied currents and their combinations on membrane potential cannot be understood without knowing the impedance of the neuron. As a basis for subsequent studies, we start with an examination of the impedance characteristics of the Hodgkin-Huxley model under the conditions that we shall place it under the various perturbation experiments.

In order to measure the impedance of the model neuron it is necessary to measure the impedance at many different frequencies since any circuit which contains reactive components, such as a neuron membrane, will have different impedances at different frequencies. Because impedance is a function of frequency and not a single number like resistance, this analysis is typically performed in the frequency domain where impedance is a complex quantity. Resistance, the component of impedance which does not change in response to changes in current, is the real part and reactance, the component of impedance which reacts to changes in current, is the imaginary part. Impedance is usually presented as impedance-plane plots (Fig. 1 A and C), where resistance is plotted against reactance at all frequencies, and as individual magnitude (Fig. 1B) and phase angle (Fig. 1D) vs. frequency plots. The two representations are related by virtue of the fact that each point on the impedance plane can be represented as a vector drawn from the origin to the point; its length is impedance magnitude, and its angle is the phase angle of the impedance. The phase angle can be positive or negative and serves to distinguish the two classes of reactance depending on whether its phase angle is positive (inductive) or negative (capacitive).

The two types of graphs complement each other. The points along the curves on the impedance plane are ordered according to frequency with the highest frequencies near the origin. Progressively lower frequency impedances are encountered by following the curve counterclockwise from the origin until the other end is reached which corresponds to the zero frequency or DC resistance of the membrane. This shows nicely how impedance changes smoothly and continuously over a range of frequencies but provides no exact information about those frequencies. That information is provided by the other graphs where frequency is the independent variable and can be read directly.

In practice impedance is measured by injecting the neuron with some time varying current signal, collecting the voltage response of the neuron to it and then calculating the impedance according to the equation $Z = \dfrac{FFT(V(t))}{FFT(I(t))}$, where Z is the complex impedance, $FFT()$ is the fast Fourier transform function $(SPFFTR())$ in Stearns and David, 1988) which converts a time domain vector into its complex frequency domain image, $V(t)$ is the voltage time series observed in response to $I(t)$, the current stimulus time series. White noise is used here as the stimulus source because it is convenient and contains nearly equal signal power at all frequencies.

At least ideally. Any single finite sample of white noise will be incomplete with unequal power at different frequencies. To mitigate this finite sampling artifact the results presented here are the averages of ten independent estimations of Z. Examples of estimates of the model neuron impedance are shown in Fig. 1. They were obtained under three different conditions: normal resting membrane potential with 0.1 msec model time steps, normal resting membrane potential with 0.05 msec model time steps, and hyperpolarized resting membrane potential with 0.05 msec model time steps.

FIGURE 1 HERE

At its normal resting potential the membrane acts as a pure resistor only at the two frequencies 0 and 20 Hz, indicated by the zero phase angle axis crossings in Fig. 1D. These points correspond to the two intersections of the resistance axis in the impedance plane plots (1A and 1C). Changing the polarization of the membrane significantly alters its impedance. This is apparent when comparing the impedance plane plots of the data from normal, depolarized and hyperpolarized membranes in Figure 1A, where the hyperpolarized membrane exhibits only reactive impedance except at 0 Hz. At the normal resting membrane potential the magnitude of the reactance rises from its DC value to peak at 45 Hz (Figure 1B) and then falls off rapidly. Depolarizing the cell as little as 3 mV significantly decreases the low frequency impedance, sharpens the impedance peak and shifts it up to 55 Hz (Fig. 1B) Hyperpolarizing the cell as little as 3 mV noticeably the low frequency impedance, broadens the impedance peak and shifts it down to about 30 Hz. Above 100 Hz the three impedance curves are similar.

Peaked impedance curves such as those in Figure 1B are characteristic of a damped oscillatory circuit which is indicative of combined inductive and capacitive elements, e.g, see [Mauro, 1970 #882; Sabah, 1970 #928; Sabah, 1969 #924]. The reactance of the normal membrane is largely inductive at and below 20 Hz, as shown by the positive reactance in Figure 1D. Three mV depolarization shifts the crossover point to 40 Hz. At higher frequencies and increasing polarization, the reactance is increasingly dominated by capacitance, as shown by the negative swing of the phase (Fig. 1D). A

pure RC circuit will exhibit a semicircle in an impedance plane plot. The deviations from this form in 1A and 1C show that even though the net reactance is capacitive, there is a smaller but still significant inductive component at the hyperpolarized potential.

As the frequency of the stimulus signal increases capacitance shunts the current, and the voltage response falls off rapidly above 45 Hz, the resonant impedance peak at rest (Fig. 1). At normal and depolarized resting potentials, and at low frequency stimulation, the membrane impedance is significantly influenced by inductive reactance arising from the dynamics of the sodium and potassium conductances.

Within the modeling parameters used in this study the integration time step size does not introduce artifacts at functionally relevant frequencies. It can be seen in Fig. 1 that the only effect of changing the time step from 0.050 to 0.100 msec is to introduce some phase distortions at frequencies above 300 Hz while most of the voltage signal power is below 200 Hz. In the remaining experiments time steps of 0.050 msec or less will be used.

3.2 *The Impulse Response Function (IRF)*

The IRF is the time domain image of the impedance and shows a three-phase time course of impedance change that would occur in the membrane in response to brief small current impulses. The significance of the IRF stems from the fact that the voltage response to any current signal can be calculated by convolution with the IRF. For a single current impulse the voltage response will be the IRF times the amplitude of the current impulse. So the IRF indicates how any current signal will be transformed and drawn out in time.

It is obtained by calculating the inverse Fourier transformation of *Z (SPIFTR())* in Stearns and David, 1988). The IRF from the two experiments with 0.05 msec time steps discussed above are shown in Figure 2. The two curves show clearly why inductive filters are considered as damped oscillators. In both cases a single current impulse causes an oscillation in the membrane impedance which diminishes over time. The membrane potential shows the same damped oscillation in response to a small current impulse (Figure 9 A and C). The depth of the negative impedance trough decreases with hyperpolarization and later than at the normal resting potential.

FIGURE 2 NEAR HERE

In an ideal linear filter these damped oscillations will continue indefinitely. In these simulations the ability to detect them is limited. The IRFs merge into ambient noise after 20 to 30 ms. The important observation about the IRF, which we shall examine further in the ACT, is that information about extremely small perturbations

(maximum amplitude of only about 1.5 x 10-12 Amps producing maximum voltage excursions of only 0.025 mV (Figure 1 legend)) is retained and still detectable over many milliseconds.

3.3 *The Average Current Trajectory (ACT): Using the output stream as the frame of reference*

The relevance of the membrane impedance, as it was described above, to the behavior of the membrane assumes that the membrane acts as a linear filter. This means that the state of the membrane at any given time is the sum of the effects of prior events. The assumption is only valid for a small range of potentials within about 5 mV of resting in squid axon [Koch, 1984 #922; Sabah, 1969 #924; Mauro, 1970 #882]. The current pulses we used were well within this range, and far from threshold, since the maximum voltage excursion to obtain the IRF was 0.025 mV above the -63 mV resting potential, approximately 10 mV below the -54 mV firing threshold.

The membrane conductances in general, especially near threshold, comprise a nonlinear system, and the steady-state impedance over the range of voltages through which the membrane potential must journey in order to achieve threshold was shown to change significantly. One should not expect that the IRF, which is obtained near the resting potential, will be a reliable predictor of the behavior of the membrane over the range of voltages up to its firing threshold. Therefore, inasmuch as we are interested in the relation between current and the timing of action potentials, a means of ascertaining how signals will interact and combine over this range is needed. The ACT described in this section correlates the occurrence of action potentials with the recent history of current perturbations. This provides a direct empirical measure of the relation between the current and the spike generating mechanism which can be compared to the IRF.

As in the case of the IRF, the neuron was activated by applying randomly varying current. With the parameters used here the cell exhibited an overall firing rate of 16 spikes per second (45,781 spikes in 2,849.1 seconds). The ACT was acquired from 30,000 spikes (65.5%). The remaining 34.5% were rejected because they were less than 50 msec apart. Fig. 3 shows an excerpt of a train of action potentials obtained in a sample simulation run. The ACT is shown in Fig. 4.

FIGURES 3 & 4 HERE

There are three statistically significant phases in the ACT time course, noted numerically, showing a damped oscillation. The ACT is an average correlation function representing the average or most likely current trajectory "chosen" by the neuron from the current waveforms presented to it. Edited portions of the ACT were used as stimulus waveforms to ascertain the functional significance of the three phases. It can

be seen from Fig. 5 that the early positive phase-3 produces no change in the voltage response that is observable at this resolution. The middle negative phase-2 is not necessary to evoke an action potential, but it does accelerate the rise of the action potential and reduce its latency. The late positive phase-1 alone is sufficient to produce an action potential, but the latency is prolonged with respect to the complete ACT stimulus waveform. The ACT therefore is not a minimal threshold current just adequate to evoke an action potential. It is a series of synergistic components which support each other. The phases of the ACT are temporally correlated with the three phases of the IRF which is a subthreshold function.

FIGURE 5 NEAR HERE

3.4   *Modified-ACT: Combining sSbthreshold Random Noise with a Spike-Evoking EPSC to Allow Changes in the Frame of Reference in Assessing Spike Trains*

3.4.1   *Information obtained using modified-ACTs from the reference of the output*

With the ACT, noise was the sole driving influence. In order to understand how impedance responds to combinations of current that might be encountered by a neuron in a circuit, we added a moderately strong synaptic event to represent a deterministic aspect of the network's business. It is deterministic because of the constancy of its time of presentation, amplitude, and shape. The aim is to influence this suprathreshold, deterministic process with subthreshold random stimulation.

Since there are now two independent stimulus sources, the noise and the synaptic current, there are two ACTs; one of the average current trajectory of the noise channel, and one of the synaptic current channel. Although the complete stimulus waveform is the sum these currents, we shall treat them separately here because they provide independent sources of information with which to analyze the response of the membrane. Moreover, because the noise is so much smaller in amplitude than the synaptic current, any details about the noise source, and of the relationship between it and its affect on the membrane, would be invisible if only the sum were observed. We shall refer to this subthreshold noise ACT as the modified-ACT to distinguish it from the standard ACT in which the noise is suprathreshold, and which did not involve the activation of the synapse. The synaptic component of the current trajectory will be referred to as the synaptic-ACT.

In these experiments, 35 ms epochs of time, were simulated rather than a single long simulation as used for the ACT above. The noise was entirely subthreshold. In each simulation an EPSC of constant magnitude was presented at a constant delay into the simulation. In the absence of noise, the EPSC evoked an action potential at 30.96 ms.

With the addition of noise, the latency of the action potential varied since each 35 ms sweep of the simulation used a different set of randomly generated noise pulses in conjunction with the EPSC. Only one or action potential was obtained in an epoch (sweep); in a few cases the action potential failed. Two intensities of noise were used to examine the modified and synaptic ACTs under different membrane conditions. With the lower noise intensity, 82,503 simulation sweeps were conducted in which there were 9326 action potential failures (0.75%). We refer to these failures as class F "latencies". With the higher noise intensity, 82,503 sweeps were run in which there were 9,326 failures (11.3%). In both experiments, 60,000 action potential latencies were used to compute the modified and synaptic ACTs. The method was the same as described for the standard ACT.

The modified-ACTs for the two noise levels are in Fig. 6A, and the synaptic-ACTs are in Fig. 6B. The shapes of the synaptic-ACTs differ from the synaptic current because from one sweep to another, different noise schedules were given that produced variation in the temporal position of the action potential with respect to the time of occurrence of the EPSC.

FIGURE 6 NEAR HERE

The most obvious differences between the modified-ACTs and the standard ACT in Fig. 5 are a difference in magnitude and a change in shape. The late positive hump in the modified-ACTs is almost a thousand times smaller, narrower and asymmetric compared to the standard ACT. In low noise, the ratio of the magnitudes in positive to negative components in the trajectory of the modified-ACT are nearly equal. In high noise, the positive phase is larger and more nearly symmetric than in low noise. The phase relation between the synaptic- and modified-ACTs changes with noise. The zero-crossing point of the low-noise modified-ACT falls near the peak of its corresponding synaptic-ACT, whereas the crossing point of the high-noise modified-ACT is displaced approximately 4 ms earlier with the peak of its corresponding synaptic-ACT.

As noise increases, the EPSC plays a diminishing role in driving the cell, and the modified-ACT begins to approach in shape and magnitude what was seen previously with the standard ACT. There is also a progressive loss of information about the synaptic current as the noise increases. This is a reciprocal relation: The information about the noise and the synaptic current provided by observing the action potential latencies are inversely related. As the noise approaches zero, the overall ACT, consisting of the combined noise and synaptic currents, approaches that of the timing, shape and amplitude of the EPSC.

3.4.2 *Using the modified-ACT contingently: observing spike trains from the inut frame of reference*

The standard method of constructing the trajectories, ignores an important source of information about the circuit in which the neuron participates (We use the term "circuit" to refer to the temporal structure of any input signal that might occur naturally or be applied experimentally). The timing of the action potential in the driven cell depends on the relation in the sequence of the driving current-sources with respect to each other. This temporal information is invisible when looking only at the postsynaptic neuron and ignoring the circuit driving its activity. The histograms of postsynaptic spike latency, as measured with respect to the start of the simulation, indicates the extent of this information (Fig. 6 C and D). Noise produces a slurred distribution of the action-potential latencies over a wide range, and the distribution is sensitive to the level of the noise. As the noise intensity increases there is a shift of the mean to shorter latencies, a broadening of the distribution, and an increased frequency of failures. Each bin of latencies represents the effect produced by particular sets of noise signals.

This additional information, which may be gained by using the input circuit as the frame of reference, causes a subtle but important change in the evaluation of the observations. With the standard ACT, our frame of reference is bound to the action potential in the postsynaptic neuron. But using the contingency of the latency histograms our observations are bound to the time frame of the afferent stream because each histogram bin represents the stimulus conditions that generate a class of latencies. An observer can exploit this binding information by collecting a family of ACT's, one for the set of current impulses associated with a given latency bin rather than a single ACT as was done before. Since the spike-evoking EPSC is used, these ACTs are modified and contingent. To distinguish them from other averaging methods above, we refer them as modified contingent ACTs (modified-CACTs).

In Fig. 7 we construct the histograms so as to divide the range of the 60,000 latencies in the low- and high-noise experiments into regions of approximately equal occupancy. These boundaries are used as criteria for collecting multiple ACTs where the inclusion of a current sweep in a particular class is contingent on the class of latencies it causes. In this way, there is one pair of current and synaptic CACTs corresponding to each of the five regions of the latency histogram. Since the averaging process is bound to the stimulus and not to the postsynaptic action potential, it is possible to collect a sixth ACT corresponding to the class, F, of current samples that suppressed action potentials. This trajectory is the lowest trace in Fig 7 (A and B) that has the most negative current dip near the peak of the EPSC.

Under these measurement circumstances, the synaptic CACT becomes a constant equivalent to the true EPSC, and is shown by the single synaptic trajectory. Variation is restricted to the modified CACTs, but they all consist of scaled versions of the filter function that was firsts encountered with the standard ACT shown in Fig. 4. The magnitude of the function is proportional to the degree to which the noise changes the action potential latency. The peak action potential advancement is caused by the current trajectory having the most negative early phase and the greatest positive late phase. Conversely, the peak latency retardation is produce by the trajectory having the most positive early phase and the most negative late phase. The form of the modified CACTs does not change with noise intensity, and neither does its relationship to the EPSC. Thus, the various CACTs shown in Fig. 7 accurately reflect the distribution of the current trajectories that were presented to the neuron and not the mechanism by which the current trajectories were chosen.

FIGURE 7 NEAR HERE

It is apparent from this that the sensitivity of the ACTs in Fig. 6 to the amplitude of the noise was a consequence of the ignorance of the observer about the timing of the postsynaptic action potential with respect to the activity in its driving network and does not accurately reflect the constancy and sensitivity of the relation between the two input streams (noise pulses and EPSC) and the postsynaptic action potential latency. This reflects the inability of an ignorant observer to extract the available information in the ACT rather than an absence of information. The results indicate that on the average knowledge of the latency of the action potential provides information about the shape of the noise that generated it. Conversely, knowledge of the average shape of the stimulus trajectory contains information about the latency of the action potential.

Importantly, the average synaptic current is not significantly affected by the noise since because the synaptic event and the averaging process are both bound to the stimulus and remain constant. From Shannon [Shannon, 1948 #726] we know that because the synaptic current is constant it contributes no information to the observation. Thus, the information in the observed variation in the latencies is solely related to the shape of the noise current stream near the synaptic current.

As small as they were, the modified-ACTs in Fig. 6 differed from zero, but the average of all of the modified-CACTs in Fig. 7 should be zero since they are properly weighted by the averaging process. To resolve this apparent paradox we need to remember that the construction of the modified-ACTs depended on the action potential as a reference point, and this required that the F-class trajectories be excluded. They need not be excluded in constructing the modified-CACTs because the selection method was independent of the action-potential reference.

The significance of this shift in the frame of reference of the observation can be appreciated by constructing modified-CACTs that are referenced to the action potential, much as is done in constructing the standard ACT. This shifts the frame of reference back to the output stream, but retains the contingency aspect by grouping the latencies into discrete ranges according to the latency of the action potentials. So, now the times of occurrence of the action potentials are fixed by definition of the construction method. The uncertainty that was previously associated with the time of occurrence of the postsynaptic action potential is transferred to the interval between the EPSC and the postsynaptic action potential.

The results are shown in Fig. 8. The five histogram bins used in the analysis in Fig. 7 were used here to construct modified-CACTs from the reference point of the action potentials. Since action potentials are used, F-class trajectories could not be constructed. Panels A and C, respectively, show the effects on the modified-CACTs of low and high noise. Panels B and D show the synaptic-CACTS for each level of noise. It can be seen that the modified-CACTs are the same as the stimulus-bound CACTs in Fig. 7, except for a translation related to the different spike latencies induced by them. As a result of this translation there is a variable causal uncoupling of the postsynaptic action potential from the afferent current stream. The duration of the uncoupling varies with the latency class of the modified-CACTs and attains a maximum value of about 2.5 ms for the longest latency class shown here. From this point of view the system appears to be capable of faithfully preserving the information about the relation of noise and synaptic currents over variable and relatively long periods of time. If these modified-CACTs are averaged together the modified-ACTs observed before for the two noise levels in Fig. 6A will result due to the unequal overlap of the offset population of trajectories, showing that the information in the modified-CACTs is contained in the modified-ACT. It is a matter of how one reads the data, but in reading it one way, one losses information that is available from the other.

FIGURE 8 NEAR HERE

For this reason, the synaptic- CACTs are no longer constant, indicating the relative ignorance about their time of occurrence with respect to the action potential. Nonetheless, the relative timing between the synaptic currents and the noise is retained. For reference, the curves for both the synaptic- and modified-ACTs are labeled numerically, but since the trajectories all progress in succession numerically, only "1" and "5" are shown. Using these numbers, it can be seen that although the synaptic-ACTs at different positions, they retain the same phase relation to their corresponding modified-ACTs. Thus, as in the case of the modified-ACTS, summing the synaptic-CACTs in Fig. 8 A and D yields the corresponding synaptic-ACTs in Fig. 6B for the

two noise levels, with the appropriate time between the modified-ACTs and the synaptic-ACTs.

The differences in the various ACTs obtained in the presence of synaptic events depend on whether the observer is ignorant of presynaptic action potential timing, postsynaptic action potential timing or both. It appears that information about the driving sources stabilizes and maximizes the information about small amplitude perturbations that can be extracted by observing the timing of the action potentials. The answer one obtains about the relationship between input stimuli and the action-potential output depends in important ways on the frame of reference from which questions are constructed to inquire into this relationship.

3.5 *Time Course of Single-Pulse Perturbations on EPSC-Evoked Spike Latencies*

These experiments show that small afferent current signals significantly affect action potential timing over long periods of time preceding the action potential. To a first approximation the relation is described reasonably well by linear filter models even though the range of membrane potentials over which the system operates under these circumstances considerably exceeds the range of potentials over which a linear model is valid.

In order to understand how linear relations persist over non-linear ranges of membrane potential we look at how the response of control parameters to small, simple perturbing currents produce changes in spike timing following an EPSC. The aim will be to obtain a better understanding of the local membrane mechanisms that transform the input stream into the output stream than is available from the white-noise experiments used above.

In the present series of experiments, the same EPSC that was used above is presented at a fixed latency in each simulated sweep. To simplify the analysis, the continuous white noise is replaced by a delta function, approximated by a single current impulse lasting one time step, is presented at some suitable time during each independent simulation while model parameters of interest are monitored.

Figure 9A contains four superimposed simulation sweeps: (1) The time course of the voltage response produced by a single depolarizing (solid line) or (2) a single hyperpolarizing (dashed line) current impulse. (3) In the absence of an EPSC, the thick solid line shows the voltage time course in response to the current impulse alone, displaying the familiar damped oscillation predicted by the IRF. (4) The voltage response to the EPSC when no conditioning pulse is presented (dotted line). At this magnification, all three EPSPs are shown by the rapidly rising thin solid line that begins at 11 ms. The nearly vertical dashed line just before the 20 ms time mark shows the descending course of the action potential that was accelerated by the hyperpolarizing

pulse. The most important feature of this illustration is that the magnitude of the voltage response to the depolarizing and hyperpolarizing pulses is less than 0.2 mV in both cases Despite such small amplitudes, it will be shown below that a single pulse can affect the latency of EPSP-evoked action potentials that precede the onset of the EPSP by as much as 35 ms.

FIGURE 9 HERE

The action potential produced by the unperturbed EPSC is shown by the dotted trace in Fig. 9B. Despite the weak immediate effects produced by the perturbing impulses, the latency is significantly advanced (dashed trace) by the presentation of the hyperpolarizing pulse, and retarded (solid trace) by the depolarizing pulse. The retardation of the action potential caused by the depolarizing impulse is greater than the advance caused by hyperpolarizing impulse of the same magnitude. The voltage response to the impulses preceding the EPSC are invisible at the display scale used in Fig. 9B.

Except for the perturbing current impulses, which are an arbitrary imposed signal, everything else in these simulations is generated by the dynamics of the model. The changes in spike latency must, of course, work through the sodium and potassium gate parameters in the simple membrane used here. The evolution of the n and m gate parameters underlying the advancement of the action potential induced by the hyperpolarizing pulse are shown in Fig. 9 D and E, respectively. The response of the membrane potential to the hyperpolarizing pulse shown in Fig. 9A is shown again in Fig. 9C for reference. Gate m inactivates rapidly but has largely recovered by the time of the EPSC onset while the slower potassium gate n is still near its nadir. This residual inactivation which advances the onset of the action potential.

A full experiment, in which current impulses of various magnitudes were presented at 0.25 ms intervals over a 30 ms time span before the EPSC and partially overlapping it, is shown in Fig. 10. The time courses of the synaptic conductance and the response of the membrane potential to it are shown for reference in Fig. 10 A and B, respectively.

FIGURE 10 HERE

The solid and dotted lines that appear in Fig. 10C and D, above the membrane-potential recording, show the change in action potential latency as a function of impulse presentation time for different current magnitudes. The lines are isopleths: i.e., each line connects all of the points obtained from impulses of the same magnitude presented at the times indicated. The dotted latency-change curves were obtained using

hyperpolarizing pulses, and the solid curves were obtained using depolarizing pulses. Some of the dotted curves are open. This indicates that the postsynaptic action potential was suppressed when the impulses were presented over that range of times. Similar sets of curves are shown for the membrane under normal polarization (Fig. 10D) and under sustained hyperpolarization (Fig. 10C). The curves for sustained depolarization are not shown.

These curves strongly resemble the filter functions seen earlier with the IRF (Fig. 2), ACT (Fig. 4) and CACTs (Figs. 7 and 8), and the different phases of the curves in Fig. !0 are numbered to coincide with the numbering scheme for the IRF and ACT. Since currents are used in these filter functions and latencies are used in Fig. 10, the deflections of the i/o curves in Fig. 10 D have the opposite deflection relative to those seen earlier. For example, the solid-line curves in Fig. 10 A, correspond to the trajectories in Fig. 7 that have positive current deflections just after the peak of the EPSC. Similarly, the solid-line curves in Fig. 10 D have inverse deflections by comparison to the ACT shown in Fig. 4.

Overall, there are two major phases of opposite effect. The larger phase peaks about 4 ms before the normal action potential and the earlier, smaller and inverted peak at 19 ms, 12 ms before the action potential. Times are approximate since as the spike latency changes the time from any feature on the curve to the start of the action potential will change with it. This is the same distinction that was made earlier with the stimulus-bound and action potential-bound CACTs. This illustration adopts the afferent-stream frame of reference. As seen before in the CACTs the maximum perturbing influence occurs at 26 ms, a little less than 1 ms after the peak EPSC. There is a null point at 22.44 ms where no current has any detectable perturbing influence on the action potential latency which corresponds to the crossover points of the stimulus-bound CACTs. Also like the CACTs, perturbing influences which tend to retard the occurrence of the action potential are stronger than those which advance the action potential. A given depolarizing current impulse at 26 ms advances the action potential less than a hyperpolarizing impulse of the same magnitude will retard it. The disparity is seen most easily with the ability of the hyperpolarizing impulses to retard the action potential by several ms while depolarizing impulses of the same magnitude are unable to advance the action potential more than 1 ms over the range of magnitudes reported here.

A constant hyperpolarizing current changes the i/o space as expected from the IRF. The null point is moved to an earlier time and the early phase is prolonged and reduced in amplitude compared to the late phase. Notice that the decay of the late phase (26-31 ms) does not change during hyperpolarization. The broadening of the late phase peak is accomplished by a broadening of its rising phase which moves the null point to an earlier time in the sweep.

A third, earlier, phase in the isopleths of Fig. 10D , noted by "3", is visible under expansion of the vertical axis, but becomes increasingly larger as the membrane is depolarized (not shown). Thus, the span of preconditioning history with detectable influences on the timing of the action potential can easily reach 30-35 ms into the past before the onset of the EPSC, depending on the polarization of the membrane.

The experiments shown in Figs. 2, 4, 6-8 and 10 have addressed a wide range of response characteristics of the membrane. The IRF, as used to generate the results shown in Fig. 2, involved sufficiently weak stimulation that the membrane remained within its linear response range. The random current used to generate the ACT (Fig. 4) forced the membrane into its non-linear range. The EPSC used to obtain the modified-ACTs (Fig. 6) and the modified-CACTs (Figs. 7,8) also operated over the non-linear range while the noise which perturbed it was within the linear range. Similarly, the isopleths in Fig. 10 were obtained with current impulses which by themselves would not exceed the linear range of the membrane. The EPSC acts as an amplifier such that the small perturbations cause significant changes in the latency of action potentials. Under all of these conditions, the history of conditioning effects appear to have similar temporal structure.

3.6 Perturbation and time-evolution of gates m , h , and n

The structure in the history of these conditioning effects must, as noted above, be related to the time and voltage dependencies of the ion gates in the Hodgkin-Huxley model. Figure 11 B-D shows the m and n gate dynamics that produce the multiphased i/o curves. Figure 11A shows two isopleths, one obtained using $+10 \times 10^{-9}$ Amp pulses, that retard the latencies over the first part of the curve and then advance them, and one using -10×10^{-9} Amp pulses that initially advance the spike latencies and then retard them. There are five labeled points of interest placed on the curves to mark important locations. Point a represents the normal or unperturbed condition. Point b is placed at 19 ms, the presentation time at which the hyperpolarizing impulse produces its maximum advancement of the action potential. Point c is at 22.44 ms, the null point, where current impulses produce no change in action potential latency. Point d is placed on the baseline at 26 ms. It belongs on the -10×10^{-9} isopleth but at that presentation time the action potential is suppressed and that region of the isopleth does not exist. Point e is near the terminal point of no effect where the action potential is no longer susceptible to perturbing influences. It is shown at 30 ms but is really somewhat later just before the moment where the membrane potential normally crosses the criterion detection threshold (-30 mV). In the absence of perturbing influences the membrane potential crosses that threshold at 30.96 ms (horizontal dashed line). The EPSC begins at 25 ms. In the following discussion, we examine the results of the

experiments using -10 x 10^{-9} Amp impulses to examine how the ion gates are related to the isopleths.

FIGURE 11 HERE

The other three panels in Fig. 11 show the evolution of the potassium activation gate parameter n and the sodium activation gate parameter m during three representative experiments. We first discuss the general features of these diagrams, and then go in to the details of each feature.

Points relating to the labeled points in Fig. 11A are placed on the trajectories. In all panels, the dotted line is the trajectory from the simulation with the EPSC alone; it is the unperturbed or control trajectory. The other trajectories are the result of paired pulse/EPSC stimulations. The dashed line is the trajectory resulting from the simulation in which the impulse was presented the at 26 ms. This trajectory is launched from the same point as the control trajectory, so the high-resolution graphs of the launch points show a combined trajectory made up of dots and dashes. The solid line is the trajectory from the simulation where the impulse was presented at 19 ms. Thus, the illustrations exhibit one normal (or control) and two extreme trajectories, the maximum retardation (dashed line) and the maximum advancement (solid line) of the action potential. The trajectory that results from the presentation of the perturbing impulse alone is shown as solid-line arc. In all cases, the sodium gate activation parameter m is presented on the vertical axis and the potassium gate activation parameter, n, is shown on the horizontal axis.

The significance of these graphs is that they constitute a reduced phase space representation of the underlying dynamics. By showing the relation between dynamic variables as the system evolves, the phase space images are especially useful for understanding how the variables interact to produce the observed behavior. The m-n plane is a reduced phase space because it is incomplete. A plot of the complete four dimensional phase space (V,m,h,n) is not feasible and an incomplete or reduced representation of the phase space is needed. The variables are not entirely independent of one another [Kepler, 1991 #958; Fitzhugh, 1961 #926]. Because V and m behave similarly, and because h and n behave similarly, we use a reduced phase-plane constructed from one variable from each pair for clarity. This is sufficient for exploring the dynamics. It is incomplete, but it is adequate as a tool for assisting thinking about the underlying process where subthreshold perturbations affect the generation of action potentials.

Figure 11B shows a medium close-up of the m-n phase plane. Time is an implicit parameter and the general flow is from the bottom left to the upper right as the sodium and potassium activation parameters increase during depolarization. The curves

continue their paths off the graph upward and to the right as the action potential progresses, leading eventually in a clockwise fashion back to the original resting state at point a after the action potential.

Trajectories to the left of the control (dotted) trajectory are advanced (reduced latency) and the trajectories to its right are retarded (increased latencies). It can be seen that the 19 ms perturbation moves the trajectory (solid line) to the left of the control trajectory. The point d marks the state of the gates where the perturbation has its maximum retardation effect (26 ms), and, in this case, the action potential is aborted (dashed line). To give a reference, the point on the unperturbed trajectory at which the voltage crosses -30 mV is labeled e. This occurs at 30.96 ms, the unperturbed action potential latency; refer to the Fig. 11A for temporal orientation. Point d occurs 1 ms after the beginning of the EPSP (25 ms) at point a and is about 5 ms before point e.

A higher resolution graph of the initial rising phase of the trajectories is shown in Fig. 11C. The divergence of the 26 ms trajectory beginning at point d is apparent. The hyperpolarizing current impulse drives the voltage down. This inactivates m, forcing the trajectory downward and also inactivates n, forcing the trajectory to the left. The reduced activation of the sodium conductances peaks near the closest approach to the separatrix which lies above the trajectories in this panel. The response time of m is short and the decrease in sodium activation dominates this response, preventing the trajectory from rising above the separatrix. (The location of the separatrix is difficult to define, and will be examined in a following section).

The interrelationships of all of the trajectories may be understood using Fig. 11D which is an extreme close-up of the foot of the trajectories. The arc acb is the subthreshold trajectory of the response of m and n to the perturbation produced by the hyperpolarizing impulse (-10 x 10^{-9} Amp). The arc begins at point a and swings clockwise. In the absence of an EPSC, the hyperpolarizing pulse would cause a succession of m-n states that follow the solid-line curve that starts at point a and continues through points c, b, and back to a eventually. The arc is broken between b and a in order to show the launch positions of the control and the two extreme-case trajectories that will be used to visualize how the perturbations affect spike genesis. The control and the maximally delayed trajectories are shown rising as a combined dashed and dotted trajectory from point a. The maximally advanced trajectory is shown by the solid line emerging from point b. The loop is a result of the fact that although the hyperpolarization of the membrane induces a decrease in both m and n, m responds more quickly than n (as shown in Fig. 9 C-E) causing a nearly vertical, downward initial motion. Later, as n responds more slowly, it pulls the curve out to the left. Recovery of m is well under way while n is still decreasing when the EPSC arrives. (A depolarizing pulse of equal magnitude would produce a mirror image of the $acba$ loop in a clockwise flow, initially up and to the right).

Point a is the sole fixed point in the complete phase space and depicts the normal resting position of the membrane, unperturbed by current pulses or synaptic currents. It is from this point that all trajectories begin. If the impulse is presented before the arrival of the EPSC, then the impulse evokes the solid-line loop described above. The earlier the impulse is presented before, the more fully the loop will evolve before it is interrupted by the EPSC. If the impulse is presented after the arrival of the EPSC, then the perturbed and unperturbed trajectories coincide, as shown by the dashed-line trajectory, until the impulse is presented. The rapidly rising trajectories are the initial response of m and n to the synaptic current.

When the hyperpolarizing perturbation impulse is presented at 19 msec, 6 ms before the onset of the EPSC, the initial decrease in sodium activation has almost completely recovered, but n is still significantly reduced. When no EPSC is presented, the combined time courses of m and n that occur in response to the impulse produce a phase-plane arc upward and to the right of point c. Thus, the trajectory launched from point b begins to the left of the control trajectory because of the residual suppression of the potassium activation and almost normal sodium activation, and it is this persistence of the potassium inactivation that reduces the action potential latency.

Point c denotes the location on the acb loop where the EPSC would interrupt the normal evolution of the response of the gates to the hyperpolarizing perturbation pulse if it had been presented at 22.44 ms. The EPSC arrives 2.56 ms later. At that point there is residual inactivation of both m and n. The balance of the two inactivations is such that the action-potential advancing influence of the decreased potassium channel activation is exactly offset by the action potential retarding effect of the decrease in m so that there is no appreciable change in action potential latency. Although it is not included here, a trajectory emanating from point c in Fig. 11D, would begin to the left of the 19 ms perturbation trajectory emanating from point b and then cross over it in order to approach the normal (dotted) trajectory and yield the same action potential latency as the control trajectory emanating from point a. As required by the Jordan curve theorem and the theorem of Poincaré-Bendixson (see discussion in (Hofbauer and Sigmund, 1988), p. 149, phase-plane trajectories of deterministic functions cannot intersect. The fact that they appear to cross here is due to the incompleteness of the reduced two-dimensional phase plane employed in constructing Fig. 11 B-D.

Many trajectories could be shown emanating from the baseline loop along acb in Fig. 11D; ones are shown only at points a and b in order to allow visualization of the loop itself. This shows how small, subthreshold perturbations impose distinct initial conditions from which similar, closely packed responses arise. The smallness of the these initial conditions can be appreciated by comparing the dimensions of the baseline arc to its phase space locations in Fig. 11B. Since the perturbation pulses used to obtain the isopleths had a presentation range of 25 ms before the EPSC, most of the acb loop in

Fig. 11D consists of m -n values obtained within 0.25 mV of the resting potential. All take-off points of the trajectories on the baseline loop are within the linear response range of the membrane.

Once the EPSC begins, the voltage of the membrane shifts rapidly into nonlinear regions. An indication of this effect is shown in Fig. 12. In all panels, the solid-line shows the trajectory leading to maximal action-potential advancement (perturbation pulse given at 19 ms), and the dashed lines represents the trajectory leading to maximal retardation (pulse given at 26 ms), as described above. The remainder of the baseline loop is made up of unfilled circles, each of which indicates the starting point of a trajectory for a different impulse presentation time. Above the baseline loop are four similar loops where each new loop represents a slice through the whole family of trajectories at different times during the simulation. Each loop is separated from the previous loop by 0.12 ms. For clarity, only the extreme trajectories and the null point trajectory are connected by lines. In Fig. 12 the scales in all four panels are the same. Compare these with scales in Fig. 11C for orientation.

FIGURE 12 here

Panel B shows two loops taken shortly after the divergence of the maximal delay trajectory at point d of Fig. 11. The course of the unperturbed trajectory, and of the trajectories that will be produced by impulse perturbations other than the one causing maximal delay, represented by the two lone points lying at the right end each loop, approximately half way between the solid and dashed trajectories. As the maximal-delay trajectory continues to diverge from the unperturbed trajectory, other non-maximally delayed trajectories emerge successively from behind the circle residing on the dashed line. These are born as impulses are presented at earlier times in the simulation with respect to point d. A total of six such trajectories have emerged from the first loop in Fig. 12C, and seven in the second loop. Also shown in Fig. 12C is that the null (dotted-line) trajectory that originated from point c in Fig. 11D has nearly converged with the circle in each loop representing the unperturbed trajectory. Along the way, the null trajectory has crossed over the maximally advanced trajectory.

The convergence between the point-c and point-a trajectories, however, is only a false impression of the two dimensional projection of the illustration. This impression also indicates that the points on the c -trajectory are advanced with the points on the a-trajectory. In higher dimensions, however, it could be seen that the two points lie on opposite sides of the cross section of a tube. These two m -n states are sufficiently close to one another that they produce similar action potential latencies.

Thus, in Fig. 12A-D, the m -n reduced phase space represents a 2-dimensional projection of an expanding cone of states. Each time-slice or loop through the cone

appears as an ellipse The effect of the EPSC is to rotate and expand the initial loop. Dividing the ellipses roughly in half horizontally in Fig. 12D, the top half contains trajectories that lead to action potentials, where the shortest latency is represented by the top solid line. The bottom half of the ellipses contain trajectories for which action potentials are not generated, where the maximal suppression of the *m -n* states is shown by the dashed trajectory.

It is also possible to relate these time-slices to the structure of the isopleths in Fig. 11A. The radial position of the points in the time slices represent points along the isopleth produced by the hyperpolarizing pulse. Starting with the solid-line trajectory of the second time slice shown in Fig. 12C and counting clockwise, the first 2 trajectories represent pulse presentation times between points *a* and *b* on the isopleth (0-19 ms). Counting counterclockwise, the first 8 trajectories represent pulse presentation times over the isopleth from point *b* to point *c* and part of the way up the segment between *c* and *d* (19-26 ms). Both of these sets of trajectories lead to action potentials. Starting at the dashed-line trajectory and counting clockwise, the first six trajectories arise from impulses presented between points *c* and *d* . In the counterclockwise direction, the first 5 trajectories emerge from pulses presented between points *d* and *e* . Neither of these sets generate action potentials. The effects along the various portions of the time slices are graded, such that there is either a progressive change in the latency of the action potentials associated with the *m-n* trajectories, or progressive changes in the depolarization of the membrane potential for trajectories that do not lead to action potentials.

Four conclusions may be summarized from the above findings on the reduced phase space.

(1) The sample series of slices in Fig. 12 appear to be transections of the surface of a tube or cone that expands in time.

(2) By labeling and examining the positions of individual circles in each time slice, it can be seen that the stretching of the surface of the cone is due to the relative motion of the trajectories such that they rotate and separate from one another but do not change their relative position. Above the separatrix, the trajectories comprise an expanding hemisection of a tube whose cross section resembles an inverted U that has the 19 ms trajectory at its apex. Expansion continues until the action potential is generated. On the rising phase of the action potential the trajectories remain more or less parallel to one another. Below the two separatrices, the trajectories form an expanding U whose base has the 26 ms trajectory. Expansion continues until the postsynaptic response plateaus. Thereafter, there is contraction of state space until the membrane returns to its resting value.

(3) The stretching of the surface of the cone pulls the dotted-line trajectory, which emerges from point *c* on the baseline slice, away from the adjacent solid-line trajectory,

which emerges from point b. This relative motion of the two trajectories on the surface of the cone produces the visual impression that the two cross. It also shows that the apparent change in relative positions of points on the surface of the structure is due to a rotation of the structure and is not due to a change in relative radial positions of points on the surface. The trajectories remain separate and distinct, they don't cross or mix.

(4) Most important is that the effect of the nonlinearities engendered by the EPSC is simply to stretch the structure of the baseline phase-space loop produced by the perturbation impulses.

3.7 *Relation of spike thresholds to the phase-space separatrix*

The separatrix divides all trajectories into those which lead to an action potential and those which do not. The two sets of trajectories represent alternative basins of attraction to the fixed point. Although the squid axon described by Hodgkin and Huxley's equations has no true threshold, the separatrix may be viewed as nonsingular-point threshold, which Fitzhugh [Fitzhugh, 1955 #929; Fitzhugh, 1960 #927; Fitzhugh, 1961 #926] has termed QTP (quasi-threshold phenomena).

The separatrix, the set of trajectories which belong to no basin of attraction, serves the purpose of the threshold. But, because the separatrix belongs to no basin of attraction any trajectory on the separatrix will not approach the fixed point in finite time. Therefore, as a trajectory approaches the separatrix from above the latency of the action potential will approach infinity. As a trajectory approaches the separatrix from below, the duration of the repolarization will approach infinity. This effect is what gives importance to the separatrix as an organizing structure in phase space.

Because they belong to no basin of attraction separatrices have probability zero and can be neither experimentally discovered nor analytically determined. As a compromise we estimate the separatrix by bracketing it and assuming the true separatrix lies somewhere between them. We used a current impulse to drive the cell (no EPSC) for this estimation by adjusting its amplitude to thirteen significant figures by trial and error until the sub- and supra-threshold responses were virtually identical for over 12 msec. The suprathreshold stimulus amplitude for the cell dimensions used here was found to be $5.123152366087 \times 10^{-11}$ Amp and the subthreshold value was $5.123152366086 \times 10^{-11}$ Amp; the membrane voltage changes produced by these two stimuli are shown by the traces in Figure 13A. The m-n plane relating to both of these voltage traces is shown in Fig. 13B, and in higher magnification in Fig. 13C. In Fig. 13D, the initial portion of the m-n separatrix phase space trajectory is shown overlapped with the trajectories originating from points a, b, c and d in Fig. 11B using a .001 ms integration step. Keep in mind that this image of the separatrix, like the trajectories projected onto the reduced phase space, is incomplete. The separatrix is a four

dimensional hyper-line in the space of (V,m,h,n), not a simple line. Trajectories originating from these points are initially lower than the separatrix because of the temporal separation between the time at which the pulse was given and the onset of the EPSC. However, as these trajectories cross the separatrix, it can be seen that the separatrix takes on a position roughly near the midpoint between the trajectories for the most advanced action potential latency (top solid line) and the most retarded latency (bottom dashed line). This position is equivalent to the lateral mid-point position on the time slice loops shown in Fig. 12C. As clearly illustrated by the latency shown in Fig. 13D,

FIGURE 13 HERE

5 *Discussion*

Our principle interest here is to understand the nature of information processing at the level of single neurons in terms of an interpretation of known biophysical mechanisms. For information to be processed, it has traditionally seemed reasonable to accept the notion that there must be some meaningful relation, supported by known mechanisms, between the information entering a neuron and the information leaving a neuron although it need not necessarily be simple or obvious. We call such transformations "single-neuron computation" and use it as the foundation concept for the inquiries presented here and in subsequent papers. We shall discuss our findings as they relate to the ability of linear membrane impedance responses to subserve input/output transformations, and to the extent to which these transformations are reliable.

The input/output transformations balance a difficult design problem in which neurons must satisfy multiple and sometimes contradictory constraints. On the one hand the neuron must accurately propagate information that it receives. This requires a predictable relation between the input and the output of a neuron so that an observer of the output can obtain reliable knowledge about the input. Balanced against this need for predictability is the need to produce novel outputs as the neuron combines information from diverse sources (such as contemporary sensory images, accumulated experience, or changes in the level of neurochemical modulation acting on the membrane) to produce an output appropriate to the circumstances that may differ in significant and unexpected ways from the form of the input.

We have explored how membrane properties may achieve aspects of these design constraints by looking at the dependence of spikes on current injection in models of simple but plausible neurons where the input signal varies in size and form from small and random to large and non-random.

A generic computer model preparation was used to allow rigorous control over input and to be able to observe otherwise unobtainable internal state parameters. One of our main observations is that surprisingly small-amplitude signals make important contributions to firing patterns. Measuring and controlling small input signals is expensive in terms of effort and ingenuity in real life. It is therefore desirable to understand how and why small signals might be important to neural function by looking at them first under ideal conditions that are only possible in a model.

Toward this end, we have modeled a single compartment neuron with the membrane electrical properties of squid giant axon. This model does not and is not intended to realistically describe any particular neuron. No neuron has exactly this impedance. But all neurons do have an impedance, and it is the need for a general understanding of how impedance relates the input of a neuron to its firing pattern that we address here. The properties of the squid axon were chosen in particular because they have been the object of extensive research and are simple enough to understand while still being complex enough to produce interesting effects.

5.1 *The membrane as a linear filter*

That the neuron membrane behaves like a filter is a trivial and uncontroversial statement because whenever a current is applied to anything a voltage will result and the relation between them, the transfer function or impedance, will be a filter of some sort. Theoretical and empirical studies have extended the utility of this statement by showing how the filter properties arise from known conductance mechanisms, and by showing in many cases that the filter will be linear over some range of voltages.

A linear filter model is desirable from our perspective because it gives a simple, compact and empirically discoverable description of the relation between input (current) and output (voltage). Most theoretical and empirical attention has been directed toward the squid giant axon ([Mauro, 1970 #882; Poussart, 1977 #890; Moore, 1980 #886; Sabah, 1969 #924; Sabah, 1970 #928]). Work by others has shown that the linear filter model of membrane impedance is not uniquely valid for the squid giant axon and can be applied to a variety of different neurons incorporating a variety of different conductances (Calcium conductance in thalamocortical neurons, trigeminal sensory cells under anesthesia [Puil, 1986 #883; Puil, 1987 #884; Puil, 1989 #885], and NMDA on lamprey spinal neurons [Moore, 1993 #889; Moore, 1985 #842]) under different conditions.

Comparing the filter properties of our model with those of squid giant axon can be used as a test of its biological validity. The only apparent discrepancy between the model and the axon is a slow increase in phase angle of the transfer function of the model from an earlier minimum at signal frequencies greater than 300 Hz which is not

present in squid giant axon. This depends on the size of the integration step and must be an artifact of the numerical methods. This presents no serious problem for the acute simulations since the behavior of the model at low signal frequencies, which is what we are interested in, is unaffected by the choice of integration step size within the range employed in the remainder of the simulations used in these studies (0.05 ms or less).

Otherwise the model captures the functionally important characteristics of the squid giant axon. As a filter, the squid giant axon behaves like a resonant RLC circuit. The model exhibits the same characteristic behavior. Like the axon the resonance frequency of the model is dependent on the steady-state resting potential maintained by various amounts of constant injected current (Fig. 1). As expected, hyperpolarizing the cell increases the damping factor and shifts the resonant frequency to lower values while depolarization decreases the damping factor and shifts the resonant frequency to higher values.

The impedance can be represented in a variety of ways. We show both the impedance plane plot in the frequency domain (Fig. 1), and the IRF in the time domain (Fig. 2). The choice of representation is a matter of convenience since they are equivalent; for any given stimulus current waveform they both predict the same voltage waveform response. The response of the system in the frequency domain is computed by multiplying the complex impedance by the transform of the current while in the time domain the current is convolved with the IRF. Frequency-domain analysis is better suited for empirically estimating the impedance and calculating the response to a stimulus in real cells and the IRF is better suited for describing the nature of the transformation of an afferent current signal into a membrane potential by reactive membrane conductances.

The duration of the IRF and its form are the two most important aspects of the filter properties of the membrane for what follows. The extent of the response, the period of time over which the IRF is non-zero, constitutes a type of memory since it indicates how long the effect of an afferent signals persist and is able to interact with currents that arrive at other times. Where the IRF is zero the current impulse has no influence on the future behavior of the system. Beyond that time the input and output are causally uncoupled. Here, the response to a single small impulse lasting less than a microsecond persists for several tens of milliseconds and the nature of this response depends upon the resting potential. This means that factors affecting the membrane potential will be able to affect the breadth of the window in time through which the neuron observes its input. In the same way, large signals may have the same effect by placing the

In the case of the squid giant axon, the membrane exhibits significant resonance. This means that the membrane potential responds to a current impulse with a damped oscillation. Not all neurons exhibit resonance and in the squid axon it can be

suppressed by hyperpolarization, e.g, [Mauro, 1970 #882; Guttman, 1974 #914]. Resonance imbues the temporal relation of multiple input signals with an importance foreign to a passive RC membrane where the interaction between two events simply diminishes with the interval of time separating them. With resonance there is also a qualitative change in the response over time where the interaction of an impulse with another event can be synergistic, antagonistic or neutral, depending the interval between them. The phase relation or temporal separation between inputs becomes a potentially significant source of information for the cell.

The relevant properties of resonance are its characteristic frequency and its strength. The characteristic or resonant frequency of the filter is the frequency at which the magnitude of the impedance peaks and the strength of the resonance can be judged by the size and damping rate of the oscillations in the IRF. This frequency depends most heavily on the characteristics of the channels involved while the damping factor depends on their density. The resonant frequency of the squid giant axon is approximately linearly proportional to the membrane potential [Sabah, 1970 #928]. The relation is more complex in other cells that have been studied but it usually exhibits polarization-dependent changes in one or both of these properties. Dorsal spinal lamprey neurons [Moore, 1993 #889] show increased resonance and higher resonant frequencies with depolarization as do trigeminal sensory neurons [Puil, 1987 #884]. Neurons of the nucleus ovoidalis of the chicken [Strohmann, 1994 #932] show a decrease in resonance away from the normal resting potential with a weak increase in resonant frequency with depolarization. In neocortical cells the resonant frequency increases with hyperpolarization [Hutcheon, 1994 #934]. In guinea pig mediodorsal thalamic neurons [Puil, 1994 #935] describe a minority of neurons which show decreased damping but no change in resonant frequency with depolarization. preference

Even though subthreshold linear impedances appear in many different neurons there is a reluctance to employ them in describing neural function. The reason for this is that linearity only holds for small signals and the range of potentials over which the filter models are linear is narrow compared to the dynamic range of operation of a neuron [Koch, 1984 #922; Koch, 1987 #680]. The range of voltage over which the impedance of the squid giant axon is linear is between 1 and 2 mV around the resting potential or about 3 mV peak-to-peak (p-p). Using subjective judgment excursions of +/- 5 mV from the resting potential have been reported to be acceptable in squid giant axon [Sabah, 1969 #924; Mauro, 1970 #882]. But voltage-clamp experiments [Moore, 1980 #886] show that linearity strictly only holds within 0.27 mV of the resting potential where current responses to voltage steps were symmetric. Nonlinearity increases beyond that point but does not become significant until the voltage steps are greater than 1 mV from the resting potential. This is supported by the observation that the

harmonic distortion increases with stimulus amplitude but only exceeds 10% for stimulus signals with peak-to-peak amplitudes above 3 mV. In addition, analysis of linearized models of the Hodgkin-Huxley equations become unstable (fail) at a critical voltage of 5.35 mV [Sabah, 1970 #928; Koch, 1984 #922] above the resting membrane potential. Thus, four different criteria (stability analysis, response symmetry, harmonic distortion and subjective judgment) concur that the linear range of the filter function in squid giant axon is not more than 5 mV from resting potential.

Despite the fact that linearity is strictly valid for only a narrow portion of the full dynamic range, the errors introduced by the failure of linearity are often relatively mild. This means that the linear approximation that is valid near the resting potential can provide important, semi-quantitative information about the behavior of the neuron beyond the range of acceptable linearity. For example, estimates of the squid giant axon admittance obtained with 2 mV p-p (linearly valid range) and 8 mV p-p (linearly invalid range) perturbations differ only in the signal to noise ratio of the estimated transfer function [Poussart, 1977 #890]. Using control voltage signals outside the valid linear range did not change the estimated characteristic frequency or other gross characteristics. Similarly, Guttman, Feldman and Lecar [, 1974 #914] reported only mild deviations from linearity as the amplitude of the white noise stimulus used to measure the squid axon filter function was increases past threshold, more than 10 mV above the resting potential. The principle effect of larger noise amplitude was a decrease in damping. The characteristic frequency was only slightly affected.

The studies looking at the range of linearity mostly used square current or voltage steps. Random or pseudo-random stimulus waveforms were used in the studies that reported only minor deviations from linearity over large voltage ranges. An obvious difference between the two methods of stimulation is that with noise a variety of membrane potentials were visited briefly while the mean voltage remained constant but with constant current or voltage steps the membrane evolves from one steady state voltage-dependent impedance to another. Under these circumstances nonlinearities are apt to be more salient.

This suggests that as long as membrane potential excursions are relatively brief with respect to the settling time of the membrane conductances, the linear behavior near the resting potential will continue to be useful over wider ranges of voltages than the limits of strict steady-state linearity suggest. This conjecture is consistent with the ACT shown here (Fig. 4). Depolarization increases the resonant frequency of the membrane, but the timing of the phases of the ACT are closer to the impedance at the resting potential than depolarized potentials near threshold.

The main difference between the IRF, which describes the behavior of the membrane over a linear range of potentials, and the ACT, which describes it over a nonlinear range of potentials, is the flattening of the early phase of the IRF. The cross

correlation function between white current noise and membrane potential, a similar statistic to the IRF, behaves the same way [Guttman, 1974 #914]; as the intensity of the noise is increased the cross correlation function evolves smoothly from a form like the IRF to one like the ACT. Theirs is the only study we know of that has explored a continuum between subthreshold and suprathreshold membrane behavior. Although Bryant and Segundo [, 1976 #815] obtained an ACT showing many of these features, from which they proposed a theory of spike train genesis based on a linear filter model, they did not try to relate that filter to membrane properties or to subthreshold filter behavior.

In significantly different experiments Bialek and coworkers [, 1991 #870] looked at the relation of spike times in the H1 neuron of the blowfly which receive visual information that is gathered from several independent receptors and has passed through several synapses. Despite the dispersed and indirect access to visual information, the acceleration of the visual field can be read accurately from the H1 spike train by applying a simple linear filter similar to the ACT described here and by others. The major difference is that they make no reference to biophysical mechanisms and the filter they extract from the spike train represents a transfer function across the entire visual system. In their theoretical analysis Bialek and Zee [, 1990 #936] show how adaptive linear filters have advantages for optimally balancing conflicting operational constrains in sensory systems and suggest that linear filtering is an important aspect of information processing in nervous systems in general [Bialek, 1993 #915].

5.2 *Determinism in membrane filter function*

For a scheme like that proposed by Bialek to work, precise phase (timing) information must be preserved through the synapses in the network. The notion that at the level of a whole cell the dynamics are mostly deterministic suggests that this should be the case and the paper by Bryant and Segundo [, 1976 #815] show the ability of single neurons to respond consistently to complex stimulus patterns. The spikes usually appear at the same places in the course of repeated presentations of a single noise sample, and when this does not happen, they appear at favored alternative times. This observation has been corroborated more recently by Mainen and Sejnowski [Mainen, 1994 #937] and Bair, Koch, Newsome, and Britten [, 1994 #938].

Three conclusions may be drawn from these research threads. First, as evidence accumulates that the information in neuronal spike-trains is not simply a mean firing rate code (as reviewed in the introduction), then we must accept that the afferent stream is unlikely to be random noise. Non-random structure in both input and output should be expected. Second, although the background afferent stream may be unpredictable and of a small magnitude, there are reasons to believe it is deterministically related to

aspects of the environment, and that its shape over time is a significant source of information for neurons. Third, in order for there to be significant information in the details of the structure or timing of the input there has to be a precise and exact relation between input and output such that small details are mapped sensitively. The transforming computations of the membrane must reliably preserve details. Stated within the context of our findings, the linear perturbations must be reliably or deterministically transformed by the nonlinear behavior of the membrane. The impedance history of the membrane, as expressed variously in the IRF, ACT, CACTs, and the isopleths indicates that this transform may be quite complex, and that features of the form of the input may dissipate or be lost.

Because deterministic systems retain information about small details it is important to consider the significance of small, subthreshold signals. Some synaptic events are unquestionably large, important and reasonably well known. They have attracted a large amount of the attention of researchers over the years. But there are also many instances where there is an on-going low-level sub-threshold stream of afferent activity. Evidence that much synaptic activity is of small magnitude and can be found scattered throughout the literature even though studies of low-level background afferent activity is scarce. For example, [Fetz, 1983 #939] report monosynaptic potentials between 0.15 and 3.1 mV (mean 0.75 mV) in cat motor neurons. In rat visual cortex [Mason, 1991 #940] show a range of synaptic potentials of 0.05 to 0.5 mV. The background synaptic activity in chicken nucleus ovoidalis neurons has a p-p magnitude of about 3 mV [Strohmann, 1994 #932]. We have shown here that small subliminal currents have a significant effect on the outcome of superthreshold events (Figures 6-10).

The deterministic Hodgkin and Huxley model tells us that this is inevitable. Is it important? Yes. In the presence of a fixed synaptic event the shape of the ACT by itself provides little information about the structure of the data stream in the input circuit. The recoverable information about the noise stream is determined by the bandpass characteristics of the resting impedance which translates the local "shape" of the stimulus into changes in the timing of action potentials from unperturbed values. This necessitates consideration of the activity of the cell within the circuit. The timing of the action potential can have no meaning without defining a frame of reference. The frame of reference is provided by using events in other members of the circuit as reference points, where the spike time is defined as the interval between the pre- and post-synaptic action potentials as a cross-correlation function. The model used here is a simple circuit where there are two distinct and independent information sources, a synaptic event and an independent subthreshold source which is either a random stream to obtain the modified-ACTs or CACTs in Figs. 6-8, or a deliberately placed but sill independent impulse to obtain the isopleths in Figs. 9-10. In a sense, the

suprathreshold synaptic event provides an observational anchor with which either the input data stream or the output action-potential latencies may be analyzed.

When this information is used the spike timing is seen to contain significant information about the shape of the subthreshold afferent channel before and immediately preceding the EPSC and that this information is a faithful scaled version of the filter function which translates magnitude to postsynaptic spike latency. Comparing the CACTs obtained from the afferent- (Fig. 7) and efferent- (Fig. 8) frames of reference shows that as information is obtained about the source, the information obtained from an observation increases. Observations bound only to the efferent frame of reference are ignorant of the events yielding no action potential and this excludes an entire class of CACT from consideration.

In this situation knowledge of the interval between the action potential and synaptic event implies knowledge of the noise channel in the vicinity of the EPSC. The limit to the amount of obtainable information here is the precision of the measurement of the postsynaptic spike timing. The CACTs consists of a smooth, graded continuum so that as the precision of the timing of the spike increases there will be a corresponding increase in the precision with which the CACTs are known. Residual ignorance can be shifted between action potential timing and EPSC form, but the correlation with the noise remains constant except for the temporal offsets associated with the latencies of each class. The offset in the CACT from the class of prolonged latencies at the tail of the histogram show that information about the noise channel during the EPSC can be preserved over several milliseconds and is immune to noise after the EPSC.

To understand how these principles can be applied in real situations requires measurements of both input and output in order to ascertain how different components in a network cooperate. In the case of the blowfly, for example, [Bialek, 1991 #870], is the observed filter function a result of prefiltering by visual elements or is it a fairly direct reflection of the local electrical properties of the neuron? If linear filters are generally appropriate then the convolution of the transfer function across H1 (the ACT), with the transfer function between the visual stimulation and the afferent current should yield the overall transfer function already described.

5.3 Degeneracy

The consequences of the deterministic nature of the Hodgkin-Huxley model raises interesting problems. From a dynamical- theoretical perspective [Takens, 1981 #54; Packard, 1980 #43], the state of the membrane can be "resurrected" from a time - series of measurements of a single variable, which in typical neurophysiological experiments is usually the membrane potential. The system of coupled differential equations is internally consistent and can be used to transmit information from one cell

to another through continuous observation of only one of the variables. This may be possible in neural networks in which transmission is relatively faithfully accomplished by graded transmitter release, as has been observed in many experimental systems since there is a one-to-one mapping of an input state with an output state [Anderson, 1981 #946; Blight, 1980 #951; Davis, 1989 #947; Fain, 1977 #950; Graubard, 1983 #729; Mendelson, 1971 #948; Pearson, 1975 #952; Shaw, 1972 #949; Siegler, 1984 #944; Werblin, 1969 #629; Maynard, 1975 #942; Roberts, 1981 #945],

In the large class of neurons that communicate with one another via action potentials the output of a neuron is discontinuous and so represents a significant transformation of its input signal, and is subject to degeneracies. In following papers, we shall examine some of these transformations [Edstrom, 1994 #912; Mpitsos, 1994 #895]. The foundation of this work is presented there. On the one hand, because the Hodgkin-Huxley equations are deterministic, we expect that each unique stimulus will produce a unique response. This is indeed the case when the full four-state description is considered or even when a single state variable is monitored continuously. But, the information in spike timing alone is not complete. Consider Fig. 10 which shows the i/o curves for several different current impulses presented at a variety of different times. A horizontal line parallel to the x-axis will intersect a number of isopleths, many will be intersected two or more times. Therefore a given impulse can produce the same change in latency when presented at two different times. Worse, for any given latency change there are infinitely many combinations of impulse amplitude/presentation time which will produce that particular latency.

Thus, even the simple network that we have used here has the potential of producing a highly degenerate, infinitely many-to-one mapping of an input data stream into an output stream. A given latency may arise from any number of combinations of different impulse magnitudes and presentation times. An impulse having a given amplituded and presentation time is correlated produces a unique(V,m,h,n) state state of the membrane; e.g, compare the states for points a, c, e in Fig. 11 that all represent the same latency. But information about these states is not contained in a spike train because observing only the moment when the voltage crosses a detection threshold collapses the full state-space trajectory onto a lower, one-dimensional point. Thus, a neuron cannot transmit complete information about its internal state by spike time alone. This raises questions about how the spike time is "meant" to be interpreted.

In principle, the shift from graded neuronal connections, which are amenable to detailed phase-space analyses of their dynamics, to spiking communication between neurons is presumed to be theoretically possible [Wang, 1992 #732]. Studies using model systems and integrate-and-fire methods have addressed the problem of whether there is a deterministic relationship between the underlying continuous dynamics and threshold-generated point processes [Longtin, 1991 #1014;Preissl, 1990 #587;Sauer, 1994

#963]. Application of a number of methods to biological neural systems have obtained evidence both for deterministic and nondeterministic activity [Longtin, 1990 #1015; Schiff, 1994 #960; Schiff, 1994 #990]. Our aim here has been to understand the input/output transformation process in its simplest expression as occurs through the history of membrane changes as in a simple two-cell network. At this level of organization, our findings indicate that there is considerable loss of information about the input stream. Moreover, the findings on CACTs (Figs. 6-8) show that there is loss of information whether an observer looks from the perspective of the input or the output data streams on cell-2. Alternatively, the information may not be necessary, and degeneracy may be necessary since it gives the network enough degrees of freedom to construct a desired particular output from a variety of inputs, as circumstances dictate [Longtin, 1990 #1015; Longtin, 1991 #1014;Longtin, 1991 #1013;Mpitsos, 1986 #38; Bulsara, 1991 #1016].

In any event, this scenario is what real-life neurons may have to work with, or must have evolved membrane mechanisms or network functions that adjust to it. Here we have defined the first components of such a scenario in the linear filter dynamics of simple membrane. In specific cases, biological systems have devised ways to accommodate or adjust for such degeneracies, as shown, for example, by the fidelity of information transfer in studies of linear models of blowfly [Bialek, 1991 #870; Glantz, 1994 #919] and crayfish visual systems. However, what we know formally of dynamical systems dynamics has come largely from studies of differential and difference equations. The application of such formalism to account for the dynamics of the simple networks described here will be quite difficult, if possible at all. Subsequent papers will deal with these networks numerically to determine how the linear filter dynamics may lead both to stable and variable firing patterns. The overall aim will be to ascertain what information of the input is retained in the output of the neuron, what is lost or dissipated, and how the characteristics of neurons and of the network architecture accommodate to such loses or are able to function accurately in the face of unresolved degeneracies.

References

Adrian ED (1928) The Basis of Sensation. Norton, New York.

Anderson WW, Barker DL (1981) Synaptic mechanisms that generate network oscillations in the absence of discrete postsynaptic potentials. J Exp Zool .

Andrade MA, Nuño JC, Moran F, Montero F, Mpitsos GJ (1993) Complex dynamics of a catalytic network having faulty replication into an error species. Phys D 63:21-40.

Bair W, Koch C, Newsome WT, Britten KH (1994) Reliable temporal modulation in cortical spike trains in awake monkey. Soc Neurosci Abstr 20:525.7.

Bialek W, DeWeese M, Ricke F, Warland D (1993) Bits and brains: Information flow in the nervous system. Physica A 200:581-593.

Bialek W, Ricke F, deRuyter van Steveninck RR, Warland D (1991) Reading a neural code. Science 252:1854-1857.

Bialek W, Zee A (1990) Coding and computation with neural spike trains. J Stat Phys 59:103-115.

Blight AR, Llinas R (1980) The non-impulse stretch receptor complex of the crab; a study of depolarization-release coupling at tonic sensorimotor synapse. Phil Trans R Soc London (Biol) 290:219-276.

Bryant HL, Segundo JP (1976) Spike initiation by transmembrane current: A white-noise analysis. J Physiol 260:279-314.

Canavier C, Clark JW, Byrne JH (1990) Routes to chaos in a model of a bursting neuron. Biophys J 57:1245-1251.

Chung S-H, Raymond SA, Letvin JY (1970) Multiple meaning in single visual units. Brain Behav Evol 3:72-101.

Cole KS (1968) Membranes, Ions, and Impulses. University of California Press, Berkeley.

Davis RE, Stretton AOW (1989) Signaling properties of Ascaris motoneurons: Graded active responses, graded synaptic transmission, and tonic transmitter release. J Neurosci 9:415-425.

Diamond DM, Dunwiddie TV, Rose GM (1988) Characterization of Hippocampal Primed Burst Potentiation *in vitro* and in the awake rat. J Neurosci 8:4079-4088.

Edstrom JL, Mpitsos GJ (1995) Predicting the influence of perturbing currents on spike latencies: Determinism and degeneracy of information transfer across simple synapses. In Preparation .

Enroth-Cugell C, Robson JG, Schweitzer-Tong DE, Watson AB (1983) Spatio-temporal interactions in cat retina ganglion cells showing linear spatial summation. J Physiol 341:279-307.

Fain GL, Granda AM, Maxwell JH (1977) Voltage signal of photoreceptors at visual threshold. Nature 265:181-183.

Fetz EE, Gustafsson B (1983) Relation between shapes of post-synaptic potentials and changes in firing probability of cat motoneurones. J Physiol 341:387-410.

Fitzhugh R (1955) Mathematical models of threshold phenomena in th nerve membrane. Bull Math Biophysics 17:257.

Fitzhugh R (1960) Thresholds and plateaus in Hodgkin-Huxley nerve equations. J Gen Physiol 43:.

Fitzhugh R (1961) Impulses and physiological states in theoretical models of nerve membrane. Biophysic J 1:445-466.

French AS, Kornberg MJ (1989) A nonlinear cascade model for action potential encoding in an insect sensory neuron. Biophys J 55:655-661.

Frishman LJ, Freeman AW, Troy JB, Schweitzer-Tong DE, Enroth-Cugell C (1987) Spatiotemporal frequency responses of cat retinal ganglion cells. J Gen Physiol 89:599-628.

Gerstein GL, Mandelbrot B (1964) Random walk models for spike activity of single neurons. Biophys J 4:41.

Gimbarzevskey B, Miura RM (1986) Quantification of membrane properties of trigeminal root ganglion neurons in Guinea pigs. J Neurophysiol 55:995-1016.

Glantz RM (1994) Direction selectivity in a nonspiking interneuron of the crayfish optic lobe: Evaluation of a linear model. J Neurophysiol 71:180-193.

Glantz RM, Nudelman HB (1976) Sustained, synchronous oscillations in discharge of sustaining fibers of crayfish optic nerve. J Neurophysiol 39:1257-1271.

Glantz RM, Nudelman HB (1988) Interval coding and band-pass filtering at oculomotor synapses in crayfish. J Neurophysiol 59:56-76.

Glantz RM, Nudelman HB, Waldrop B (1984) LInear integration of convergent visual inputs in an oculomotor reflex pathway. J Neurophysiol 52:1213-1225.

Graubard K, Raper JA, Hartline DK (1983) Graded synaptic transmission between identified spiking neurons. J Neurophysiol 50:508-521.

Grüneis F, Nakao M, Yamamoto M, Musha T, Nakahama H (1989) An interpretation of 1/f fluctuations in neuronal spike trains during dream sleep. Biol Cybernetics 60:161-169.

Guttman R, Feldman L, Lecar H (1974) Squid axon membrane response to white noise stimulation. Biophys J 14:941-955.

Hodgkin A, Huxley AF (1952) A quantitative description of membrane current and its application to conduction and excitation in nerve. J Physiol 117:500-544.

Hutcheon B, Miura RM, Yarom Y, Puil E (1994) Low threshold calcium current and resonance in thalamic neurons: A model of frequency preference. J Neurophysiol 71:583-594.

Kepler TB, Abbott LF, Marder E (1991) Order reduction for dynamical systems describing the behavior of complex neurons. Morgan Kakufmann Publishers, San Mateo, CA.

Knuth DE (1981) Seminumerical Algorithms. 2nd Edn., Addison-Wesley, REading, MA.

Koch C (1984) Cable theory in neurons with active, linarized membranes. Biol Cybern 50:15-33.

Koch C, Poggio T (1987) Biophysics of computation: Neurons, synapses, and membranes. In: Edelman G, Gall WE, and Cowan WM, (ed) Synaptic Function, Wiley & Sons, New York, pp 637-697.

Krause HI, Naka K-I (1980) Spatiotemporal testing and modeling of catfish retinal neurons. Biophys J 29:13-36.

Llinas R, Steinberg IZ, Walton K (1980) Transmission in the squid giant synapse: A model based on voltage clamp studies. J Physiol Paris 76:413-418.

Mainen ZF, Sejnowski TJ (1994) Reliability of spike initiation in neocortex. Soc Neurosci Abstr 20:627.9.

Mason A, Nicoli A, Stratford K (1991) Synaptic transmission between individual pyramidal neurons of the rat visual cortex *in vitro*. J Neurosci 11:72-84.

Mauro A, Conti F, Dodge F, Schor (1970) Subthreshold behavior and phenomenological impedance of the squid axon. J Gen Physiol 55:497-523.

Maynard DM, Walton KD (1975) Effects of maintained depolarization of presynaptic neurons on inhibitory transmission in lobster neuropil. J Comp Physiol 97:215-243.

McClurkin JW, Optican LM, Richmond B, Gawne T (1991) Concurrent processing and complexity of temporally encoded neuronal messages in visual perception. Science 253:675-677.

Mendelson M (1971) Oscillator neurons in crustacean ganglia. Science 171:1170-1173.

Moore LE, Buchanan JT (1993) The effects of neurotransmitters on the integrative properties of spinal neurons in the lamprey. J Exp Biol 175:89-114.

Moore LE, Christensen BN (1985) White noise analysis of cable properties of neuroblastoma cells and lamprey central neurons. J Neurophysiol 53:636-651.

Moore LE, Fishman HM, Poussart DJM (1980) Small-signal analysis of K+ conduction in squid axons. J Membrane Biol 54:157-164.

Mpitsos GJ, Edstrom J (1995) Bifurcation dynamics and variation in computer simulation of biologically realistic neural networks. .

Nakahama H, Yamamoto M, Ishi N, Fujii H, and Aya K (1977) Dependency as a measure to estimate the order and the values of Markov .

processes. Biol Cybernetics 25:209-226.

Packard NH, Crutchfield JP, Farmer JD, Shaw RS (1980) Geometry from a time series. Phys Rev Lett 45:712-716.

Patlak J (1991) Molecular kinetics of voltage-dependent Na+ channels. Physiol Rev 71:1047-1080.

Pearson KG, Fourtner CR (1975) Nonspiking interneurons in walking system of the cockroach. J Neurophysiol 38:33-52.

Perkel DH, Schulman JH, Bullock TH, Moore GP, Segundo JP (1964) Effects of regularly spaced synaptic input. Science 145:.

Poussart D, Moore LE, Fishman HM (1977) Ion movements and kinetics in squid axon: I. Complex admittance. Ann N Y Acad Sci 303:355-379.

Press WH, Flannery BP, Teukolsky SA, Vetterling WT (1988) Numerical Recepies in C: The Art of Scientific Computing. Cambridge University Press, Cambridge, MA.

Puil E, Gimbarzevsky B, Miura RM (1986) Quantification of membrane properties of trigeminal root ganglion neurons in guinea pigs. J Neurophys 55:995-1016.

Puil E, Gimbarzevsky B, Miura RM (1987) Voltage dependence of membrane properties of trigeminal root ganglion neurons. J Neurophysiol 58:66-86.

Puil E, Meiri H, Yarom Y (1994) Resonant behavior and frequency preferences of thalamic neurons. J Neurophysiol 71:575-582.

Puil E, Miura RM, Spiegelman I (1989) Consequences of 4-aminopyradine applications to trigeminal root ganglion neurons. J Neurophysiol 62:810-820.

Rall W (1977) Core conductor theory and cable properties of neurons. .

Roberts A, Bush BMH (1981) Neurones Without Impulses. Cambridge University Press, Cambridge.

Rose GM, Dunwiddie TB (1986) Induction of Hippocampal long-term potentiation using physiologically patterned stimulation. Neurosci Let 69:244-248.

Sabah NH, Leibovic KN (1969) Subthreshold oscillatory responses of teh Hodgkin-Huxley ca ble model for the sqid giant axon. Biophys J 9:.

Sabah NH, Spangler RA (1970) Repetitive response of the Hodgkin-Huxley model for the squid giang axon. J Theor Biol 29:155-171.

Sakuranaga M, Naka K-I (1983) Signal transmission in the catfish retina. III. Transmission to typs-C cells. J Neurophysiol 53:411-427.

Sakuranaga M, Naka K-I (1985a) Signal transmission in the catfish retina. I. Transmission in the outer retina. J Neurophysiol 53:373-389.

Sakuranaga M, Naka K-I (1985b) Signal transmission in the catfish retina. II. Transmission to type-N cell. J Neurophysiol 53:390-410.

Segundo JP, Moore GP, Stensaas LJ, Bullock TH (1963) Sensitivity of neurones in *Aplysia* to temporal pattern of arriving impulses. J Exp Biol 40:643-667.

Segundo JP, Perkel DH, Wyman H, Hegstadt H, Moore GP (1968) Input-output relations in computer-simulated nerve cells. Kybernetik 5:157-171.

Shannon CE (1948) The mathematical theory of communication. Bell Syst Tech J 27:379-423.

Shaw SR (1972) Decremental conduction of the visual signal in barnacle lateral eye. J Physiol 220:145-175.

Siegler MVS (1984) Local interneurons and local interactions in Arthropods. J Exp Biol 112:253-281.

Stearns SD, David RA (1993) Signal Processing Algorithms in Fortran and C. Prentice-Hall, Inc., New York.

Stein RB, French AS, Holden AV (1972) The frequency response, coherence, and information capacity two neuronal models. Biophys J 12:295-322.

Strohmann B, Schwartz DW, Puil E (1994) Subthreshold frequency selectivity in avian auditory thalamus. J Neurophysiol 71:1361-1372.

Takens F (1981) Detecting strange attractors in turbulence. In: Rand DA, and Young LS, (ed) Dynamical Systems and Turbulence, Vol. 898. Springer-Verlag, Berlin, pp 366-381.

Tsukada M, Aihara T, Mizuno M, Kato H, Ito K (1994) Temporal pattern sensitivity of long-term potentiation in hippocampal CA1 neurons. Biol Cybern 70:495-504.

Wang X-J, Rinzel J (1992) Alternating and synchronous rhythms in reciprocally inhibitory model neurons. Neural Commputation 4:84-97.

Werblin FS, Dowling JE (1969) Organization of the retina of the mud puppy, *Necturus maculosus*. J Neurophysiol 32:339-355.

Wolf A, Swift JB, Swinney HL, Vastano JA (1985) Determining Lyapunov exponents from a time series. Physica 16D:285-317.

Yamamoto M, Nakahama H (1983) Stochastic properties of spontaneous unit dischargess in somatosensory cortex and mesencephalic reticular formation during sleep-waking states. J Neurophysiol 49:1182-1198.

FIGURE LEGENDS

FIGURE 1: White noise analysis of complex impedance Z. A: Comparison of impedance-plane plots of the normal, depolarized and hyperpolarized membrane with 0.05 msec time step at three membrane potentials. The open circles designate data from the normal resting potential (E_m= - 63.32 mV); filled triangles are for the hyperpolarized membrane (E_m = -66.40 mV using sustained current of -9.5 x 10^{-11} Amp) and open triangles is for depolarized membrane (E_m = -60.208 mV using sustained current of 13 x 10^{-13} Amp). White noise current was subthreshold for spike genesis in all cases. B: The vector length or magnitude of Z as a function of frequency. Filled and open circles are for the data presented in (C) at normal membrane polarization. C: The vector Z as a plot of reactance vs. resistance for two integration step sizes at the normal membrane potential. Open circles are for step = 0.05 msec; filled circles are for step = 0.10 msec. D: The phase of Z (vector angle in (A and C)) as a function of frequency. Symbols are as in (A-C).

At the normal resting potential there is a significant resonant peak at about 40 Hz that is shifted up to 55 Hz when the membrane is depolarized and down to 30 Hz when it is hyperpolarized. Above 300 Hz the modeling process introduces some phase distortions. In D the phase reaches a minimum around 300 Hz and then angles back up. This distortion is more severe for the simulation using a 0.1 msec time step than for the simulation using a 0.05 msec time step. There is no apparent difference between the two at frequencies below 300 Hz.

Typical Current (all cases; example is from 0.05 msec time step simulation, N = 16384):
Mean: 1.5493 x 10^{-14} Amps.   SD: 4.1111 x 10^{-13} Amps.   Max: 1.5443 x 10^{-12} Amps.

                                                                  Min: -1.4915 x 10^{-12} Amps.

Typical Voltage responses:

Mean (normal):	-0.063319 Volts.	SD: 7.9827 x 10^{-6} Volts.
Max:	-0.063293 Volts.	Min: -0.063342 Volts.
Mean (depolarized):	-0.060208 Volts.	SD: 8.0384 x 10^{-6} Volts.
Max:	-0.060182 Volts.	Min: -0.060232 Volts.
Mean (hyperpolarized):	-0.066403 Volts.	SD: 7.3067 x 10-6 Volts.
Max:	-0.066378 Volts.	Min: -0.066425 Volts.

The cell was injected with white noise for 0.8192 sec in all cases (8192 points @ 0.1 msec integration steps; and 16384 points @ 0.05 msec integrations) so that the minimum resolvable frequency step is 1.2207 Hz. The Nyquist frequency was 10 kHz with 0.05 msec and 5 kHz with 0.1 msec time steps.

FIGURE 2: Time course of the impulse response function (IRF): back transformation of the complex impedances shown in Fig. 1. Circles show every 10th point in a five-point center weighted running mean of the IRF from normal. The running average is needed to suppress high frequency noise, remnants of which can be seen on the two curves, resulting from phase distortions at the high frequency end of the spectrum.

FIGURE 3: Noise-activated action potentials. Two time scales are shown. The top trace is an expansion of the region in the lower trace noted by the dashed lines, and shows example of spike intervals that were excluded from the computation of the ACT. Current was injected continuously. Mean noise: -1.676 x 10^{-13} Amp; SD = 3.73 x 10^{-10} Amp, Time step = 0.05 msec.

FIGURE 4: Time course of the ACT. Vertical axis: average current. Horizontal axis: time preceding the occurrence action potentials; N = 30,000. Mean current Mean noise: -1.676 x 10^{-13} Amp; SD = 3.73 x 10^{-10} Amp. Dashed horizontal lines: 96% Confidence Limit, $CL = 2\left(\frac{SD}{\sqrt{N}}\right)$ = Mean ± 4.3 x 10^{-12} Amp. The analysis was on the same time series as shown by the excerpt in Fig. 4. This shows clearly that the average stimulating membrane current has a complex three-component waveform lasting approximately 30 msec before the occurrence of the action potential. The first component (0 to 5 msec preceding the action potential) is depolarizing. The second (5 to 20 msec) is hyperpolarizing, and the third, just barely above the 96% confidence limit, is depolarizing. Since the autocorrelation function of the injected current is flat, except for the first 7 points, these correlations between the action potentials and their preceding history of membrane currents are introduced by the membrane. The time course of the first two components is identical to the time course of the two components obtained in the IRF. The third is only slightly depolarizing, and is not observed in the IRF.

FIGURE 5: Effects produced by the three phases of the ACT. The waveshape and amplitude of the three phases of the ACT were used as stimuli for injecting current into the cell. A: Membrane potential. B: Full ACT wave shape. C: ACT with phase three removed. D: Phase one of the ACT. Thick line in the voltage trace is the response to phase three. Thin line is the combined responses to the full ACT and the ACT less phase three.

FIGURE 6. Modified ACTs: In the next three illustrations, EPSC-evoked action potentials will be used to examine the effect of subthreshold noise stimulation. A: Low and high noise modified ACTs in which random stimulation is paired with an EPSC. B: Synaptic ACTs. 60,000, 35-ms simulation sweeps were conducted in which random noise perturbation was paired with an EPSC in each sweep. Since the synaptic ACT is calculated using the timing of the action potential, the preceeding currents of the EPSC are shifted from one sweep to the

next, causing a slurring of the synaptic currents. C and D: Frequency histograms of latencies obtained with low and high noise levels. The integration step size was 0.001 msec. In order to show an expanded scale, the traces here, and in Figs. 7 and 8, are of 1500 integration-step excerpts. In each sweep a different seed was used to generate pulses having random amplitude variation (same parameters as used in Fig. 5). At 25 ms into each sweep a single EPSC was given that had $G_{syn} = 3 \times 10^{-8}$ Siemens. Each EPSC generated and action potential whose latency was defined using the start of the sweep as time zero.

FIGURE 7: Average currents can be calculated from the input-stream frame of reference using modified-ACTs contingently. The latencies used in the low- and high-noise experiments of Fig. 6 were placed into 5 histogram bins having equal occupancy. Each range of latencies provided the contingency for selecting the particular noise-sweeps to use in the averages. A and C: Modified-contingent ACTs (modified-CACTs) for low and high noise. All are scaled selectively for each latency bin. Trajectories producing the longest latencies dip most negatively near the EPSC, and those generating the shorter latencies deflect more positively. B and D: Synaptic CACTs for all latency are equivalent to the EPSC. Averages obtained using only the output frame of reference (Figs. 5 and 6) lose information about the input perturbations and of timing of the EPSC. This information was uncovered by forcing the data into the histogram. This information is lost to an observer who has information only about the spike intervals generated in the postsynaptic neuron.

FIGURE 8. Observing spike latencies from the frame of reference of the output data-stream using modified-CACTs. Same histogram data as used to construct Figs. 6 and 7. A: Modified-CACTs constructed using the action potentials as the reference point. B: Synaptic ACTs corresponding to each trajectory in (A); the numbers used to identify the synaptic trajectory progress serially and are matched with the numbers in (A). C and D: Same as in (A and D) but with a higher level of random noise. The relative timing between the classes of spike latencies and the corresponding noise currents is retained. But information is lost between the timing of the occurrence of the EPSC and the action potential.

FIGURE 9. Weak preconditioning current pulses affect EPSC-evoked action potential latencies after membrane potential changes occurring in response to the pulses have almost died out. A: Preconditioning current pulse duration: 0.010 msec, given at 5 msec. Dashed line: hyperpolarizing pulse. Dotted line no preconditioning pulse. Thick-solid line: depolarizing pulse. Note that the membrane potential has recovered before the onset of the EPSC which occurs at 11.16 msec. B: Same as (A) but at different scales, showing the EPSC and the action potentials; dotted, dashed, and thick-line traces are for the same conditions as in (A). C: Membrane response to a hyperpolarizing pulse; EPSC onset is indicated by the thin vertical line. D and E: Time course of changes in the potassium gate n and sodium gate

m during the voltage time course shown in (C). Magnitude of the current pulses (±) 1 x 10⁻⁹ Amp. Integration time step = 0.010 msec.
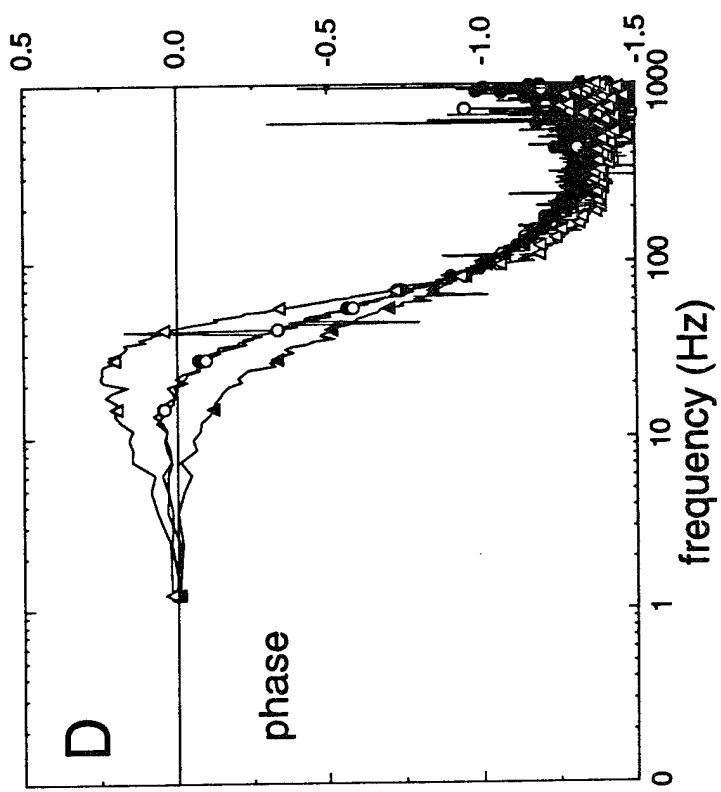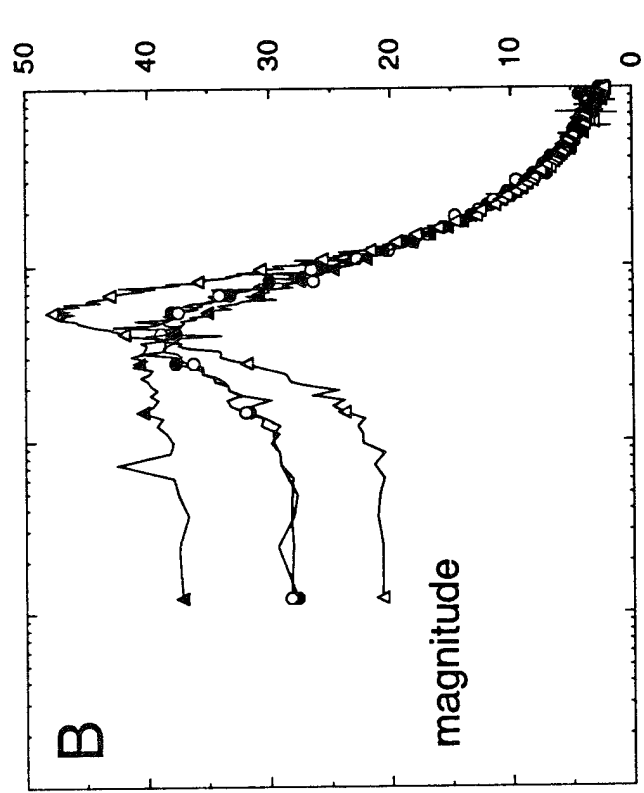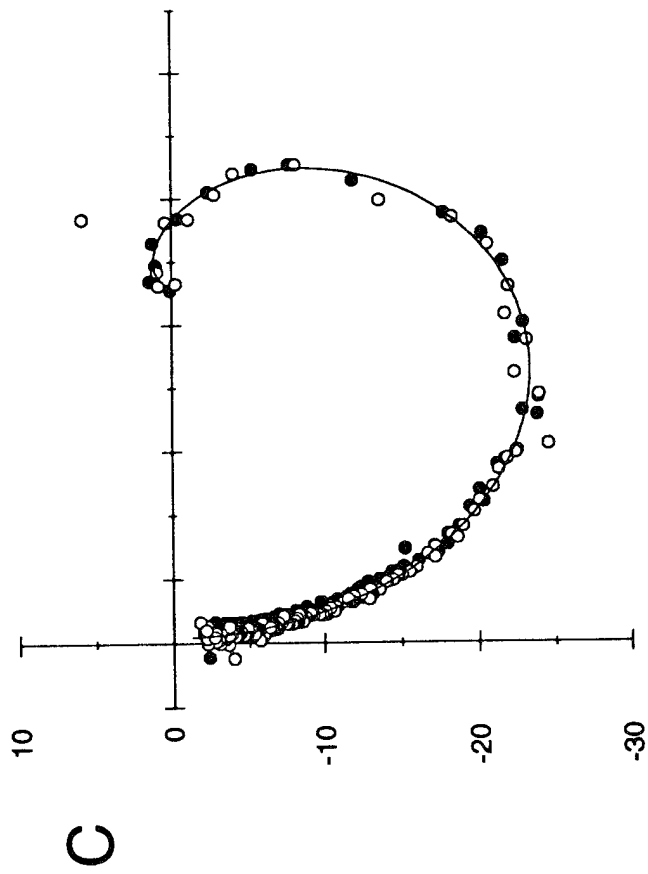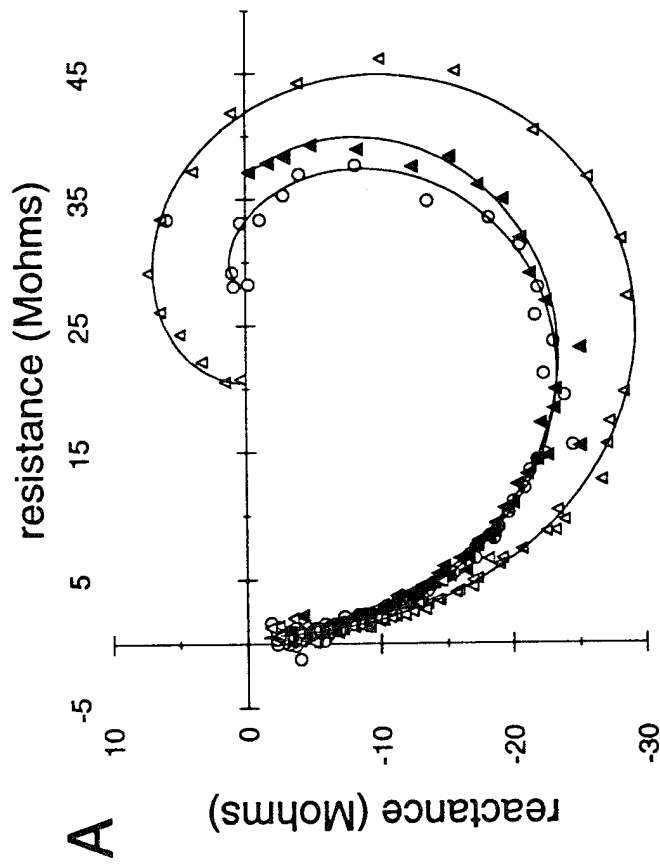
FIGURE 10: The timing of single preconditioning current pulses produces complex changes in action potential latencies. In each 40 msec sweep of the simulation a single pulse was given before the onset of the EPSC. A: Onset (24 msec) and time course of the EPSC. B: Action potential produced by the EPSC in the absence of a preconditioning current pulse. C and D: latencies of action potentials produced in hyperpolarized and normal membrane to depolarizing (solid curves) and hyperpolarizing (dotted) current pulses; hyperpolarization used here is the same as in Figs. 1 and 3. Each curve was obtained using a different amplitude of the current pulse. The incomplete lines in some of the negative current isopleths indicate suppression of the EPSC-evoked action potential at those current/time combinations. The interval between the points on the curves is 250 msec. The amplitude for the five 0.010 ms depolarizing and hyperpolarizing current pulses was, in multiples of 10^{-10} Amp: (±) 2, 4, 6, 8, 10. G_{syn} = 3 x 10^{-8} Siemens at the normal resting potential and 4.0536 x 10^{-8} Siemens at the hyperpolarized potential, a value chosen by trial and error to give the same unperturbed action potential latency as the normal control EPSC. Integration time step = 0.010 ms.

FIGURE 11. Relationship of i/o curves to the *m* and *n* gate dynamics. A: Two i/o curves or isopleths obtained using ± 10 x 10^{-10} Amp pulses. Labeled points: a, the normal unperturbed resting state; b, the point of maximum action potential advance at 19 ms; c, the null point of no effect (22.44 ms); d, the point on the zero isopleth corresponding to the pulse-presentation time that yields the maximum retardation (26 ms; in this case, the action potential is suppressed entirely and the point *d* does not exist on the -10 x 10^{-10} isopleth); and e, the terminal point of no effect that corresponds to the moment the membrane potential crosses the criterion threshold (-30 mV). In the absence of perturbing influences the action potential crosses that threshold at 30.96 ms. The EPSC begins at 25 ms. B: Medium close-up of the *m-n* phase plane. Trajectories to the left of the control (dotted) trajectory are advanced (reduced latency) and the trajectories to its right are retarded (increased latencies). At this magnification the state of the membrane is roughly the same at points *a*, *b*, and *c*. The state at point *d* (26 ms into the simulation) is different than at *a*, *b*, or *c* because the EPSC precedes it. Point *e* labels the *m-n* state when the membrane crosses the spike-detection threshold (-30 mV). C: Initial section of the trajectories in (B). D: Extreme close-up of the foot of the trajectories in (B) where points *a*, *b*, *c* are also the same as those leveled in (B). Arc *acb* is the trajectory of *m-n* states that are produced by a -10 x 10^{-10} Amp pulse when no EPSC is given. Trajectories are also shown for the *m-n* states that emerge in time for action potentials that are most advanced (solid line emerging upward from point *b*) and for a control
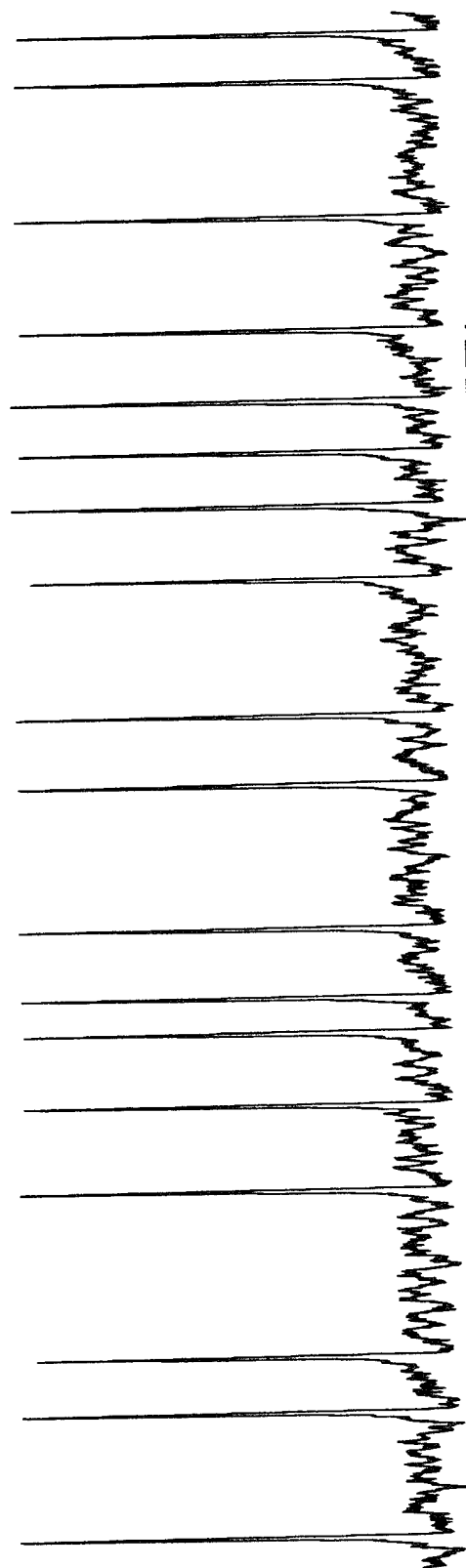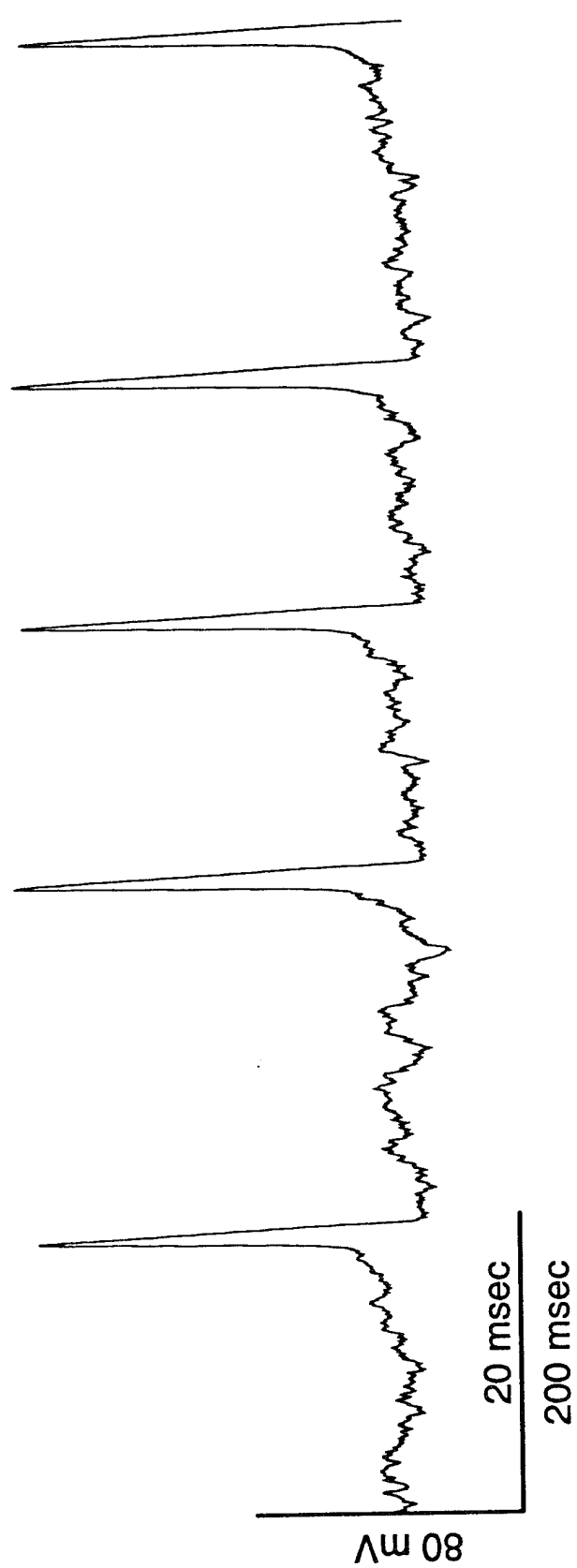
trajectory in which the EPSC is not paired with a conditioning pulse (dots emerging from point a). Point a is also the take-off point for the trajectory relating to action potential latencies that are most delayed(dashes overlying the dots). This trajectory diverges from the control when the conditioning pulse is presented at 26 ms into the simulation, 1 ms after the onset of the EPSC. When using paired pulse/EPSC stimulation, trajectories originate along the baseline arc, starting successively from point a (25 ms before the EPSC) and progress toward point b .

FIGURE 12. Stretching of m-n phase space in time after the onset of the EPSC. A: Base arc of open-circle points are take-off positions on the acb arc shown in Fig. 10D for a selected number of trajectories; this arc represents the state of the membrane just before the onset of the EPSC. Dashed line: trajectory emerging from point c. Solid line: trajectory emerging from point b. Dashed line: trajectory emerging from point a. A-D: Time-slices at selected times after the onset of the EPSC. The range of phase space dimensions are the same in all panels in order to show the stretching of the loops in time. In panel B, the time slices have been taken just after the separatrix (see Fig. 12) of m-n states that are above and below the level for generating action potentials. Thus, the bottom-most solid line now represents the trajectory of the most retarded action potential latency (here the spike is aborted), and the control trajectory is now shown by the point lying between the two solid lines.

FIGURE 13. Separatrix between phase-space states for spiking and nonspiking membrane. A: Membrane potential obtained using a 0.001 ms depolarizing pulse that way just suprathreshold ($512.3152366087 \times 10^{-15}$ Amp) and subthreshold ($512.3152366086 \times 10^{-15}$ Amp) for generating an actin potential. B: Phase space states of gates m and n relating to the membrane potential traces shown in (A). C: High-gain phase space of spiking and non-spiking regions in (B). D: The initial portion in (C) is shown at an even higher gain as the in m-n phase space as the separatrix between trajectories that led to action potentials and those that do not. These trajectories (shown by the) solid, dotted, and small-dash lines are these same as the trajectories labeled $a,b,c,$ and d in Fig. 10. Integration step = 0.001 ms.
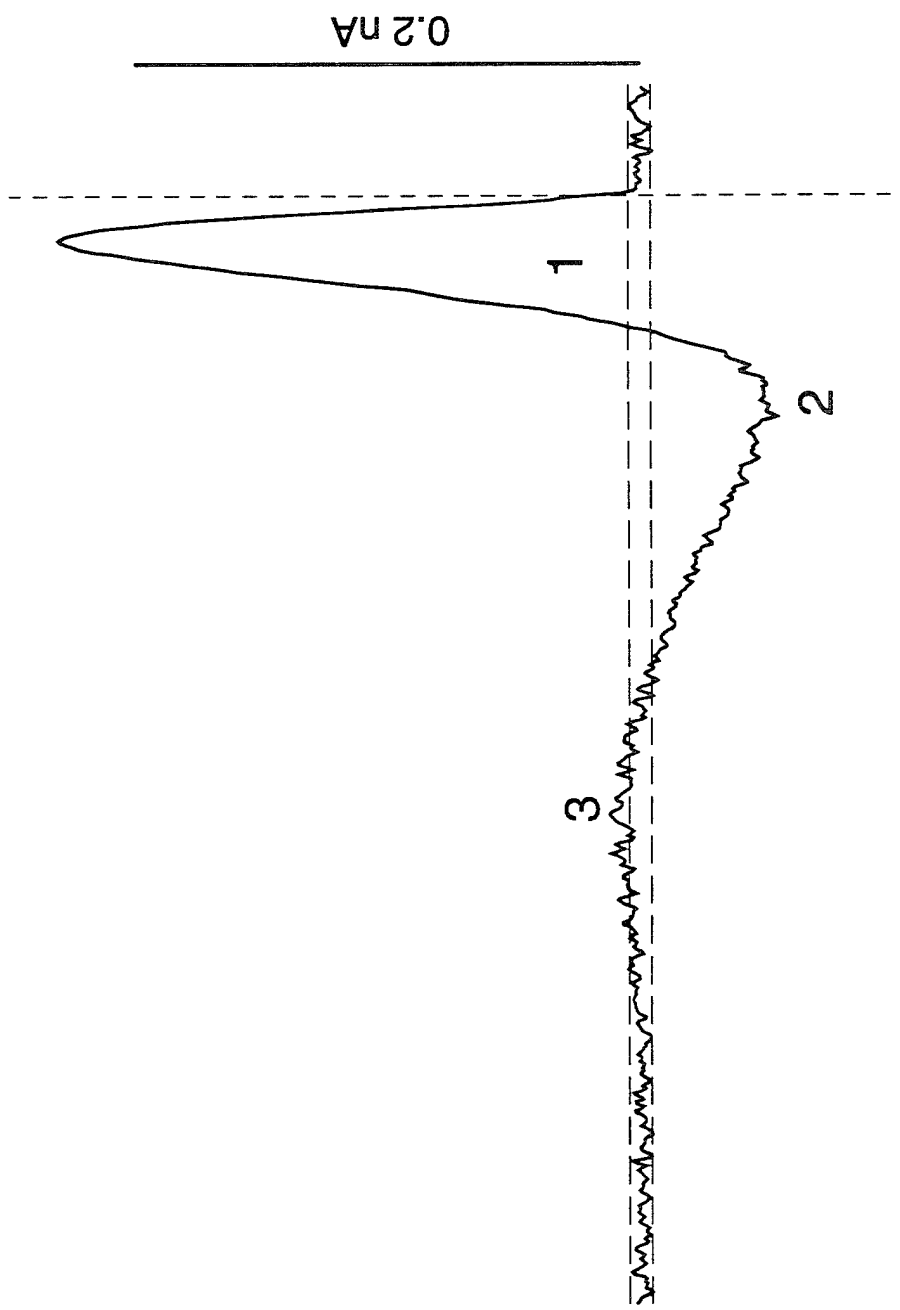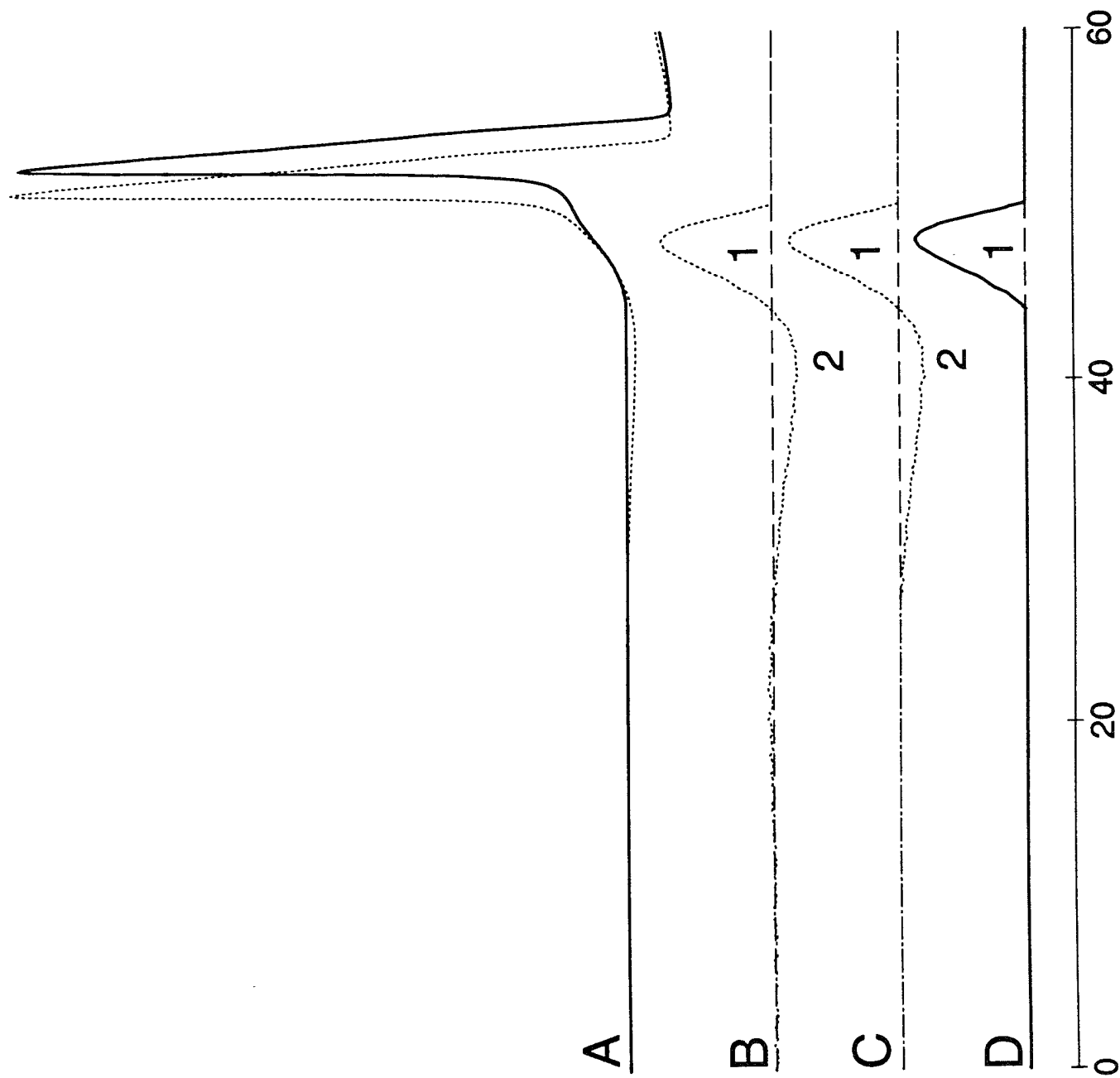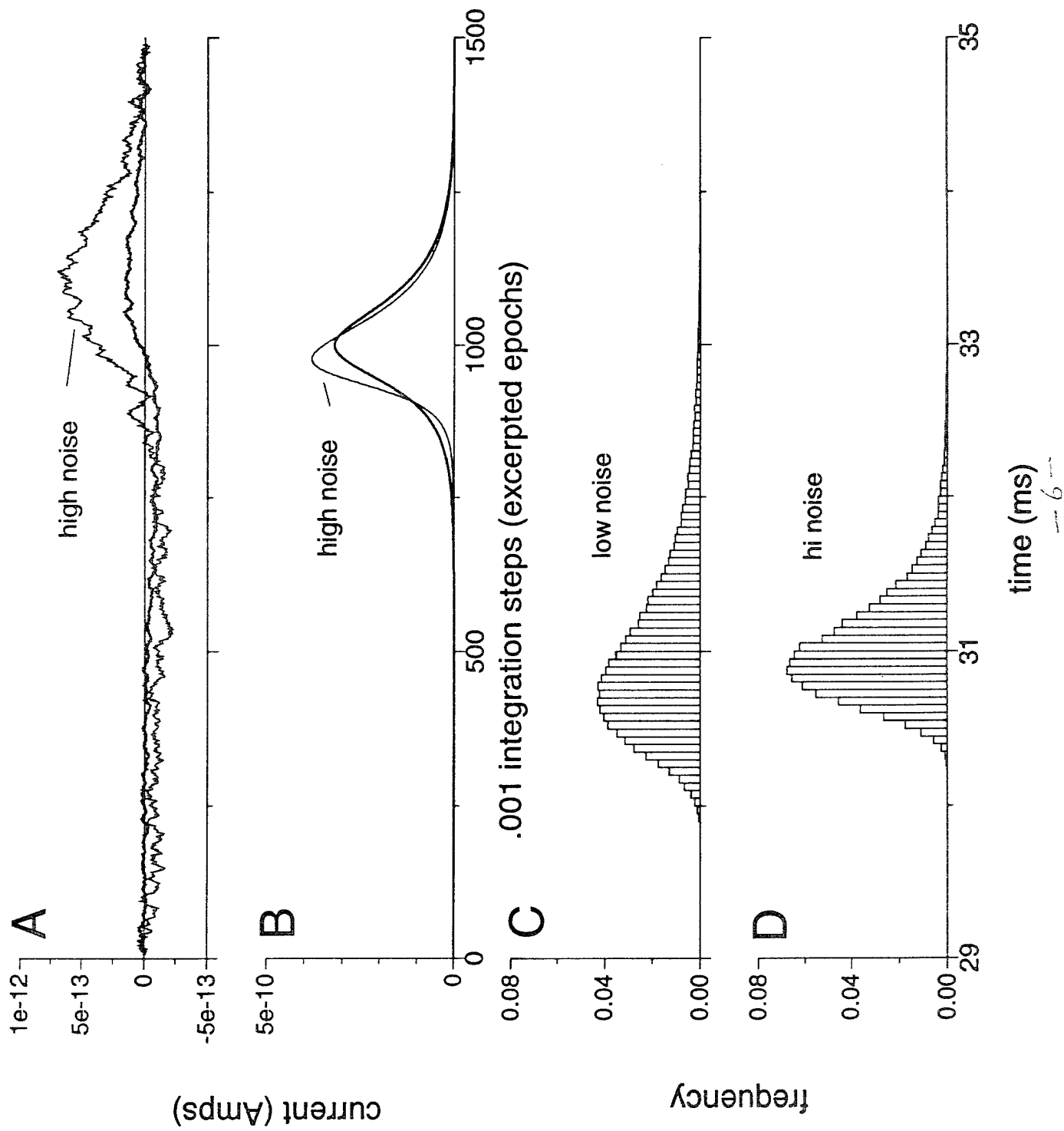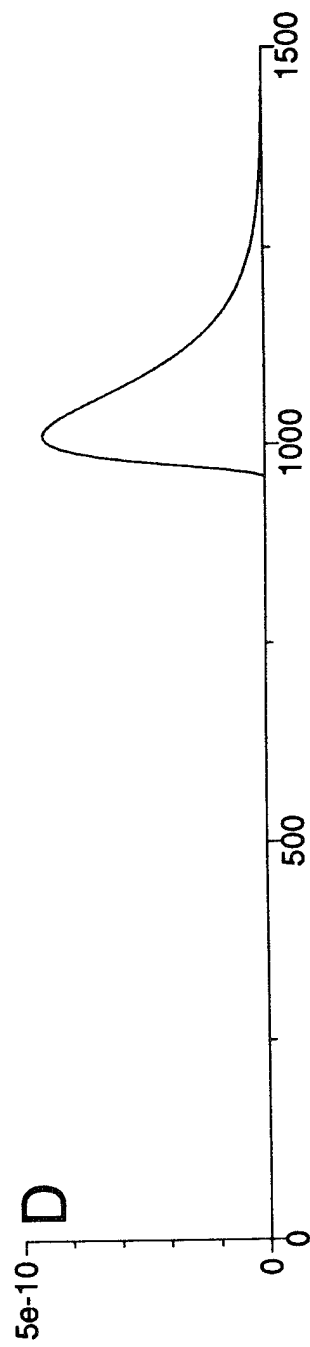
A

resistance (Mohms)

reactance (Mohms)

B

magnitude

C

D

phase

frequency (Hz)

– / –

IFFT(Z)

20 msec

80 mV

20 msec

200 msec

0.2 nA

20 msec

1

2

3

msec

A

B

C

D

0   20   40   60

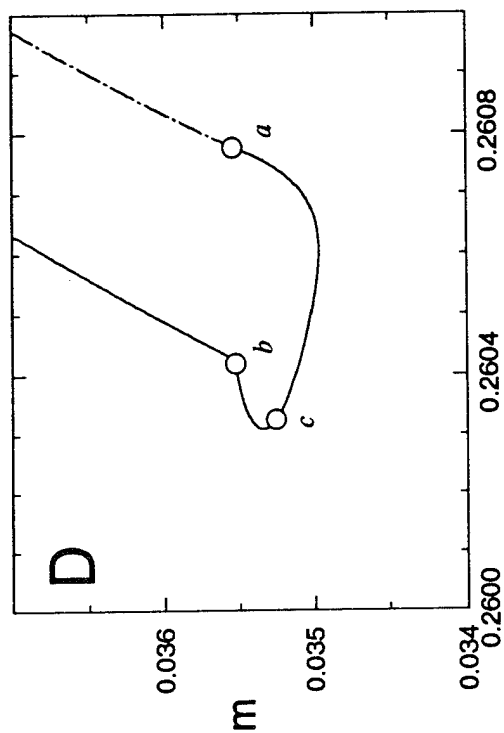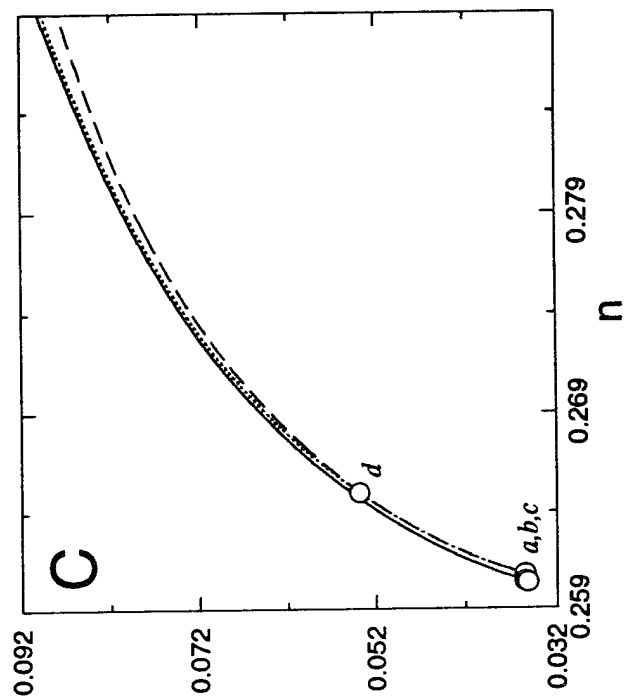**A**

current (Amps)

1e-12
5e-13
0
-5e-13

high noise

B

5e-10
0

high noise

.001 integration steps (excerpted epochs)

0   500   1000   1500

C

frequency

0.08
0.04
0.00

low noise

D

0.08
0.04
0.00

hi noise

29   31   33   35

time (ms)

A

low noise

B

C

high noise
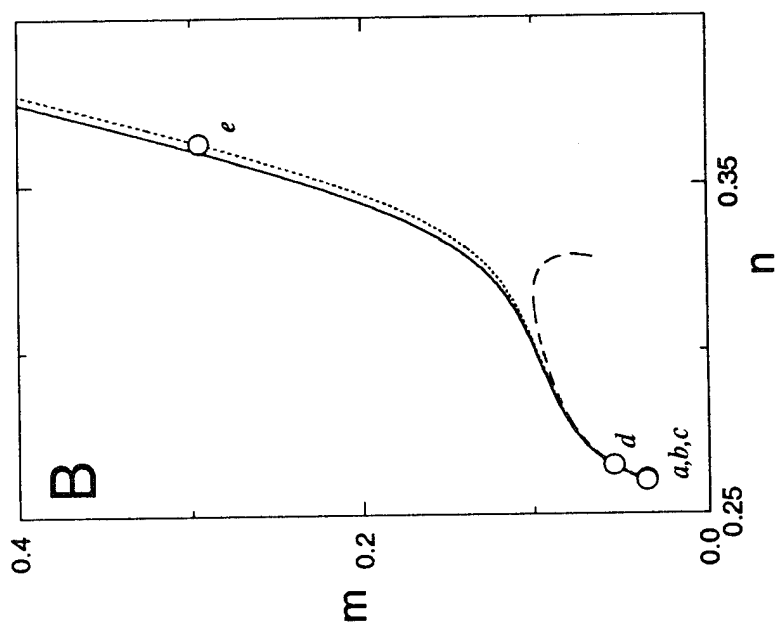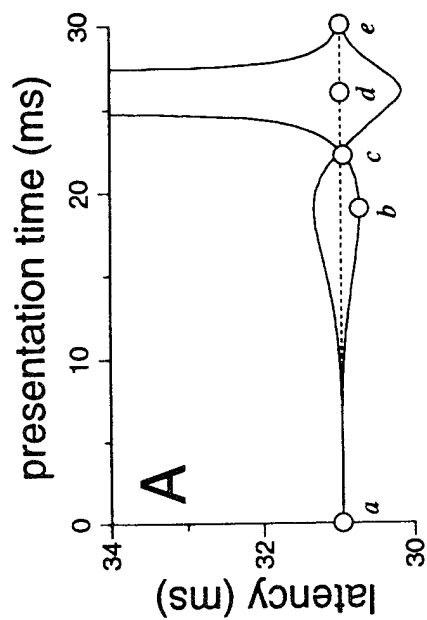
D

3.5e-12

-3.5e-12

5e-10

0

3.5e-12

-3.5e-12

5e-10

0

0   500   1000   1500

.001 integration steps (excerpted epochs)

current (amps)

low noise

high noise

.001 integration steps (excerpted epochs)

current (Amps)

~ /0 ~

legend:
······· no perturbation
——— -10 @ 19 msec
– – – -10 @ 26 msec
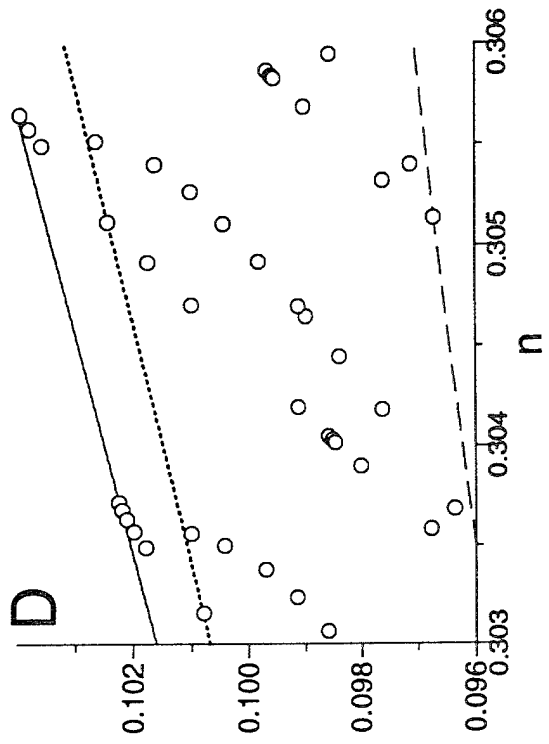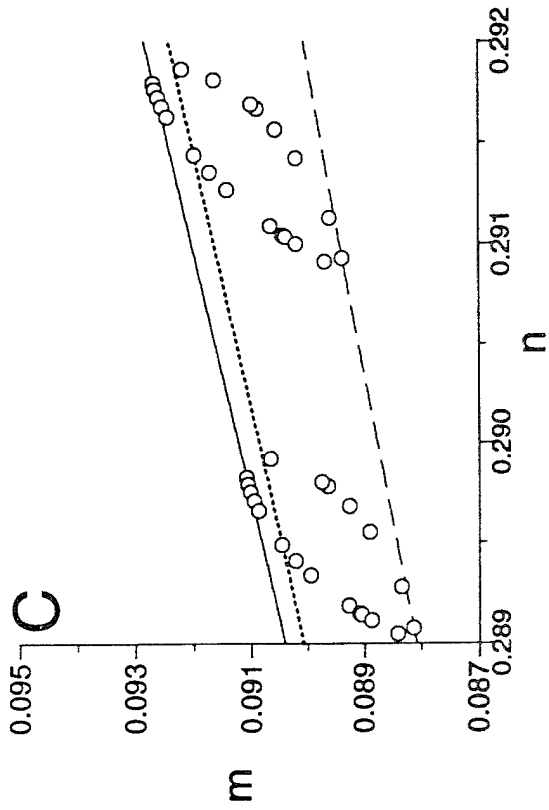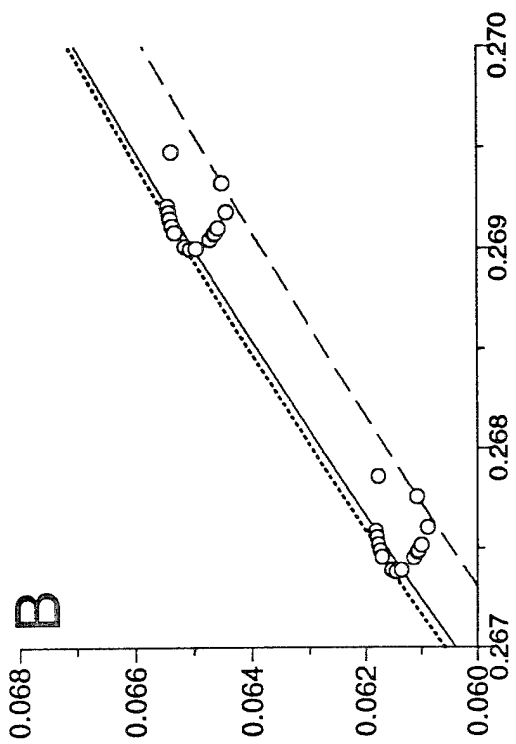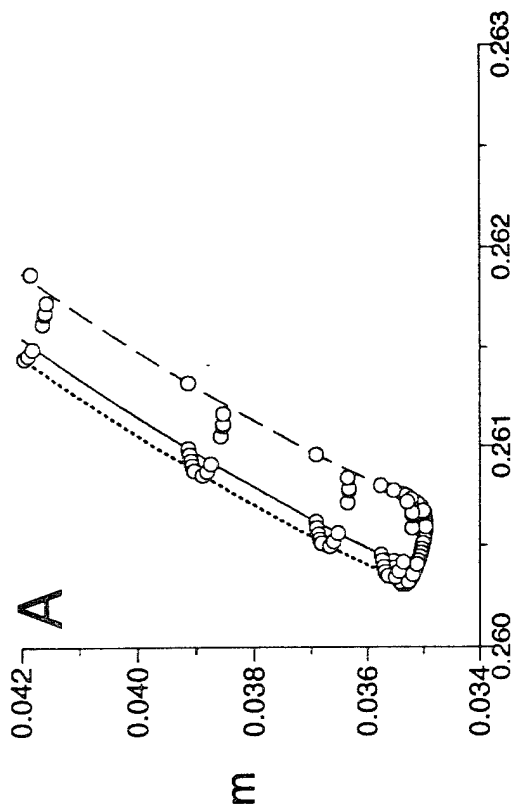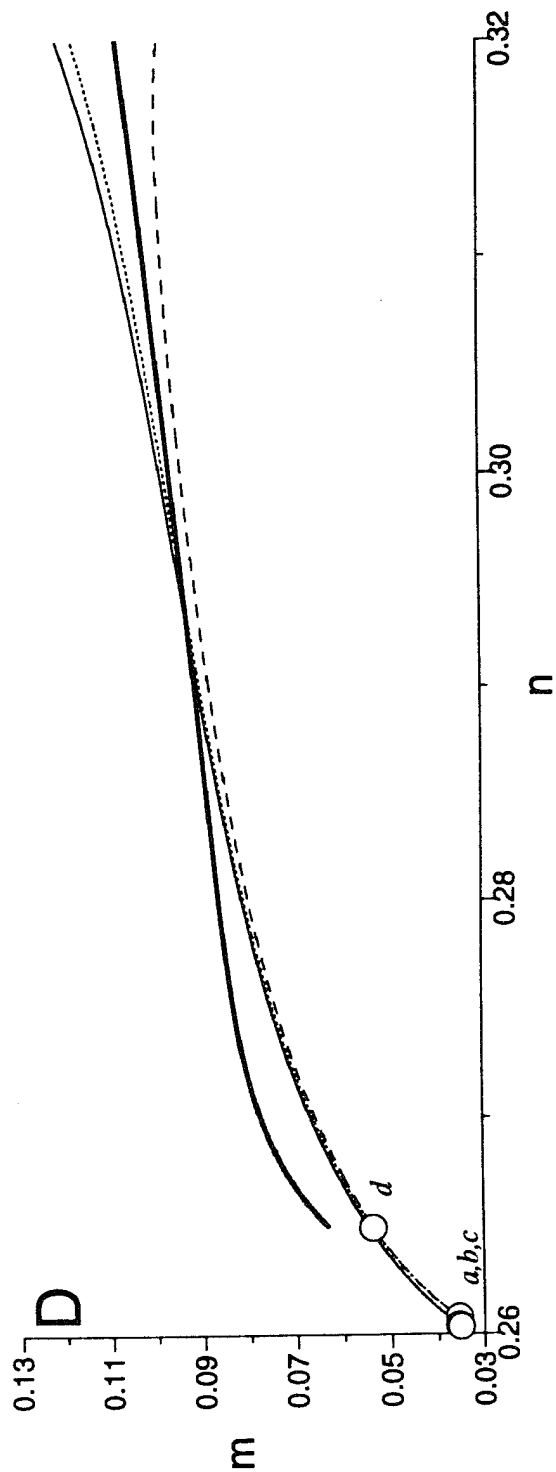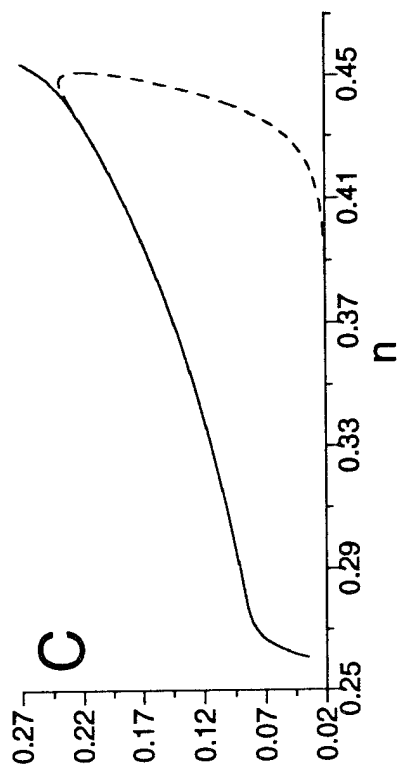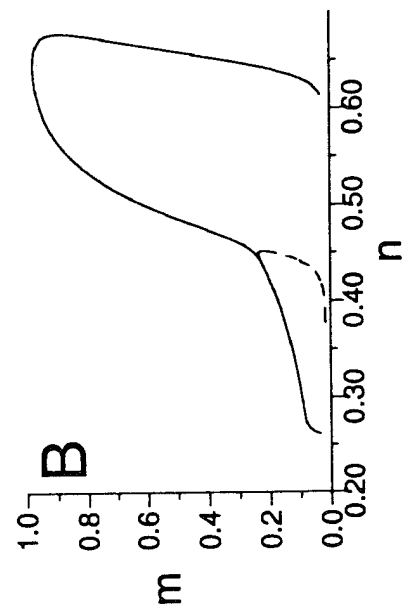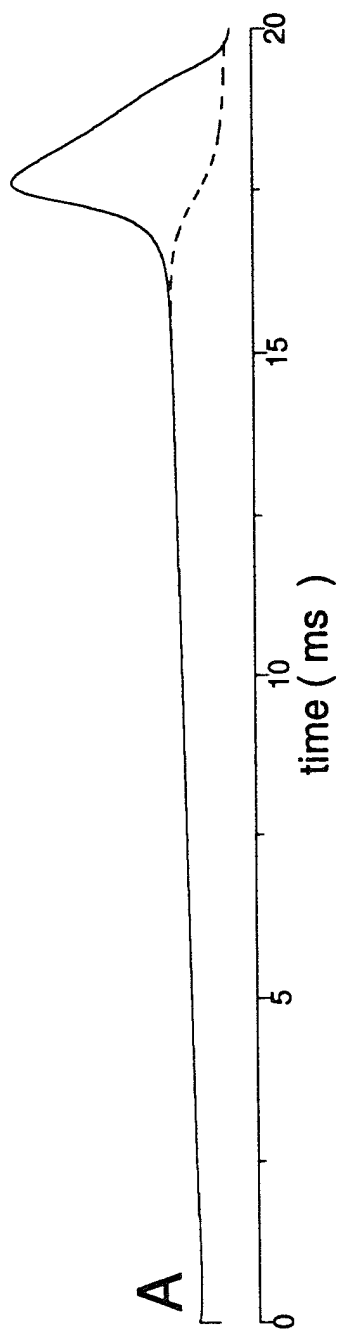
A

presentation time (ms)

latency (ms)

34 32 30

0 10 20 30

a b c d e

B

m

0.4

0.2

0.0

n

0.25 0.35

a,b,c d e

C

m

0.092 0.072 0.052 0.032

n

0.259 0.269 0.279

a,b,c d

D

m

0.036 0.035 0.034

0.2600 0.2604 0.2608

a b c

-12-

A

B

C

D

time (ms)

m

n

m

n

m

n

a,b,c

d

—/3—

Simple Neuronal Membrane is Sensitive to the Temporal Structure of Input Signals

By

John Edstrom

and

George J. Mpitsos

Oregon State University
The Mark. O. Hatfield Marine Science Center
Newport, OR 97365
USA

ABSTRACT. We have examined how a Hodgkin-Huxley model of the squid axon membrane responds to patterned stimulation. The present work extends the methods reported in the accompanying paper whereby a single, low-level current impulses is used in each simulation to perturb the latency of action potentisls (spikes) evoked by an excitatory postsynaptic current (EPSC). A chaotic logistic function controlled the presentation time (or the amplitude) of the impulse. Over a number of simulations, the change in the timing of the impulse provided temporally structured trains of stimuli that could be compared to the changes in the latency of the EPSC-evoked spikes. At fixed presentation times, spike latencies were found to be a linear function of the amplitude of the perturbing impulse. This yielded a temporal structure in the sequence of spike latencies that was similar to the structure in the sequence of different impulse amplitudes. Using fixed impulse amplitudes and presenting them at different times produced complex sequences of spike latencies. The output pattern was significantly distorted by comparison to the input and is transformed into a higher phase-space dimension. The distortions are attributable to the shape of the functions relating the timing of the perturbation to the latency of the action potential which we examined in the preceding paper with respect to membrane impedance under perturbation. Using two perturbing impulses in each sweep, one having a fixed timing and one variable, produced amplitude changes in the distortion but no new distortions. Owing to the sensitivity of the membrane to stimulus patterns, multiple, temporally varying input stimuli would produce complex firing patterns. Together the findings reported here and previously provide evidence both for deterministic and nondeterministic pattern detection and generation in single neurons.

1 *Introduction*

A large body of research has indicated that structure in the temporal firing of action potentials in neurons may provide a basis of information transfer between neurons rather than, or in addition to, other response characteristics, such as the mean firing frequency, e.g., (Adrian, 1928; Diamond, et al., 1988; Gerstein and Mandelbrot, 1964; Glantz and Nudelman, 1976; Glantz and Nudelman, 1988; Glantz, et al., 1984; Grüneis, et al., 1989; Nakahama, et al., 1977; Perkel, et al., 1964; Rall, 1977; Rose and Dunwiddie, 1986; Segundo, et al., 1963; Tsukada, et al., 1994; Yamamoto and Nakahama, 1983). Along this line, the aim of the simulations reported in the preceding paper was to establish a foundation defining how membrane impedance, acting as a linear filter, might provide the mechanism for pattern detection and generation in simple neuron membrane (Edstrom and Mpitsos, 1995). We examined the ability of a simple neuron to generate synaptically-evoked action potentials under conditions when the impedance state of the membrane had been preconditioned using the injection of brief low-level current impulses. The neuronal membrane characteristics were defined using the Hodgkin-Huxley (1952) parameters for sodium and potassium ion channels. An excitatory postsynaptic current (EPSC) was used whose effect was simply to produce smoothly changing unimodal membrane changes having the time course of the squid giant synapse. The temporal history of impedance changes that occur between the perturbing impulse and the EPSC-evoked action potential (spike) had complex structure that resembled i/o functions obtained using sub- and suprathreshold white-noise perturbation methods of neurons in a number of animals (Bryant and Segundo, 1976; Guttman, et al., 1974; Sakuranaga and Naka, 1983; Sakuranaga and Naka, 1985a; Sakuranaga and Naka, 1985b). The findings are consistent with the possibility, also proposed in animal studies, that membrane may a act as a linear filter for pattern detection or generation e.g., (Bialek, et al., 1993; Bialek, et al., 1991; Enroth-Cugell, et al., 1983; Frishman, et al., 1987; Glantz, 1994; Glantz, et al., 1984; Krause and Naka, 1980). Our findings also suggested that the same i/o functions may impose a form of degeneracy in the transfer of information across the synapse.

In the present paper we extend these studies to show that the postsynaptic neuron responds differentially when the same input pattern is presented at different regions of the temporal span of the i/o function. However, depending on the timing of the input stimuli, the output spike patterns exhibit distortions

and increases in complexity by comparison the same measures of the input pattern. Such differences include multiple folding regions in the return maps (phase-space autocorrelations of one spike latency against the preceding one in the time series) that require increases in phase-space embedding to resolve some of the degeneracies. The aim here will be to show these effects graphically. Papers that follow will report on quantitative measures of spike trains using information-theoretic methods and symbolic dynamics.

2 Methods and Results

Except for the the addition of a chaotic logistic function to control the presentation of the perturbation current impulses, methods used in the present series of experiments were the same as those reported in the preceding paper (Edstrom and Mpitsos, 1995). A two-cell network was used in which the presynaptic neuron activated the postsynaptic by means of an EPSC. A single low-level delta-function current impulses, lasting one integration step, was presented to the postsynaptic cell in each 35 ms simulation sweep. The impulse was presented in some temporal relationship with an EPSC whose onset was at 25 ms. The membrane potential was reset to the normal resting potential after each sweep. The impulses were well below the firing threshold of the membrane, whereas the EPSC was suprathreshold and generated a single action potential. In the last set of experiments reported here, two impulses were given, one acting as a preconditioning stimulus to the other. In both sets the aim is to examine the effect of the conditioning impulses on the latency of the action potential produced by the EPSC.

The temporal position of the impulses in the simulation sweep was controlled either by sequences of computer generated random numbers (routine ran0 in (Press, et al., 1988, pp. 207-208), or by the recursive logistic function $X_{i+1} = R(1-X_i)X_i$, where X is in the unit interval. For R = 3.7, this function generates values that cover the unit interval densely and chaotically. Both sets of numbers were scaled so as to cover the first 30 ms of the simulation sweeps, or some portion of them. The sum of many such simulation sweeps defines input/output (i/o) functions that relate the time of occurrence of the input perturbation impulse(s) to the output latency generated by the EPSC.

2.1 *The perturbation history of the membrane imposes structure on randomly spaced stimuli*

An example of an i/o function is shown in Fig. 1A. The time-axis of the simulation sweeps rises vertically, and the associated latencies produced by the EPSC are on the horizontal axis. One perturbation current impulse (5×10^{-10} Amps) was randomly timed to occur within the 7-30 ms portion of each simulation sweeps. Earlier presentation times were not used because at the normal resting potential, small perturbation currents produce little effect on the spike latencies. A total of 100,000 sweeps were run in which the random signals covered the 7-30 ms interval homgeneously (Fig. 1B). This generated 100,000 action-potential latencies having a non-homogeneous frequency distribution (Fig. 1C), showing that the membrane imposes structure on the input data stream that it receives.

2.1 *The perturbation history of the membrane distorts and adds complexity to the temporal structure of the signals that it receives*

The chaotic logistic shifts the timing of the perturbing impulse back and forth with respect to the occurrence of the EPSC. Being deterministic, the logistic provides a well-defined pattern of shifts that can be compared with the pattern of latencies in the output spike train. Figure 2A shows a sample time series. Figure 2B shows the structure of the time series as the return map, where a given interval (X_{i+1}) is mapped against the interval preceding it (X_i). For reference, the first four points are mapped in the return map with the same symbols as the first four points in the time series.

FIGURE 2 HERE

In some experiments, we held the presentation time constant and used the logistic to control the amplitude of the impulses using $L_i = (X_i - 0.5) \times 10^{-10}$ Amp. In all cases the impulse width was the same as the integration time step (usually 0.010 msec). In other experiments we held the impulse amplitude constant and varied the presentation times T using $T_i = C + (X_i - 0.5)D$, where X_i is the ouput of the logistic equation. The constant D controls the range of the logistic values, and C slides the critical point of this range along the time axis. The value of the

critical point in the logistic itself is 0.5, and is the center of folding in the return map by which the points mix with respect to one another, as shown in Fig. 2B (and see (Devaney, 1986; May, 1976)). The i/o function representing the complete set of latencies obtained in the experiment is shown by the curve in Fig. 3C. Using the 45° line in Fig. 3B, it can be seen how the time series of current impulses (Fig. 3A) are mapped back and forth onto the temporal position of successive simulation sweeps (Fig. 3C). The symbols in Fig. 3 A-D identify each impulse with the corresponding latency in the output time series (Fig. 3D).

FIGURE 3 HERE

When holding the presentation times constant, the changes in the latency are nearly a constant function of amplitude (Fig. 4B), and the return maps of the latencies, constructed by plotting the latency obtained in one simulation sweep against the latency in the preceding sweep, are quite similar to the return map of the logistic-generated amplitudes (compare Fig. 4A with Fig. 2B). Minor stretching and compression may occur in the latency return maps at other constant presentation times along the isopleths, but overall their shape is similar to the shape shown in Fig. 2B for the input logistic function.

Holding the amplitude constant and presenting the impulses at different times produces complex changes in the spike latencies. The results of two experiments are in Fig. 4D, where the two sets of impulses range over different times and have their critical points shifed with respect to one another in the simulation sweep. The latencies arising from impulses in one experiment are shown by open circles, and those from the other are shown by small dots that coallesce into a line at this resolution. The utility of using the logistic to control the impulse-presentation times becomes evident when plotting the latency changes as return maps in Fig. 4C. Both return maps have two folding regions, wheres the input logistic has only one. The effect of changing the position and range of the impulses is shown more fully in Fig. 5. The thin, unbroken line in Fig. 5A is a fuller representation of the standard i/o function obtained from membrane at resting potential using 10^{-10} Amp impulses shown in Fig. 4D. The presentation times of seven different sets of input stimulus trains are shown by the filled circles; they are shifted vertically with respect to one another in order to illustrate their positions. Figure 5B shows the return maps of the spike latencies; each map is identified numerically by the range of the input stimulus times that

generated it. Like the findings in Fig. 4C, the return maps are significantly distorted variously by comparison to the input stimulus pattern often resulting in more than one folding region and even in ones having crossed trajectories (Fig. 5B "14-19"). Crossed trajectories occur whenever the stimulus pattern sufficiently spans a humped (vertically convex or concave) region of the i/o functions. Four of these regions are shown in Fig. 6A, two each for depolarizing and hyperpolarizing impulses. The corresponding return maps are in Fig. 6B. Together the findings in Figs. 4(C and D), 5B, and 6 indicate that the conditioning history, introduced by a single low-level current impulse, significantly distorts or increases the complexity of the spike-latency return maps obtained in response to a test EPSC.

In biological systems, neurons are bombarded by many synaptic events. These conditions are not controllable in biological systems to obtain the kind of perturbation studies we have attempted here, though they may be approximated in simulations (Mpitsos and Edstrom, 1995). In the experiments presented up to now in the present and in the preceding paper, we have used only one conditioning impulse and one test EPSC in each simulation sweep. Between sweeps the membrane was returned to the normal, unperturbed resting potential. A step toward creating controlled, multiple stimulation conditions may be made by presenting two conditioning pulses in conjunction with the EPSC. The general design of these experiments is as follows: A first conditioning impulse was presented at some fixed position in each simulation sweep. This impulse preconditioned the state of the membrane to the arrival of a second conditioning impulse. The timing of the second impulse was controlled by the chaotic logistic; as before, the use of the logistic provides a structured train of stimuli from one sweep to the next that can be used to assess the effect of the stimulus environment on the output of the postsynaptic neuron.

Figure 7A provides an example of one such experiment. The fixed impulse, lasting one integration step, was given at 19 ms in the simulation sweep. In one experiment the amplitude of this impulse was 10^{-10} Amps (open circle); in a second experiment its amplitude was -10^{-10} Amps (filled circles). The dashed lines running through these points indicate the latency of the action potential obtained when only this first impulse was paired with the EPSC. The long-dashed line lying between these indicates the latency obtained when presenting only the EPSC. In order to provide a reference for the results obtained using the second im pulse that was controlled by the logistic function, Fig. 7A contains i/o

functions (solid-line curves) in which the position of the second impulse is moved successively along the time axis in each sweep from left to right, as was done to generate Fig. 10 of the preceding paper. There are two sets of solid-line curves for each experiment, one in which the amplitude of the second impulse was 4×10^{-10} Amps and one in which it -4×10^{-10} Amps; in both cases each of these movable impulses was paired with one of the fixed 10^{-10} Amp impulses and the EPSC. The effect of the fixed-position impulse is to shift the two sets of curves vertically, one set above the control position shown by long-dashed line, and one set below; i.e., the fixed-position impulse acts as bias on the membrane potential, or equivalently, on the state of the gate parameters. A third set of experiment is superimposed on these results by the thickened region of the i/o curves obtained using the $4 \times !0^{-10}$ Amp impulses. In this set of experiments, the fixed impulses were used in conjunction with the EPSC, but the timing of the 4×10^{-10} Amp impulses was controlled by the logistic over the simulation times that are indicated by the thickened curves.

The return maps of the latencies delimited by the thickened curves in Fig. 7A are plotted in Fig. 7B, showing that the depolarizing preconditioning states produced by the fixed impulse expand the maps whereas hyperpolarizing shrink them. Thus, adding the fixed impulse produced no new changes in the maps except for amplification, and, since the fixed impulses shifted the i/o functions vertically, the two return maps were shifted to different regions of phase space. The changes in amplification, however, would further complicate the return maps if both impulses had variable timing.

3 Discussion

As suggested by a number of studies in biological systems, noted above and reviewed in the accompanying paper, the findings reported here illustrate that the membrane acts as an active linear filter, responding differentially to the same stimulus pattern presented at different times, and adding structure to randomly spaced input signals. The output of the cell represents a distortion of the input, producing several folding regions in return maps and changing the shape and amplitude of the input pattern.

Overall the output represents an increase in complexity with respect to the input pattern, since a single-folded return map of the chaotic logistic that is characterizable as by a second order polynomial, is converted to a doubly-folded

map requiring a higher order polynomial to define it. The input stimulus is a 1-dimensional process, and the phase-space dynamics of the input pattern can be characterized accurately by simple 2-dimensional return maps (Fig. 2B) that represent autocorrelations between adjacent input values. The inter-spike intervals are also a 1-dimensional process, but under some impulse presentation timing, the membrane forces the output dynamics into higher phase-space dimensions than the input since autocorrelations between several intervals in succession are required to resolve the dynamics. These instances occur when the return maps have crossed ends (Fig. 5B ("14-19"), Fig. 6B, and Fig. 7B). Owing to the Poincaré-Bendixson theorem (Hirsch and Smale, 1974) and the Jordon curve theorem, phase-space trajectories can not cross in deterministic systems. Although it is not shown here, casting the return maps in 3-dimensions (X_n, X_{n+1}, X_{n+3}) and rotating the image, the trajectories do not cross, showing that a changing the reference from a 2-dimensional return map to a 3-dimensional one resolves at least this degeneracy in the input/output transformation, though higher dimensional embedding may be necessary to characterize the dynamics accurately.

Two important and possibly interrelated phenomena have been identified in our studies that may be useful in extending the understanding of how individual neurons may become involved in the integrative capabilities of networks. Both emerge from the input/output functions relating the linear perturbation history of the membrane impedance. One, reported in the accompanying paper, is the apparent degeneracy of how information in the input data stream may relate or be decipherable in the output data stream. The second, reported here, shows that that there is also a deterministic component, though there is distortion and increase in complexity of the output firing pattern by comparison to the input signal.

These findings speak to both sides of a controversy that has had a long existence, e.g., (Adey, 1972; Adrian, 1946; John, 1972). To use Adey's words, are neurons inefficient, "noisy processor" or do they process information efficiently and deterministically? Recent work on hippocampal slices has obtained evidence for determinism (Schiff, 1994), but also for a substantial, perhaps in most cases, of nondeterministic activity (Schiff, et al., 1994). The problem has been one not only of neuronal function in mammals, but also one of "simple" function in lower animals (Mpitsos and Cohan, 1986; Mpitsos, et al., 1988b; Wu, et al., 1994). In our own biological work (Mpitsos, 1989; Mpitsos, et al., 1988a; Mpitsos, et al., 1988b),

the search for low-dimensional deterministic activity has not been encouraging, and has prompted the present simulations to gain some understanding of where the apparent nondeterministic activity arises. In a commentary on a deterministic model proposed by Shalden and Newsome (1994), Softky (1995) has discussed that their model of 'balanced inhibition', used to account for variations in cortical neuron firing, is based on the assumption that the cell is insensitive to the temporal structure of the input signal. Our findings indicate that any neuron having complex, humped or multi-humped i/o functions will be highly sensitive to the temporal structure of its input signal. Although the process is deterministic, it is also highly subject to degeneracies that can lead to variations. Our subsequent papers will examine how the humped i/o functions lead both to stable and unstable firing when the neuron is placed in a network, and will examine the information transfer quantitatively.

References Cited

Adey RW (1972) Organization of brain tissue; Is the brain a noisy processor? Int J Neurosci 3:271-284

Adrian ED (1928) The Basis of Sensation. Norton, New York

Adrian ED (1946) The physical background of perception. Clarendon Press, Oxford

Bialek W, DeWeese M, Ricke F, Warland D (1993) Bits and brains: Information flow in the nervous system. Physica A 200:581-593

Bialek W, Ricke F, deRuyter van Steveninck RR, Warland D (1991) Reading a neural code. Science 252:1854-1857

Bryant HL, Segundo JP (1976) Spike initiation by transmembrane current: A white-noise analysis. J Physiol 260:279-314

Devaney RL (1986) An Introduction to Chaotic Dynamical Systems. Benjamin/Cummings, New York

Diamond DM, Dunwiddie TV, Rose GM (1988) Characterization of Hippocampal Primed Burst Potentiation *in vitro* and in the awake rat. J Neurosci 8:4079-4088

Edstrom JL, Mpitsos GJ (1995) Predicting the influence of perturbing currents on spike latencies: Determinism and degeneracy of information in the linear filter properties of neuron membrane. In Preparation

Enroth-Cugell C, Robson JG, Schweitzer-Tong DE, Watson AB (1983) Spatio-temporal interactions in cat retina ganglion cells showing linear spatial summation. J Physiol 341:279-307

Frishman LJ, Freeman AW, Troy JB, Schweitzer-Tong DE, Enroth-Cugell C (1987) Spatiotemporal frequency responses of cat retinal ganglion cells. J Gen Physiol 89:599-628

Gerstein GL, Mandelbrot B (1964) Random walk models for spike activity of single neurons. Biophys J 4:41

Glantz RM (1994) Direction selectivity in a nonspiking interneuron of the crayfish optic lobe: Evaluation of a linear model. J Neurophysiol 71:180-193

Glantz RM, Nudelman HB (1976) Sustained, synchronous oscillations in discharge of sustaining fibers of crayfish optic nerve. J Neurophysiol 39:1257-1271

Glantz RM, Nudelman HB (1988) Interval coding and band-pass filtering at oculomotor synapses in crayfish. J Neurophysiol 59:56-76

Glantz RM, Nudelman HB, Waldrop B (1984) LInear integration of convergent visual inputs in an oculomotor reflex pathway. J Neurophysiol 52:1213-1225

Grüneis F, Nakao M, Yamamoto M, Musha T, Nakahama H (1989) An interpretation of 1/f fluctuations in neuronal spike trains during dream sleep. Biol Cybernetics 60:161-169

Guttman R, Feldman L, Lecar H (1974) Squid axon membrane response to white noise stimulation. Biophys J 14:941-955

Hirsch MW, Smale S (1974) Differential Equations, Dynamical Systems, and Linear Algebra. Academic Press, New York

Hodgkin A, Huxley AF (1952) A quantitative description of membrane current and its application to conduction and excitation in nerve. J Physiol 117:500-544

John ER (1972) Switchboard versus statistical theories of learning and memory. Science 177:850-864

Krause HI, Naka K-I (1980) Spatiotemporal testing and modeling of catfish retinal neurons. Biophys J 29:13-36

May RM (1976) Simple mathematical models with very complicated dynamics. Nature 261:459-467

Mpitsos GJ (1989) Chaos in brain function and the problem of nonstationarity: A commentary. In: Basar E, and Bullock TH, (ed) Dynamics of Sensory and Cognitive Processing by the Brain, Springer-Verlag, New York, pp 521-535

Mpitsos GJ, Burton RM, Creech HC, Soinila SO (1988a) Evidence for chaos in spike trains of neurons that generate rhythmic motor patterns. Brain Res Bull 21:529-538

Mpitsos GJ, Cohan CS (1986) Comparison of differential Pavlovian conditioning in whole animals and physiological preparations of *Pleurobranchaea:* Implications of motor pattern variability. J Neurobiol 17:498-516

Mpitsos GJ, Creech HC, Cohan CS, Mendelson M (1988b) Variability and chaos: Neurointegrative principles in self-organization of motor patterns. In: Kelso JAS, Mandell AJ, and Shlesinger MF, (ed) Dynamic patterns in complex systems, World Scientific, Singapore, pp 162-190

Mpitsos GJ, Edstrom J (1995) Bifurcation dynamics and variation in computer
simulation of biologically realistic neural networks.

Nakahama H, Yamamoto M, Ishi N, Fujii H, and Aya K (1977) Dependency as a
measure to estimate the order and the values of Markov
processes. Biol Cybernetics 25:209-226

Perkel DH, Schulman JH, Bullock TH, Moore GP, Segundo JP (1964) Effects of
regularly spaced synaptic input. Science 145:

Press WH, Flannery BP, Teukolsky SA, Vetterling WT (1988) Numerical Recepies
in C: The Art of Scientific Computing. Cambridge University Press,
Cambridge, MA

Rall W (1977) Core conductor theory and cable properties of neurons.

Rose GM, Dunwiddie TB (1986) Induction of Hippocampal long-term
potentiation using physiologically patterned stimulation. Neurosci Let
69:244-248

Sakuranaga M, Naka K-I (1983) Signal transmission in the catfish retina. III.
Transmission to typs-C cells. J Neurophysiol 53:411-427

Sakuranaga M, Naka K-I (1985a) Signal transmission in the catfish retina. I.
Transmission in the outer retina. J Neurophysiol 53:373-389

Sakuranaga M, Naka K-I (1985b) Signal transmission in the catfish retina. II.
Transmission to type-N cell. J Neurophysiol 53:390-410

Schiff SJ (1994) Controlling chaos in the brain. Nature 370:615-620

Schiff SJ, Jerger K, Chang T, Sauer T, Aitken PG (1994) Stochastic versus
deterministic variability in simple neuronal circuits: II. Hippocampal slice.
Biophys J 67:684-691

Segundo JP, Moore GP, Stensaas LJ, Bullock TH (1963) Sensitivity of neurones in *Aplysia* to temporal pattern of arriving impulses. J Exp Biol 40:643-667

Shalden M, Newsome W (1994) Noise, neural codes and cortical organization. Curr Opin Neurobiol 4:569-579

Softky WR (1995) Simple codes versus efficient codes. Curr Opin Neurobiol 5:239-247

Tsukada M, Aihara T, Mizuno M, Kato H, Ito K (1994) Temporal pattern sensitivity of long-term potentiation in hippocampal CA1 neurons. Biol Cybern 70:495-504

Wu JY, Tsau Y, Hopp HP, Cohen LB, Tang AC, Falk CX (1994) Consistency in nervous systems: trial-to-trial and animal-to-animal variations in teh responses to repeated applications of a sensory stimulus in *Aplysia*. J Neurosci 14:1366-1384

Yamamoto M, Nakahama H (1983) Stochastic properties of spontaneous unit dischargess in somatosensory cortex and mesencephalic reticular formation during sleep-waking states. J Neurophysiol 49:1182-1198

FIGURE LEGENDS

FIGURE 1: Recent history of impedance changes that occur under random perturbation generates nonrandom firing of EPSC-evoked action potentials. A: Relation of impulse presentation time to action potential latency (horizontal axis). B: Density of randomly generated impulse presentation times; vertical axis is the same as in (A). A single randomly timed current impulse (4×10^{-10} Amps, lasting one .010 ms integration step) was presented in the 7-30 ms interval of each 35 ms simulation sweep. A suprathreshold EPSC was initiated 25 ms into the simulation. C: Histogram of the EPSC-evoked action potentials the resulted from 100,000 simulation sweeps.

FIGURE 2: The chaotic logistic, $f(x) = 3.7(1-x)x$ was used to generate deterministic sequences of impulse presentation times. A: Time series. The values were scaled (see text) to control the impulse presentation times within each simulation sweep. B: Return map showing the deterministic structure of the logistic. One value (X_{i+1}) of the time series is plotted against the preceding value (X_i). For reference, the symbols are the same in (A and B) for the first four points. The 1:1 line shows how the points fold over the critical point ($X = .5$).

FIGURE 3: Method for presenting the logistically-driven constant current pulses to the postsynaptic neuron variably in time. A: Logistic-driven current pulses. B: the 1:1 line is used to match time axes so that the current pulses can be superimposed on the time axis of the isopleth (C) to show how they bounce back and forth in time. D: Symbols show the observed EPSC-evoked action potential latencies arising from each pairing of the impulse with the EPSC.

FIGURE 4: The effect of the amplitude (A and B) and timing (C and D) of perturbation pulses on EPSC-evoked action- potential latencies. A and C: return maps of the latencies. B and D: latencies as a function of current-pulse amplitude and time of occurrence, respectively. For each presentation of a 0.010 msec perturbation pulse and an EPSC, a single action potential was obtained whose latency was measured as the time from the onset of the simulation. Both amplitude and time were modulated by the 3.7 logistic. When changing the presentation time, the amplitude was constant at 2×10^{-10} A. The presentation times for two experiments are shown min C and D: The solid line is for
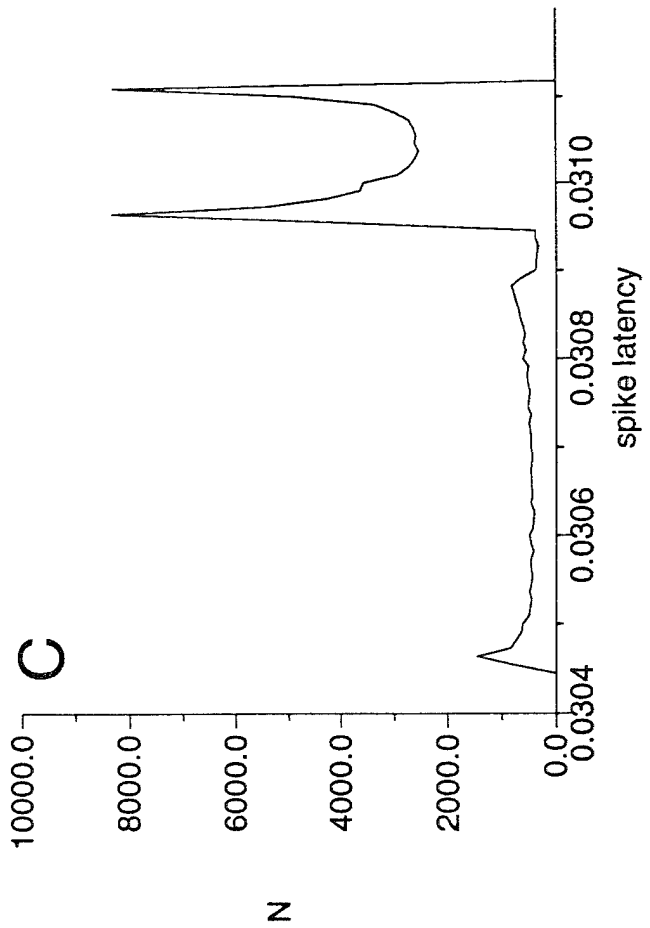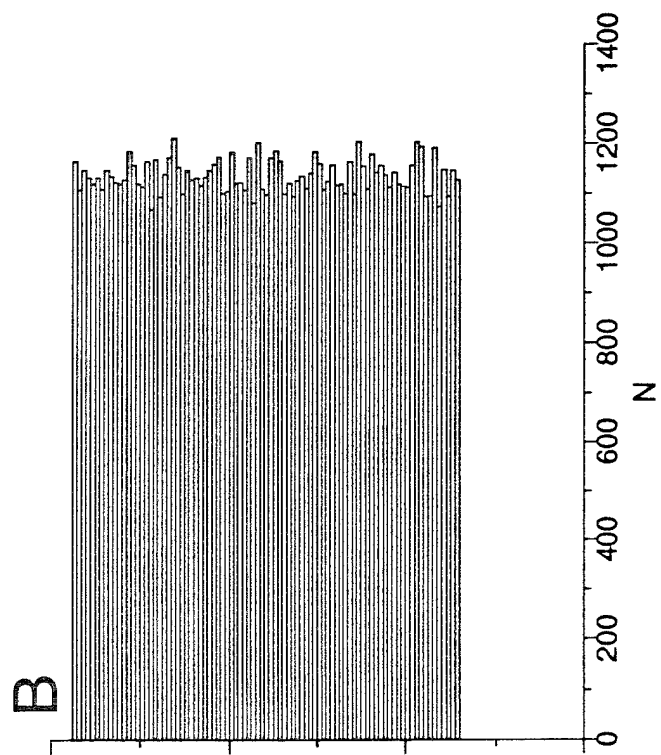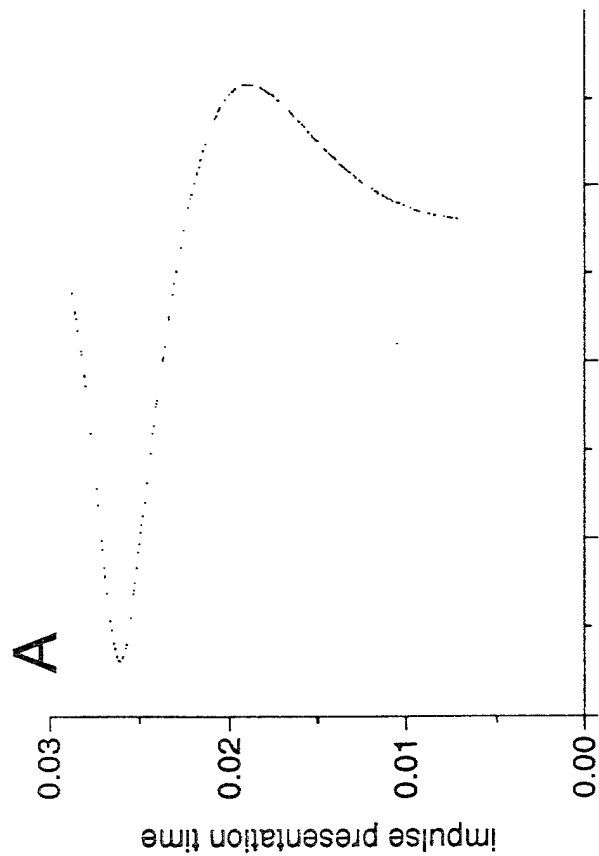
presentation times shifted earlier and covered a smaller range than the times shown for the experiment shown by the open circles. The EPSC onset was at 25 msec

FIGURE 5: The temporal position along the latency isopleths represent different distortions of the structure of the input function generating the perturbation pulses. A: The thin line shows the action potential latencies arising from a composite of logistic-activated sequence of current pulses having constant amplitude (9×10^{-10} Amp; .010 ms). Seven of these sequences are shown by the dotted curves which have been shifted vertically to identify them. The irregular spacing between the dots in each line arises from the logistic scaling function T described in the text. B: Return maps of the intervals in six of the sequences in (A). The numbers identify the approximate range of times spanned by each sequence along the isopleth. Note that each map is a different distortion of the input function return map shown in Fig. 8, and, in particular, that the two legs of the map for the presentation of the input function at the 14-19 msec span on the isopleth cross over one another.
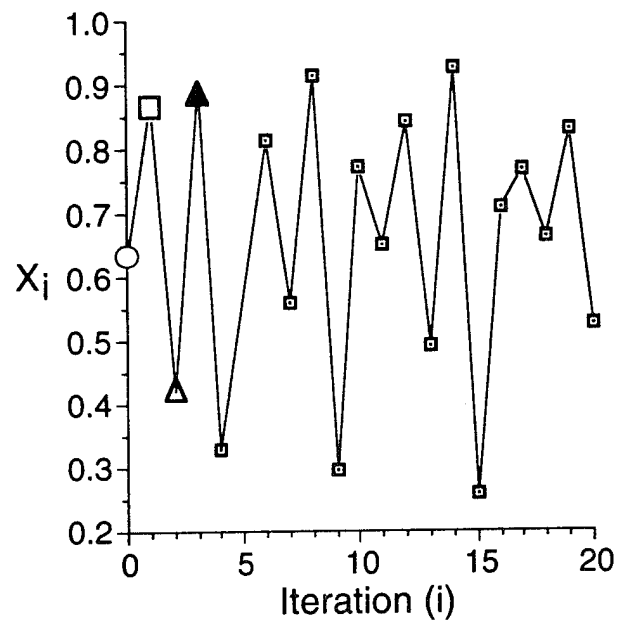
FIGURE 6: Trains of stimuli falling over four humped regions (normal and inverted) of the isopleths (A) produce different looped latency return maps (B). The two smaller humps occur before the onset of the EPSC. The second two partially overlap the EPSC, showing that the EPSC amplifies the latency changes by comparison to the latencies produced by stimuli falling over the first set of humps, but does not change the overall structure of the maps.

FIGURE 7: Interaction between multiple perturbation impulses amplifies changes in EPSC-evoked latencies, but does not change overall output dynamics. A: To show the effect, three experiments were conducted involving two conditioning impulses and a suprathreshold EPSC). In two experiments (two sets of thin-line curves), a fixed conditioning pulse was presented at 19 ms in the simulation sweep (filled circle = 10^{-10} Amps; open circle = -10^{-10} Amps). The timing of the second impulse (4×10^{-10} or 4×-10^{-10} Amps) was moved progressively from left to right in each simulation sweep, and enough sweeps were conducted to cover the full sweep. To show the shapes of the i/o curves, only the 15-30 msec range of times is shown. The third experiment paired the fixed-position impulses with the movable impulse whose timing was controlled

by the logistic to occur over the range shown by the thickened line segments. B: Return maps of the latencies shown by the two thickened lines. Not that the two maps are simple linear amplifications of one another. Middle, long-dashed line: latency obtained with only the EPSC. Top dashed line: latency obtained by pairing the 10^{-10} Amp impulse with the EPSC. Bottom dashed line: latency obtained by pairing the -10^{-10} Amp impulse with the EPSC.

A: Time Series

B: Return Map

○	0.623
□	0.869
△	0.421
▲	0.902

latency (msec)

time (msec)

iteration

D observed AP latencies

A modulatory current pulses

time (msec)

latency (msec)

C

B

-3-

A

time of spike (msec)

spike time without perturbation

time (msec) from start of simulation

B

time of spike(n+1)

5 - 10
9 - 14
10 - 15
12 - 17
13 - 18
14 - 19
14 - 19
13 - 18
12 - 17

time of spike(n) in msec

- 5 -

A

latency (n+1)

latency (n)

latency (msec)

time (msec)

- 6 -

A

B

latency(n+1) msec

latency(n) msec

time (msec)

latency (msec)

17.2
17.0
16.8
16.6
16.4
16.2
16.0

16.2 16.4 16.6 16.8 17.0 17.2

0   5   10   15

16   17   18   19   20

— 7 —